Dissertation

Dynamic Electrochemistry of Organic Radicals in solution

Muhammad Tahir Soomro

Graz, im August 2011

zur Erlangung des akademischen Grades
des Doktors der Technischen Wissenschaften

vorgelegt bei
O.Univ.-Prof. Dipl.-Chem. Dr. Günter Grampp
Institut für Physikalische und Theoretische Chemie
der Technischen Universität Graz

...dedicated to my parents
in love and gratitude

Contents

List of Tables

List of Figures

Abstract

This work presents the experimental determination of the half-wave oxidation/reduction potentials for irreversible, one electron transfer, electrochemical processes. A variety of structurally related series of organic compounds e.g., aromatic amines, methoxybenzenes, pyrroles, bicarbonyls, adenine, thymine, thymidine, adenosine, histidine, methionine, alanine, 2,2´-bipyridine, and 3,3´,4,4´-benzophenone tetracarboxylic acid are observed for their redox behavior. Many of these compounds are used for photoinduced electron transfer (PET) reactions.

The $E_{1/2}$ ($E_{1/2}^{ox}, E_{1/2}^{red}$) values can be determined by analyzing the cyclic voltammogram at various sweep rates. Based on the free energy relationships given by Marcus, Rehm-Weller, and Marcus-Levine the dependence of the peak potentials on the electron transfer coefficient have been evaluated and plotted. From the intercept the thermodynamic half-wave potentials were obtained after some simple calculations. This relatively uncomplicated methodology provides an opportunity to find out the standard potential for irreversible systems. It is somewhat surprising that only a limited number of systems have been examined with this method.

Alternatively, for highly irreversible redox systems, the phase-selective second-harmonic ac voltammetric approach can be capable of yielding reliable thermodynamic half-wave potentials even when the half life of the electrode reaction product is 10^{-4} s. The method has been exploited for the determination of the thermodynamic half-wave potentials of all oxidative/reductive quenchers. Finally the results obtained from cyclic voltammetric and from phase-selective second-harmonic ac voltammetric methods have been compared.

Zusammenfassung

In dieser Arbeit wird über die Messung elektrochemischer Redoxpotentiale irreversibler Elektronentransferreaktionen berichtet. Eine Vielzahl von strukturverwandten organischen Verbindungen, z.B. aromatischen Aminen, Methoxybenzolen, Pyrrolen, sowie Adenin Thymin, Adenosin, Histidin, Methionin, Alanin, 2,2´-Bipyridin und 3,3´,4,4´-Tetracarboxybenzophenon wurden bezüglich ihres Redoxverhaltens untersucht. Viele dieser Verbindungen werden bei Untersuchungen des photoinduzierten Elektronentransfers (PET) als Quencher eingesetzt. Zur Interpretation solcher Ergebnisse müssen die Redoxpotentiale der Reaktionspartner bekannt sein.

Die Halbwellenpotentiale für Oxidation und Reduktion können aus den Zyklischen Voltamogramen entnommen werden. Durch Anwendung der Elektronentransfertheorien nach Marcus, Rehm-Weller und Marcus-Levine lassen sich aus den Potentialmaximas und den Elektronentransferkoeffizienten die Redoxpotentiale irreversibler Elektrodenreaktionen bestimmen. Diese Methode wurde bisher nur für sehr wenige Redoxsysteme angewandt.

Zusätzlich wurden die Redoxpotentiale irreversibler Systeme mit Hilfe der phasenselektiven Wechselstromvoltametrie bestimmt. Mit dieser Methode können sehr kurzlebige Oxidations- oder Reduktionsprodukte an der Elektrode untersucht werden. Die erzielten Ergebnisse aus beiden elektrochemischen Verfahren wurden miteinander verglichen und interpretiert.

Acknowledgements

I owe my profound thanks and deepest sense of gratitude to Almighty Allah who blessed me with determination, potential and ability to complete my Ph.D. I don't have words to describe my feelings of respect about my affectionate parents, for the understanding, unlimited support and encouragements they have shown to me. I also would like share my feelings of admiration about my brothers and sisters for their moral support. My deepest thanks go to Amna, no doubt you have charming and impressive personality and you have contributed a lot in grooming my individual qualities.

It is my pleasure to acknowledge many people for their patience and contributions to my scientific and personal development. Obviously I can not mention all of them individually but I am very thankful to all with owed gratitude.

To Prof. Dr. Mahboob Mohammad because of his enthusiastic supervision and great contribution that eventually build up my interest in physical chemistry and bring me to the stage of honor. I will always remember his inspiring guidance, constant encouragement, constructive criticism and friendly discussions.

I don't find myself in position to pay compliments to Professor Günter Grampp, from whom I have learnt a lot about electron transfer reaction, practical laboratory work, and instrumental work. His enthusiasm in research and his thinking freedom are contagious and stimulating.

I wish to express my warm and sincere thanks to Dr. Stephan Landgraf, who helped me much with setting, building, rebuilding, designing and reforming the apparatuses used in this work. His advice in the practical work has been essential.

Helmut Eisenköbl, Marion Hofmeister and Hilde Freißmuth, all of them really deserve recognition for making things to keep running in smooth way, providing chemicals, solvents, glassware, electric and mechanical help and cover all administrative stuff, all of it sum together to say thank to all of you for making work smooth and comfortable.

Special thanks are due to all my colleagues in last four years (Boryana, Faiza, Christine, Tajamal, Noureen, Zahid, Asim, Sadia, Truong, Kriwan, and Kenneth) for sharing time with me related to both scientific and non-scientific contents. It was my pleasure to work and learn from all of you with many good memories of time.

Finally, the financial support given by the Higher Education Commission of Pakistan for this research project is acknowledged.

Chapter 1. Introduction

Research is what I'm doing when
I don't know what I'm doing.

(*Wernher von Braun*)

Electronically excited states molecules are highly energetic species and this energy can be transferred to other molecules, more often to quenchers, by the process of electron transfer reactions. The properties associated with the quenchers that determine the extent of the actual electron transfer reactions are the redox potentials.[1-2] Electrons usually are relocated in the direction of increasing redox potentials and therefore it is important to know the redox potentials of reductants and oxidants. The knowledge of the redox potentials further provide understanding of how the actual electron transfer processes occur from reductants to oxidants or either way. Regardless of its importance the thermodynamically meaningful oxidation/reduction potentials for many quenchers (e.g., aromatic amines, methoxybenezes, and biologically relevant quenchers such as thymine, adenosine etc) are not available or have not been determined precisely by electrochemical methods because of the irreversible nature of this one-electron oxidation/reduction on the time scale of electrochemical measurements. There is not any established methodology exist for the determination of redox potentials of these irreversible systems e.g., quenchers.

The present work writes with hopes to contribute to the better and deeper understanding of the determination of the standard potentials for irreversible electrochemical systems. A relatively easy and simple approach has been utilized for the determination of the half-wave redox potentials in irreversible systems.[i] First the basic understanding of the free energy relationships given by Marcus, Rehm-Weller, and Marcus-Levine is presented and developed.[3-9] In the second step the theory of stationary state polarography has been linked to the free energy relationships. The methodology employed has few steps which are

- All three free energy relationships, Marcus, Rehm-Weller, and Marcus-Levine, are derivatized with respect to free energy change.

[i] Fukuzumi and coworkers had already done some work in this regard, see reference 3.

- The cyclic voltammograms obtained for all compounds at different scan rate are analysed.
- From the width of the CV waves the electron transfer coefficients will be obtained.
- The electron transfer coefficients are plotted against the peak potentials obtained at different scan rate.
- From the linear plots the intercept values will be calculated which subsequently provide half-wave oxidation/reduction potentials.
- The criteria for electrochemical reversibility will also been checked.

Beside cyclic voltammetric method, the second approach that we will utilize is the phase-selective second-harmonic ac voltammetry.[ii] For rapid follow-up chemical reactions compared to the charge transfer step, the second-harmonic ac voltammetry with its excellent potential provides us simple and precise determination of the reversible half-wave potentials. The method also offered some advantages over conventional dc techniques i.e., zero current contribution from double layer charging current and also fast analysis time. The phase-selective second-harmonic response will be characterized by two symmetrical positive and negative lobes around zero current minimum.[10-14] We will individually record in phase (I) and quadrature (Q) components of the voltammograms. Both components will intersect at zero or nearly zero current minimum on the dc axis and this intersection offers us straightforward determination of the half-wave redox potentials.

The third approach photomodulated voltammetry[iii] will be applied for the determination of the redox potential for transient species, species with a lifetime of milli-second. The radicals are generated using photolysis and flow through the cell where subsequent oxidation/reduction of the radicals will be taking place. The small alternating current is generated, when potential is scanned between certain limits, and will be detected by the lock-in-amplifier.[15-17] The resulting PMV voltammogram has a typically sigmoid shaped. The presentation of photomodulated voltammetry is very simple however in practice the technique to some extent more complicated than the theory suggests.

[ii] Numbers of publications are available on second-harmonic ac voltammetry by different authors.
[iii] Not many workers are using this technique due to its complicated setup.

This thesis is organized as follows: The chapter 2 presents the theoretical foundations of the experimental work which will further extend in next three chapters. The following experimental section provides necessary information regarding the used substances and solvents, measurements procedures and instrumental setups. The next chapter presents the experimental results obtained from all three methods, their analysis and discussions about findings. In the end a short summary and an outlook of the possible future work will be presented.

Chapter 2. Theoretical Contemplations

> If you're not part of the solution,
> you're part of the precipitate.
>
> (*Henry J. Tillman*)

This chapter presents the descriptions and explanations of the main theoretical concepts used in this work. First we illustrated here the free energy relationships from Rehm-Weller, Marcus and Marcus-Levine in terms of relationship between free energy of activation and free energy change. In the next section, application of the theory of stationary electrode polarography together with the above mentioned free energy relationships, the dependence of the CV peak potential on the electron transfer coefficient has been established. Later, this relation has been used to extract the thermodynamic standard potential from the intercept of the linear plot between peak potential vs. electron transfer coefficient.

2.1 Treatment of Rehm-Weller Equation

Although an electronically excited molecule has higher electron affinity and lower ionization potential which means excited state is both a stronger oxidant and a stronger reductant[2, 18-19] and can easily transfer electron when encounter quencher, the electron transfer reactions adequately depend on the redox properties of the quencher.[2, 20] This intermolecular electron transfer reaction between excited molecule, M, and non-excited ones, Q, which in strongly polar solvents generally results in fluorescence quenching. The theory that describes the fluorescence quenching by electron transfer in polar solvents first formulated by Rehm and Weller[3] and later extensively studied by others.[2, 18-19, 21-22]

Equation (2.1) is an adapted version of the general reaction proposal submitted by Rehm and Weller.

$$M^* + Q \underset{k_{diss}}{\overset{k_{diff}}{\rightleftarrows}} \left(M^*Q\right) \underset{k_{-et}}{\overset{k_{et}}{\rightleftarrows}} \left(M^{\mp}Q^{\pm}\right) \xrightarrow{k_{decay}} M + Q \qquad (2.1)$$

The excited state molecule represented by the asterisk which can be either the donor M^* or the acceptor Q^* molecule. The rate constants for the diffusion and the dissociation processes are k_{diff} and k_{diss} whereas the rate constants for forward and back electron transfer from the encounter complex to the radical ion pair expressed by k_{et} and k_{-et}. k_{decay} is the rate constant for the processes by means radical ion pair can disappear. These processes include dissociation, diffusion and back electron transfer leading to the ground state / triplet state.

Quenching reaction proceeds via the deactivation of the excited state molecule M^* by single electron transfer to quencher Q. Conversely, depending on the redox potentials of both M and Q, it is also rational to consider electron transfer from M to Q.[18, 22] The quenching rate constant k_q more or less equal to the diffusion controlled rate constant[23] and can be depicted in the form of the individual rate constants shown in equation (2.1).[3, 22] It has been reported that the quenching by electron transfer bring about the relationship between the quenching rate constant and the redox potential of the quenchers.[3, 18, 24] Rehm and Weller have set up the quantitative relationship between the quenching rate constant and the free energy change of the electron transfer process.[3] The first equilibrium step described the diffusion of the reactants to the encounter complex and the rate of formation of encounter complex or non-radiative decay rate of the molecule M to its ground state is shown below.

$$\text{rate} = k_{diff}\left[M^*\right][Q] - k_{diss}\left[M^*Q\right] \qquad (2.2)$$

The concentration of the encounter pair can be obtained by allowing for the steady state approximation. The concentrations of the intermediates are put to zero

$$\frac{d\left[M^*Q\right]}{dt} = k_{diff}\left[M^*\right][Q] - \left(k_{et} + k_{diss}\right)\left[M^*Q\right] + k_{-et}\left[M^{\mp}Q^{\pm}\right] \approx 0 \qquad (2.3)$$

$$\frac{d\left[M^+Q^-\right]}{dt} = k_{et}\left[M^*Q\right] - \left(k_{decay} + k_{-et}\right)\left[M^{\mp}Q^{\pm}\right] \approx 0 \qquad (2.4)$$

By rearranging equation (2.4), the radical ion pair equals

$$\left[M^{\mp}Q^{\pm}\right] = \frac{k_{et}\left[M^{*}Q\right]}{k_{decay} + k_{-et}} \tag{2.5}$$

Substituting the steady state $\left[M^{\mp}Q^{\pm}\right]$ into the equation (2.3) for the encounter complex

$$\left[M^{*}Q\right] = \frac{k_{diff}\left[M^{*}\right][Q]}{\left(k_{et} + k_{diss}\right) - \dfrac{k_{-et}k_{et}}{k_{decay} + k_{-et}}} \tag{2.6}$$

One may further proceed and substitute the above $\left[M^{*}Q\right]$ into equation (2.2) to get the final expression for the over-all quenching rage constant k_q.

$$k_q = \frac{k_{diff}}{1 + \dfrac{k_{diss}}{k_{et}} + \dfrac{k_{diss}}{k_{decay}} \cdot \dfrac{1}{K_{et}}} \tag{2.7}$$

where $K = \dfrac{k_{et}}{k_{-et}}$ is the equilibrium constant for electron transfer reaction between the encounter pair and the radical ion pair. The equilibrium constant can be articulated in the form of Gibbs free energy of the electron transfer reaction.

$$K = \exp\left(\frac{-\Delta G^{0}}{RT}\right) \tag{2.8}$$

Rehm and Weller illustrated that the Gibbs free energy change arrived from the difference between the minimal potential energy for the encounter complex and the radical ion pair (**Figure 2.1**). It has been reported by many authors[18, 21, 23] that, for the electron transfer from Q to M, ΔG_{et} can be estimated from the oxidation and reduction potential of Q and M as shown below.[iv]

$$\Delta G^{0} = E(Q/Q^{\bullet+}) - E(M^{\bullet-*}/M) + w_p - w_r \tag{2.9}$$

Where w_p, the work is utilized to bring the products together and consequently w_r is the term used for bringing the reactants together. The work terms are due only to Coulombic attraction and usually they are very small and negligible,[18, 21, 23] therefore ΔG^{0} can be taken as the difference in the standard redox potential of the two couples.

[iv] Remember $\Delta G = -nFE$.

Such potentials are obtained by means of cyclic voltammetric experiments. Because M is in the excited state and one must consider excitation energy of M , such as

$$E^0(M^{\bullet -*}/M) = E^0(M^{\bullet -}/M) + \Delta E_{0,0} \qquad (2.10)$$

where $\Delta E_{0,0}$ is the zero-zero transition energy which can be obtained from the spectroscopic data.

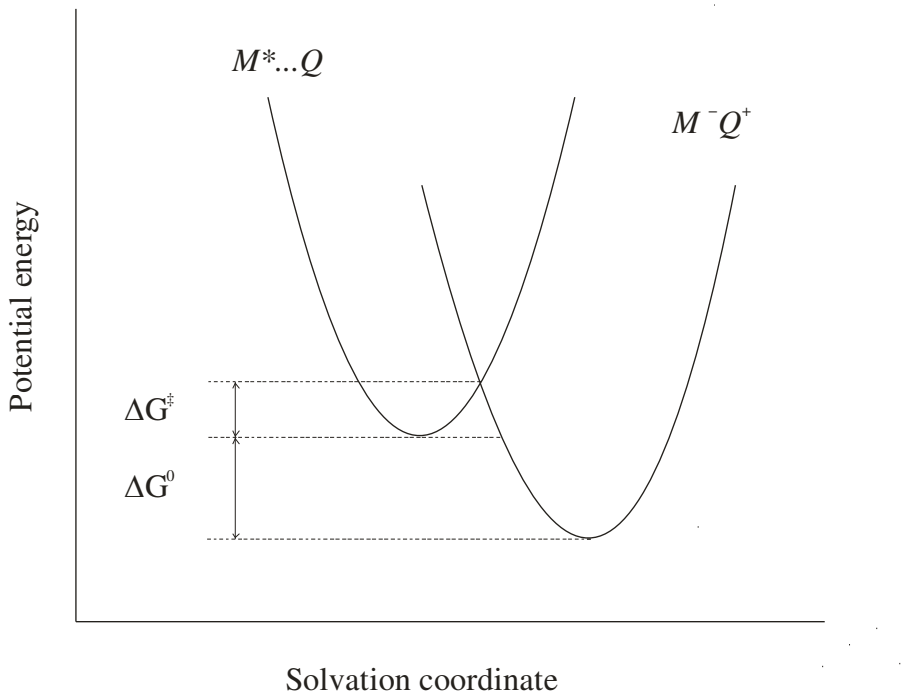

Figure 2.1: Potential curves that illustrate an exothermic electron transfer process. In this illustration, the abscissa represents changes that occur upon electron transfer in (a) the salvation shell surrounding the $M-Q$ pair, and (b) the configuration of nuclei in the $M-Q$ pair.[v]

The rate constant for the diffusion limited processes can be shown as a function of the solvent dependent diffusion coefficients D_M and D_Q of the reactants in accordance with the Smoluchowski equations. The bimolecular rate constant k_{diff} for the encounter complex is shown in equation (2.11).[3, 22]

[v] Figure 2.1 is taken from L. Poulsen et al., 2003; see reference 22.

$$k_{diff} = 4\pi N_A \left(D_M + D_Q\right) a \tag{2.11}$$

where N_A is Avogadro's number and a is the distance at which reactants interact to each other.

Similarly the unimolecular rate constant of the dissociation process is as follows

$$k_{diss} = \frac{k_{diff}}{N_A \Delta V_{diff}} = B\frac{\left(D_M + D_Q\right)}{a^2} \tag{2.12}$$

D_M and D_Q are the diffusion coefficients. B is the dimensionless parameter which is a function of shape and relative size of the reactants where as the volume of the encounter complex symbolize as $\Delta V = \frac{k_{et}}{k_{-et}}$.[18]

According to Arrhenius equation, the rate constant for the electron transfer can be articulated in terms of activation free energy, ΔG^0 between encounter complex and radical ion pair. For a given process from i to j, the rate constant,

$$k_{ij} = k^{\ddagger} \exp\left(-\frac{\Delta G^{\ddagger}}{RT}\right) \tag{2.13}$$

that means the rate constant equal to product of a pre-exponential frequency factor $k^{\ddagger}$, with the same unit as k_{ij}, and a unitless exponential factor $\exp\left(-\frac{\Delta G^{\ddagger}}{RT}\right)$. The frequency factor $k^{\ddagger}$ will be on the order of $10^{-11}s^{-1}$. As we discussed before k_{decay} is the rate constant for all the possible modes of the decay of the radical ion pair to ground state and here we assumed as these authors already did,[3, 22] the back electron transfer process is adequately exothermic process and $\Delta G^{\ddagger}$ will be close to zero, so that

$$k_{decay} = k^{\ddagger} \tag{2.14}$$

under these condition the electron transfer rate constant is defined as

$$k_{et} = k_{decay} \exp\left(-\frac{\Delta G^{\ddagger}}{RT}\right) \tag{2.15}$$

So that the rate constant for electron transfer between M and Q become the function of the $\Delta G^{\ddagger}$. Substituting equations (2.11), (2.12) and (2.15), equation (2.7) can be transformed into equation (2.16)

$$k_q = \frac{k_{diff}}{1+\frac{k_{diff}}{N_A \Delta V_{diff} k_{decay}}\left(\exp\left(\frac{\Delta G^{\ddagger}}{RT}\right)+\exp\left(\frac{\Delta G^{0}}{RT}\right)\right)} \tag{2.16}$$

where ΔG^0 and $\Delta G^{\ddagger}$ are the free-energy difference and the free energy of activation between encounter complex and radical ion pair. Rehm and Weller,[3] assumed that for a series of related donors (or vice versa), k_{diff}, k_{decay}, and ΔV_{diff} can be considered as constant. In that case, k_q can be expressed as a function of only ΔG^0 and $\Delta G^{\ddagger}$. In turn $\Delta G^{\ddagger}$ depends only on ΔG^0, and therefore, k_q formulated as a function of only ΔG^0. It is this correlation of rate constant with the energetics of the electron transfer, ΔG^0, that can provide the kinetic information for an electron transfer in a reaction scheme. For diffusion controlled limited electron transfer reaction, k_q is independent of ΔG^0 in that case equation (2.16) reduces to equation (2.17)

$$k_q = \frac{k_{diff} N_A \Delta V_{diff} k_{decay}}{N_A \Delta V_{diff} k_{decay} + k_{diff} \exp\left(\frac{\Delta G^{\ddagger}_{et}}{RT}\right)} \tag{2.17}$$

where ΔG^0 becomes large and negative (i.e., $k_{et} = k_{iff}$).

And endergonic electron transfer reaction for which, k_q depends strongly on ΔG^0 and equation (2.17) becomes equation (2.18)

$$k_q = \frac{N_A \Delta V_{diff} k_{decay}}{2} \exp\left(-\frac{\Delta G^0}{RT}\right) \tag{2.18}$$

where ΔG^0 is large and positive and can be evaluated directly from redox potentials of reacting couples as in Eq.(2.9). According to Rehm and Weller,[3] the free energy of activation for an electron transfer reaction, $\Delta G^{\ddagger}$, is related to the overall free-energy change, ΔG^0, by equation (2.19):

$$\Delta G^{\ddagger} = \left[\left(\frac{\Delta G^{0}}{2}\right)^{2} + \left(\Delta G^{\ddagger}(0)\right)^{2}\right]^{1/2} + \frac{\Delta G^{0}}{2} \tag{2.19}$$

In equation (2.19) $\Delta G^{\ddagger}(0)$ is the intrinsic barrier representing the activation free energy for electron transfer when the driving force is zero i.e., $\Delta G^{\ddagger} = \Delta G^{\ddagger}(0)$ at $\Delta G^{0} = 0$. The value of $\Delta G^{\ddagger}$ which, in turn, can be utilized to obtain k_{et} from equation (2.13).

The two general features of the Rehm and Weller's correlation are (a) k_q is independent of ΔG^{0} when electron transfer reaction is diffusion controlled limited (b) k_q strongly depends on ΔG^{0} for the endergonic electron transfer reaction. The third feature that has been suggested by Schuster is that, there should be no correlation between ΔG^{0} and k_q when the electron transfer reaction is both endergonic and irreversible.[25]

2.2 Treatment of the Marcus Quadratic Equation

In many aspects electron transfer reactions are omnipresent in chemistry, biology and biochemistry.[26] The field of electron transfer processes has been extensively studied during last 60-70 years.[6] The main contribution in the electron transfer field came from Marcus.[4-6, 8] Early experiments in the field of electron transfer were on "self-exchange reactions" (isotopic) and, afterward, on "cross reactions".

Marcus proposed that the reaction rate of an electron transfer decreases when ΔG^{0} is too large. The theory was originally devised for outer-sphere electron transfer reactions, in which the two reactants are not directly bonded to each other, and later it was extended to inner-sphere electron transfer reactions, in which the two reactants are bonded or linked (via bridge) known as Marcus-Hush theory.[27-28] Alongside outer and inner sphere electron transfer reactions the theory has also been extended to deal with heterogeneous electron transfer reactions.

The theory based on the Classical Arrhenius Equation in two ways

- Afford expression for the pre-exponential factor in the Arrhenius equation
- Afford expression for the activation free energy in terms of reorganization energy and Gibbs free energy.

The driving force that is, ΔG^0, determines the extent to which the reaction proceeds. The more negative is ΔG^0, the rate of electron transfer will increase as the electron transfer reaction becomes more exergonic. This is true until a certain point called the "Normal region." However afterward, the electron transfer rate will decreases because the reaction turn into more exergonic, in the generally called "Marcus Inverted region."

The key features of the Marcus theory have shown in a schematic representation of the potential energy surfaces for the reactants and products (**Figure 2.2**). The nature of the chemical reactions is often established by examining the motion of the atoms of the reactants on a potential energy surface. In other words potential energy can be obtained by considering the translational, vibrational and rotational coordinates of the reacting species and of the surrounding molecules and the potential energy surface is merely a plot of the entire electronic energy of the system versus the positions of all the atoms.[6]

In the potential energy profile (**Figure 2.2**) the abscissa is showing the "reaction coordinates" whereas ordinate is representing the potential energy. The surface R denotes the nuclear motion of the reactants before the actual electron transfer, while surface P corresponds to the final stage when the electron has transferred. Together surface R and surface P, described an essential aspect of the electron transfer reactions that is the change in the equilibrium nuclear configuration of the reactant and the product results from either its gain or loss of an electron.[29] The process by which reactants converted into products depends on precisely how the barrier is passed over (classical theory), tunneled through (quantum theory) or otherwise avoided.[8, 26] There are two mechanisms for electron transfer, the electron transfers adiabatically if the distance between two surfaces or reactants is negligibly small and in the second case when the electronic interactions are very weak the process called non-adiabatic electron transfer process.[6, 28] The Marcus relationship of free energy of activation is the result of an adiabatic electron transfer reaction.

The potential energy surfaces more or less approximated a parabola.[26] Hook's gave the relationship between energy and the bond length. This relation gives a parabolic curve and set up the framework for the discussion of the energy on the vibrational state and on temperature. The energy just simply depends on the square of the distance when molecule swing along the parabola or from their equilibrium position. Both reactant and product have different equilibrium nuclear positions on the abscissa scale and after the

actual electron transfer their equilibrium nuclear position change from the earlier positions.

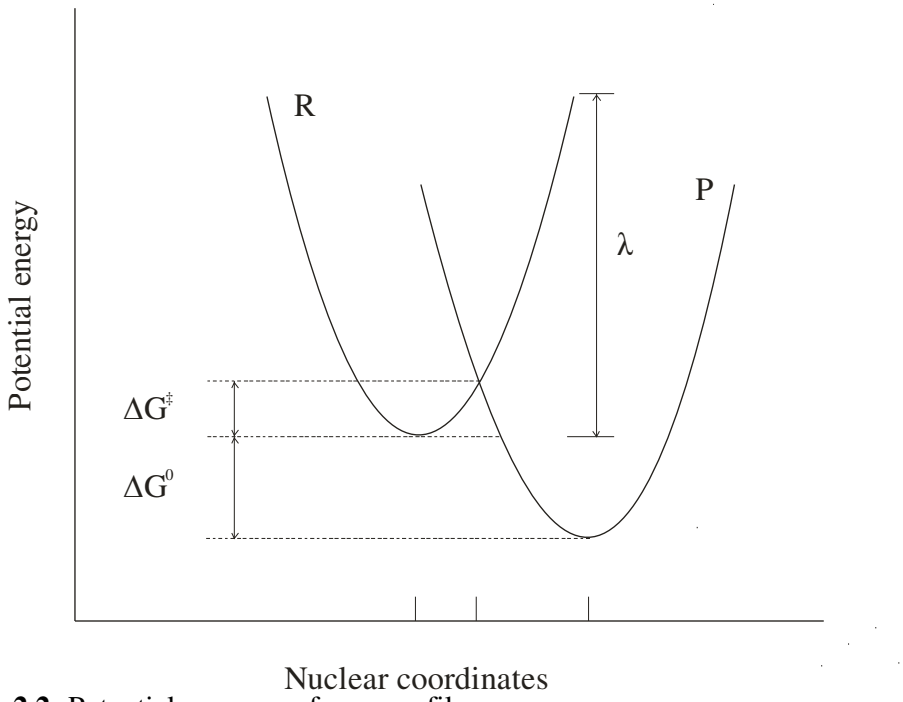

Figure 2.2: Potential energy surfaces, profile.

In this energy profile ΔG^0, is the free energy change between the minima of the reactant parabola and the minima of the product parabola and $\Delta G^{\ddagger}$ is the activation energy. The energy that actually force the reactants to have the same nuclear configuration as the products before or without an electron transfer is the reorganization energy and represented by λ.

The relationship[vi] for free energy of activation given by Marcus is as follows

$$\Delta G^{\ddagger} = \frac{(\Delta G^0 + \lambda)^2}{4\lambda} \tag{2.20}$$

where ΔG^0 is the standard free energy (Gibbs energy) of reaction which is zero for a self exchange reaction i.e., $\Delta G^{\ddagger} = \Delta G^{\ddagger}(0)$ at $\Delta G^0 = 0$ and equation (2.20) becomes

[vi] The derivation of the Marcus free energy relationship found elsewhere.

$$\Delta G^{\ddagger} = \Delta G^{\ddagger}(0)\left[1+\frac{\Delta G^{0}}{4\Delta G^{\ddagger}(0)}\right] \tag{2.21}$$

and λ is the reorganization energy composed of two terms such as salvation energy (λ_0) and vibrational energy (λ_i).

$$\lambda = \lambda_0 + \lambda_i \tag{2.22}$$

Therefore, the free energy of activation for the self exchange reaction is simply one-fourth of the reorganization energy. From the standard Arrhenius relationship the expression for the rate constant k of the reaction is given by

$$k = A\exp(\frac{-\Delta G^{\ddagger}}{k_b T}) \tag{2.23}$$

where A is a pre-exponential function which depends on the nature of the electron transfer reaction (e.g., intramolecular or biomolecular) and k_b is the Boltzmann constant.

2.3 Treatment of Marcus Levine Equation

Another free energy relationship that correlates the activation free energy to the free energy change in electron transfer reactions is Marcus-Levine-Agmon equation. The theory first derived by Marcus for atom and proton transfer reactions and later formulated by Agmon and Levine.[9, 21, 30-31] The theory developed for the concerted type of reactions on the basis of a thermodynamic like treatment.[31]

The Marcus-Levine hyperbolic equation of free energy is shown below

$$\Delta G^{\ddagger} = \Delta G^{0} + \frac{\Delta G^{\ddagger}(0)}{\ln 2}\ln\left[1+\exp\left(-\frac{\Delta G^{0}\ln 2}{\Delta G^{\ddagger}(0)}\right)\right] \tag{2.24}$$

It has been reported that the equation (2.24) share the general features of the Rehm and Weller free energy relationship[21, 30], equation (2.19), and it is preferable when applied over a range where $\Delta G^{0} >> \Delta G^{\ddagger}(0)$.

2.4 Totally Irreversible Oxidation / Reduction Wave

The most essential properties associated with electron transfer reactions are the redox potentials of the reactant molecules, donor and acceptor in this case.[1, 32] Because electrons are relocated in the way of the increasing redox potentials, therefore, it is crucial to know the redox potentials of reductants and oxidants for understanding the actual electron transfer processes from reductants to oxidants or either way. Despite its importance the thermodynamically meaningful oxidation potentials[33] for many quenchers are not available or have not been determined precisely by electrochemical methods because of the irreversible nature of this one-electron oxidation on the time scale of electrochemical measurements.[19] There is not any established methodology exist for the determination of redox potentials of these irreversible systems (quenchers).

Some attempts have been made for the determination of the redox potentials of these irreversible systems through electrochemical methods. Velasco from Spain,[34-35] he proposed a method for the determination of the redox potential of electrochemically totally irreversible processes. According to him the formal potential $E^{o`}$ can be obtained at $I = 0.82 I_p$. This methodology may be applicable for single system but could not be applied to cover the whole range of compounds. Another procedure was reported which offer the possibility that the half-wave potential can be estimated as 0.028 V before the anodic peak potential.[36]

We have given the free energy relationships between $\Delta G^{\ddagger}$ and ΔG^{0} in the forgoing sections from Rehm and Weller, Marcus and Marcus-Levine. We will utilize these free energy relationships for the irreversible electrochemical oxidations of quenchers to determine the thermodynamic oxidation potential $E_{1/2}^{ox}$ from the cyclic voltammetry measurements. The procedure first formulated by Fukuzumi[19] to be followed.[37-38] We have elaborated the method in more sophisticated way on the basis of the theory of the stationary electrode polarography.[39-41] The $E_{1/2}\,(E_{1/2}^{ox}, E_{1/2}^{red})$ values can be determined by analyzing the cyclic voltammogram at various sweep rates. This method provides an opportunity to find out the standard potential and it is somewhat surprising that only a limited number of systems have been examined with this method.

2.4.1 Application of Cyclic Voltammetry

Over the past couple of decades potential sweep techniques, such as cyclic voltammetry, have been applied to an ever increasing range of systems,[42] and at the same time the mathematical description[40-42] of these techniques has been developed sufficiently to enable kinetic parameters to be determined for a wide variety of mechanism. It is, however, in the area of preliminary mechanistic investigations that sweep techniques, in particular cyclic voltammetry, are probably most useful. An 'electrochemical' spectrum indicating the potential at which processes occur can be rapidly obtained, while from the sweep rate dependence the involvement of coupled homogeneous reactions is readily identified, and other complications such as adsorption can be recognized. In view of these capabilities, cyclic voltammetry is nearly always the technique of choice when studying a system for the first time, through better techniques probably exist for determining precise kinetic data. A full description about cyclic voltammetry and several reviews are available elsewhere.[42-49] This details are outside the scope of this work and we will only consider the application of cyclic voltammetry to totally irreversible systems.

2.4.2 Totally Irreversible Oxidation

The thermodynamic parameter $E_{1/2}$ ($E_{1/2}^{ox}, E_{1/2}^{red}$) can not be inferred from the analysis of the cyclic voltammogram obtained for the irreversible systems. There is no direct method available like for reversible systems.[46-47, 49] Though we can find $E_{1/2}$ through the dependence of the electron transfer coefficient β on E_p and here we will derive the relationship between β and E_p.

The irreversible one step oxidation of the species, in this case quencher, at a plane electrode can be described on the basis of the simple kinetic scheme shown below

$$Q \underset{k_{-et}}{\overset{k_{et}}{\rightleftharpoons}} Q^+ + e \qquad (2.25)$$

$$Q^+ \xrightarrow{k_d} \text{product} \qquad (2.26)$$

The follow up rate constant k_d is much faster than the reverse electron transfer rate constant and under this condition the rate of forward electron transfer becomes rate limiting step. In the CV experiment, total irreversibility can be explained in terms of the (i) chemical reactivity of the intermediate generated by one electron transfer and / or (ii)

increasing the rate of mass transport of species from the electrode surface by variation of the sweep rate.[50] The electrochemical oxidation is designated as totally irreversible process that means no cathodic wave in the reverse direction.[50] For this case we will derive the expression for the rate constant for the heterogeneous electron transfer at the CV peak potential.

The general expression for the rate constant for heterogeneous electron transfer adopted from Nicholson and Shane[40, 51] paper is given below

$$k(E) = k_s \exp\left[\frac{\beta nF}{RT}\left(E - E_{1/2}^{ox}\right)\right] \tag{2.27}$$

where E is the electrode potential, n is the number of electrons transferred from the electroactive species Q in the rate-limiting step, β is the transfer coefficient for the electrode process, and $E_{1/2}^{ox}$ is the standard oxidation potential, which fixes the value of k_s (i.e., $k_s = k_{et}$ at $E = E_{1/2}^{ox}$), the standard rate constant. F is the Faraday constant, and R and T have their usual implication. The expression for the rate constant derived from the Fick's laws of diffusion further leads us to established quantitative tests for total irreversibility based on (i) the dependence of E_p^{ox} and $E_{p/2}^{ox}$ on the CV sweep rate, (ii) the consistency of the transfer coefficient estimated from various properties of CV wave, and (iii) the shape of the anodic / cathodic wave. The heterogeneous rate constant in equation (2.27) depends on the applied electrode potential E and varies with it.

Nicholson and Shane also predicted a peak current at the applied voltage such as

$$E_p^{ox} = E_{1/2}^{ox} + \left[\frac{RT}{\beta nF}\right]\left[0.780 + \ln\left(\frac{D\beta nFv}{RT}\right) - \ln k_s\right] \tag{2.28}$$

where[vii]

$$0.780 = \ln\left(\sqrt{\pi}\,\frac{\chi(bt)}{(j-1)}\right) \tag{2.29}$$

For a totally irreversible wave, E_p^{ox} is a function of scan rate, shifting (for a oxidation) in a positive direction with increase in v. Also E_p^{ox} occurs beyond $E_{1/2}^{ox}$.[42] Rearrangement of equation (2.28) accomplished following expression

[vii] See following references (a) Nicholson et al., 1964 (b) A. Bard et al., 2001.

$$k_s \exp\left[\frac{\beta nF}{RT}\left(E_p^{ox} - E_{1/2}^{ox}\right)\right] = 2.18\left[\frac{D\beta nFv}{RT}\right]^{1/2} \tag{2.30}$$

which on comparison with equation (2.30) and equation (2.27) finally results the heterogeneous rate constant at the CV peak potential

$$k\left(E_p^{ox}\right) = 2.18\left[\frac{D\beta nFv}{RT}\right]^{1/2} \tag{2.31}$$

where

$$2.18 = \left(\frac{F}{RT}\right)^{1/2} \sqrt{\pi} \exp\left(1.875\frac{RT}{F}\right)^{1/2} \tag{2.32}$$

Conclusion is, for a totally irreversible process, the electron transfer rate constant at the CV peak potential $k(E_p^{ox})$ is directly related to the sweep rate and the diffusion coefficient D. It is worth mentioning that equation (2.31) is independent of the system related parameters $E_{1/2}^{ox}$ and k_s which is difficult to get for totally irreversible systems. Thus, by changing the sweep rate (and therefore the rate of diffusion of species Q), it is possible to measure the potential dependence of the rate of electron transfer at the CV peak potential.

Combining equation (2.31) and the general expression in equation (2.27) yield equation (2.33) in which the potential dependence of the rate constant $k(E)$ for electron transfer is expressed in terms of the CV parameters E_p^{ox} and β.

$$k(E) = 2.18\left[\frac{D\beta nFv}{RT}\right]^{1/2} \exp\left[\frac{\beta nF}{RT}\left(E - E_p^{ox}\right)\right] \tag{2.33}$$

The electron transfer coefficient, β (tangent of the free energy relationship $\frac{\partial \Delta G^{\ddagger}}{\partial \Delta G}$), can be determined independently from the width of the CV wave for the anodic wave, as described by Nicholson and Shain,[40] i.e.,

$$\beta = \frac{1.857\ \mathrm{RT}}{\mathrm{nF}}\left[E_p^{ox} - E_{p/2}^{ox}\right]^{-1} \tag{2.34}$$

where $E_{p/2}^{ox}$ is the potential where the current is at half peak value. The β value can be determined also from the dependence of the oxidation peak potential E_p^{ox} on the sweep rate v according to the following equation

$$E_p^{ox} = \frac{2.3RT}{2\beta nF}\log v + \text{constant} \tag{2.35}$$

The value of electron transfer coefficient can be obtained from the slope of the linear plot between E_p^{ox} and $\log v$. The constant term in Eq.(2.35) is equal to:

$$\text{Const} = E_p^{ox} + \frac{2.3RT}{\beta nF}\log\frac{2.18D\beta nF}{k\left(E_{1/2}^{ox}\right)RT} \tag{2.36}$$

Where $k\left(E_{1/2}^{ox}\right)$ is the electron transfer rate constant at the oxidation potential $E_{1/2}^{ox}$.

Similar expression found for the dependence of the half peak potential $E_{p/2}^{ox}$ on the sweep rate as given below

$$E_{p/2}^{ox} = \frac{2.3RT}{2\beta nF}\log v + \text{constant} \tag{2.37}$$

Another reversibility criteria is the expression between E_p^{ox} and the peak current i_p which also furnish the β value from the slope value as shown below

$$E_p^{ox} = \frac{2.3RT}{\beta nF}\log i_p + \text{constant} \tag{2.38}$$

Here the constant term almost the same as given above.

As we established before that the heterogeneous electron transfer rate constant $k(E_p^{ox})$ depends on two variables one is sweep rate and the other is diffusion coefficient. The diffusion coefficient can be determined from the expression for the peak current

$$i_p = (2.99x10^5)\beta^{1/2}AC_0^*D_0^{1/2}v^{1/2} \tag{2.39}$$

where

$$2.99x10^5 = F\left(\frac{F}{RT}\right)^{1/2}\sqrt{\pi}\chi(bt) \tag{2.40}$$

An alternative expression for i_p in terms of E_p^{ox} derived by Nicholson and Shane is

$$i_p = 0.227\, FAC_0^* k_s \exp\left[\frac{\beta nF}{RT}(E_p^{ox} - E_{1/2}^{ox})\right] \tag{2.41}$$

The description for the constant term is given in Nicholson and Shain's paper.[viii] Thus, a plot of $\ln(i_p)$ vs. $E_p^{ox} - E_{1/2}^{ox}$ for different scan rates would be a straight line with a slope proportional to β, and intercept proportional to k_s provided that $E_{1/2}^{ox}$ already be known from some other means. This approach is very convenient for determining the kinetic parameters, though scan rate would have to be varied over several orders of magnitude. One can also obtain kinetic information from stationary electrode voltammograms illustrated by Reinmuth[52] who showed that for an irreversible reaction, the current flowing at the foot of the wave is independent of the rate of voltage scan.

2.4.3 Use of Rehm-Weller Free Energy Relationship

We have already given Rehm and Weller free energy relationship in equation (2.19). Here we are going to derive the linear relationship between E_p^{ox} and β from the first derivative of Rehm-Weller equation with respect to ΔG^0 as shown below

$$\beta = \frac{\Delta G^0}{4}\left[\left(\frac{\Delta G^0}{2}\right) + \left(\Delta G^{\ddagger}(0)\right)^2\right]^{-1/2} + \frac{1}{2} \tag{2.42}$$

which on substituting the value of free energy change such as $\Delta G^0 = E_{1/2}^{ox} - E_p^{ox}$, the equation (2.42) becomes

$$E_p^{ox} = E_{1/2}^{ox} + \frac{(1-2\beta)}{\left[\beta(1-\beta)\right]^{1/2}}\Delta G^{\ddagger}(0) \tag{2.43}$$

At this instant the relationship between the standard oxidation potential and oxidation peak potential has been established. The oxidation potential $E_{1/2}^{ox}$ can be evaluated from the intercept of the linear plot between E_p^{ox} and $\frac{(1-2\beta)}{\left[\beta(1-\beta)\right]^{1/2}}$, and intrinsic barrier can be obtained from the slope $\Delta G^{\ddagger}(0)$.

[viii] $(j-1) = \left[\chi(bt)\right]\exp\frac{FE}{RT}$ (potential value in Nicholson and Shain's scale) $= \frac{C_0(O,t)}{C_0^*}$.

2.4.4 Use of Marcus Free Energy Relationship

Similar treatment of the Marcus free energy equation (2.21) relationship that is the first derivative with respect to the free energy change ΔG^0 give up the transfer coefficient as given below

$$\beta = \frac{1}{2} + \frac{\Delta G^0}{8\Delta G^{\ddagger}(0)} \tag{2.44}$$

The relationship between E_p^{ox} and β formulated by substituting the value of free energy $\Delta G^0 = E_{1/2}^{ox} - E_p^{ox}$.

$$E_p^{ox} = E_{1/2}^{ox} + 4(1-2\beta)\Delta G^{\ddagger}(0) \tag{2.45}$$

The intercept will furnish the value of the oxidation potential $E_{1/2}^{ox}$ from the linear plot between E_p^{ox} and $4(1-2\beta)$. The intrinsic barrier $\Delta G^{\ddagger}(0)$ can be evaluated from the slope.

2.4.5 Use of Marcus-Levine Free Energy Relationship

The Marcus-Levine free energy relationship is given in (2.24). We have done the same handling as we did with Rehm-Weller and Marcus equations. The final outcome which is the relationship between E_p^{ox} and β is given below

$$E_p^{ox} = E_{1/2}^{ox} + \frac{\Delta G^{\ddagger}(0)}{\ln 2}\ln\left(\beta^{-1} - 1\right) \tag{2.46}$$

The $E_{1/2}^{ox}$ value can be obtained from the intercept and the intrinsic barrier $\Delta G^{\ddagger}(0)$ is estimated from the slope.

2.4.6 Totally Irreversible Reduction

For the irreversible one electron reduction taking place at the planar electrode the simple kinetic scheme is given below

$$Q + e \underset{k_{-et}}{\overset{k_{et}}{\rightleftarrows}} Q^- \tag{2.47}$$

$$Q^- \xrightarrow{k_d} \text{product} \tag{2.48}$$

The relationships for the rate constant, peak current and the electron transfer coefficient are similar with those already given for the irreversible one electron oxidation case. The only difference is the sign of the direction of the electron transfer.

The general expression for the rate constant for heterogeneous electron transfer is;

$$k(E) = k_s \exp\left[\frac{-\beta nF}{RT}\left(E - E_{1/2}^{red}\right)\right] \tag{2.49}$$

and the expression for the peak current at the applied voltage is defined as,

$$E_p^{red} = E_{1/2}^{red} - \left[\frac{RT}{\beta nF}\right]\left[0.780 + \ln(\frac{D\beta nFv}{RT}) - \ln k_s\right] \tag{2.50}$$

The heterogeneous electron transfer rate constant at the CV peak potential for the irreversible reduction case is shown below,

$$k\ \left(E_p^{red}\right) = 2.18\left[\frac{D\beta nFv}{RT}\right]^{1/2} \tag{2.51}$$

The electron transfer coefficient is also evaluated from the width of the cathodic wave such as

$$\beta = \frac{\text{-1.857 RT}}{\text{nF}}\left[E_p^{red} - E_{p/2}^{red}\right]^{-1} \tag{2.52}$$

For estimating the reduction potential $E_{1/2}^{red}$ we have three similar relationships from the Rehm-Weller, Marcus and Marcus-Levine free energy relationships as in the case of the irreversible oxidation process. Here in this case the value of free energy change is $\Delta G^0 = E_p^{red} - E_{1/2}^{red}$. The equations are representing below

1) From Rehm-Weller relationship

$$E_p^{red} = E_{1/2}^{red} - \frac{(1-2\beta)}{\left[\beta(1-\beta)\right]^{1/2}}\Delta G^{\ddagger}(0) \tag{2.53}$$

2) From Marcus relationship

$$E_p^{red} = E_{1/2}^{red} - 4(1-2\beta)\Delta G^{\ddagger}(0) \tag{2.54}$$

3) From Marcus-Levine relationship

$$E_p^{red} = E_{1/2}^{red} - \frac{\Delta G^{\ddagger}(0)}{\ln 2} \ln\left(\beta^{-1} - 1\right) \tag{2.55}$$

From the linear plots of all three equations mentioned above one can obtain $E_{1/2}^{red}$ from the intercept and the intrinsic barrier $\Delta G^{\ddagger}(0)$ from the slope.

2.5 Simulation of Cyclic Voltammograms

Cyclic voltammetry is perhaps the most widely used electrochemical technique which readily provides information about the stability of the oxidation states and the electron transfer kinetics of a redox system. However, it is very difficult to obtain mechanistic information using cyclic voltammetry alone. Computer simulation[ix] is usually done for mechanistic investigation and also for confirming the electron transfer kinetics[53] and for this commercially available program DigiElch 4.F (from Elcsoft, Germany) was used in the present case.

Quantitative measurements can be made using digital simulation programs. A mechanism and the appropriate parameters are entered into the program, and the software calculates the cyclic voltammogram for the entered data. However, there are some typical problems of using this software such as:

- limited to specific mechanisms
- only usable over a limited range of kinetics parameter values
- required a high level of mathematical sophistication

Digital simulation, a cyclic voltammetry simulation program is truly general, and can accept any mechanism that can be entered in terms of single- or multiple-electron transfer reactions and first- or second-order chemical reactions. It is also efficient, and can rapidly calculate the simulated voltammograms for a wide range of kinetic parameter values.

DigiSim can be used not only for investigating the electrochemical mechanisms of real redox systems, but it can also be used for understanding the basic concepts and behavior of cyclic voltammetry. It is therefore a highly effective tool for teaching cyclic voltammetry.

The DigiElch 4.F program simulates the electron transfer reactions and chemically coupled reactions using the theory of stationary electrode polarography.[40] The theory of stationary electrode polarography is based on the Butler – Volmer equation:

[ix] Commercially two simulation software's are available (a) DigiSim from Bioanalytical Systems (b) DigiElch from Elcsoft Germany.

$$i = i_0 \left\{ \exp\left[(1-\alpha) nF / RT \right] - \exp\left[-\alpha nF / RT \right] \right\} \tag{2.56}$$

where i_o is the exchange current density, n is number of electrons and α is electron transfer coefficient.[x] It provides a general simulator that can be used for almost any solution based redox mechanism over the full range of appropriate thermodynamic and kinetic parameter values.

We have used the simulation program for confirming our findings such as diffusion coefficient, heterogeneous electron transfer and the oxidation / reduction potential. In order to simulate our experimental findings, the program required proposal of an electrochemical mechanism and its parameters.[53] We began our simulations by looking at the experimental cyclic voltammograms, specifically the oxidation / reduction potentials and whether or not the peaks were reversible. We would propose a mechanism, insert the oxidation / reduction potentials and would estimate other required parameters based on the reversibility irreversibility of the system. Thus, if we observed a reversible cyclic voltammogram, the parameters defining reversibility such as the transfer coefficient α and the heterogeneous rate constant k_s should be α = 0.5 and k_s greater then 10^{-3}. For the case of irreversible cyclic voltammogram, the parameters defining irreversibility i.e., β and the heterogeneous rate constant at the CV peak potential $k\left(E_p\right)$ obtained from the experiment should be used. For chemically coupled reactions the equilibrium constant, K_{eq} must also be entered. In order to obtain CV's fitting our experimental findings we had to enter numbers in the ranges states above in different permutations. Following parameters can be modified such as the k_s, α and K_{eq}. Those that can not be modified during the experiment, are the temperature (298K), the scan rate (V/s), the initial concentration of the species (varied but usually between 1-4 mM), the diffusion rate (semi-infinite) and the geometry of the electrode (planar).

[x] α is a transfer coefficient for reversible electron transfer processes.

Chapter 3. Voltammetric Studies on the Oxidation of DNA Bases, Nucleosides, Amino Acids, and Two Oxidative Quenchers

> Scientific knowledge is in perpetual evolution; it finds itself changed from one day to the next.
>
> (*Jean Piaget*)

Purine and Pyrimidine bases and their derivatives play an imperative role in many biological processes. It has been reported that the in vivo oxidation of DNA contributed to cell damage, ageing, and age-related diseases[54] and causes mutagenesis and carcinogenesis. Determining individual concentrations of purine and pyrimidine bases and their corresponding derivatives or their ratio in DNA has become increasing important in the field of biomedical and biological research.[54] The detection will be indicative of certain type of diseases related to enzymatic degradation of tissues, dietary habits and catabolism of nucleic acid.[55-56] Studies on the determination of concentrations of DNA components found elsewhere.

The most generally used methods for the detection and quantification of DNA components in nucleic acids are the spectroscopic methods coupled with chromatography or electrophoreses and electrophoresis with electrochemical detection.

Voltammetric methods are also being actively explored for the investigations of DNA and its components, because of, voltammetric techniques are particularly suitable for the analysis of a wide variety of organic compounds and provide valuable insights into biological redox behaviour of such compounds.[54, 57] Numerous studies for the determination of purine and pyrimidine bases and their corresponding derivatives upon electrochemical oxidation or reduction at various electrodes (e.g., glassy carbon, carbon paste, pyrolytic graphite electrode, and chemically modified electrodes) have been published.[55-56, 58-62]

A significant amount of research has also been done for the sensitive, selective and precise determination of amino acids. The significance of amino acids can be

understand on the basis of their role in nutritional, clinical, and biotechnological field and in many biochemical processes.[63]

Extensive studies have been carried out for the development of the methods for their detection and quantification. The methods include chemoluminescne, fluorescence, mass spectrometry, UV visible absorption, liquid chromatographic separation and electrochemical techniques.[64] Such methods can be used for the investigation of the amino acids. In general one of the major problems of all these methodologies is the need of derivitisation of the amino acids.

The electrochemical methods have significant benefits over other methods and offer direct measurements of amino acids at solid electrode without any derivative process. These methods are simple and cost effective. We have found several reports on the investigation of amino acids at solid electrode particularly using voltammetry.[65] For example, Reynaud et al. described electrochemical oxidation of all amino acids. They have found that, of amino acids, only 6 can be oxidized at solid electrodes (gold, platinum, vitreous carbon, carbon paste): cystine, cysteine, methionine, tryptophan, tyrosine, and histidine.[66-68]

It is well known that the purine and pyrimidine bases and their derivatives showed irreversible oxidation wave at positive potentials.[57, 69-70] This behavior is indicating the formation of reaction products upon oxidation which further undergo chemical reaction. It is also well established that amino acids can also be irreversibly oxidized at solid electrodes (gold, platinum, graphite electrode, modified carbon electrode, carbon paste, and silver). Because of irreversible oxidation of DNA bases and its components and amino acids, these compounds can be used as effective quenchers (donors, reductive) in the quenching reactions and therefore it is important to know the half-wave oxidation potential for the one step irreversible oxidation of these compounds.

Our interest has been developed due to the following reason: in our group we are studying photoinduced electron transfer reaction between donor and acceptor molecules. For this purpose we are using following as donors molecules;[xi] DNA bases and its components e.g., thymine, thymidine, adenine, adenosine, and amino acids e.g.,

[xi] Donor molecules behave as reductive quenchers whereas acceptor molecules behave as oxidative quenchers.

methionine, histidine, alanine, and acceptor molecules are; 2,2´-bipyridine, 3,3´,4,4´-benzophenone tetracarboxylic acid.

Voltammetric investigations on the irreversible oxidation of the following reductive quenchers e.g., adenine, adenosine, thymine, thymidine, alanine, histidine, methionine and two oxidative quenchers 2,2´-bipyridine, 3,3´,4,4´-benzophenone tetracarboxylic acid are demonstrated here.[71-73] Glassy carbon electrode is used throughout the study for the examinations. Irreversible oxidation waves are observed for thymine, adenosine, methionine and histidine. No oxidation peak has observed for adenine, thymidine, and alanine. The irreversible reduction waves are also detected for the 2,2´-bipyridine, 3,3´,4,4´-benzophenone tetracarboxylic acid. The half-wave redox potentials of the following compounds will be used for establishing the relationship between pH and the potentials.[xii] From the dependence of the potentials on pH the nature of the photoinduced electron transfer can be deduced.[74-75]

[xii] Cyclic voltammetry has been applied to determine the apparent standard potential as a function of pH, see following papers from Cyrille et al., July 2009, and October 2009.

Chapter 4. Determination of Thermodynamic Reversible Potentials from Phase-Selective Second-Harmonic AC Voltammetry

Observations always involve theory.

(*Edwin Hubble*)

4.1 Introduction

The significance of half-wave potential is largely understood on the basis of its relationship with thermodynamic parameters. Reduction and oxidation half-wave potentials of carbon centered radicals are key quantities and if known, render the calculation of equilibrium constant, kinetic parameters, and other physical parameters that will give insights into molecular or ionic properties.[76-80] Such potentials also provide basis for establishing the mechanism of organic electrode reactions.

There are different approaches to have these quantities e.g., (a) radicals may be generated as transient species and investigated by photomodulated voltammetry for their half-wave potentials, the method is described in next chapter (b) instead of generating radicals start with cation, or anion of corresponding radical and use electrochemical techniques such as cyclic voltammetry to measure a half-wave oxidation, or reduction potential (c) and when the electrode reaction products are unstable and undergo further chemical reaction the phase-selective second-harmonic alternating current voltammetry can be a method of choice.[11]

Phase-selective second-harmonic ac voltammetry has excellent potential for the direct and precise determination of thermodynamically important half-wave potential for irreversible electrode reactions.[81-84] Conventional dc voltammetry though it's a very simple technique suffered from some limitations such as contribution from the double layer charging current, sometimes difficult to measure the accurate wave heights due to non-ideal exponential shape current-potential curves, and required a long time to record a voltammogram.[85] These limitations are overcome by second harmonic ac

voltammetry which practically afford zero double layers charging current and relatively shorter analysis time.[86] Surprisingly, phase-selective second-harmonic ac voltammetry has not found many applications in organic electrochemical studies because of the complexity of data collection and data analysis.

Predominantly the phase-selective second-harmonic ac voltammetric method is useful to measure the redox potentials of species that react rapidly when electrolyzed or to study the electrochemical processes that generate very reactive intermediates. McCord and Smith have established that with the method the reversible half-wave potentials of the reactive intermediates having half-life in the order of 10^{-4}s can easily be determined.[12-13] In other words the phase-selective second-harmonic ac voltammetry is less perturbed by the follow-up chemical reaction than the normal dc voltammetry and ac voltammetry.

4.2 Application of Second-Harmonic AC Voltammetry

The electrochemical objects such as electrodes have non-linear relation with potential, usually an exponential dependence. It is well known that an ac current response to the ac potential is always not linear and when ac voltage applied, produces an ac current with appreciable amount of higher harmonics.

Upon application of small amplitude sinusoidal potential that is superimposed on to the dc potential applied to the working electrode, the capacitative impedance of the electrical double layer behaves as an almost perfectly linear electrical element and does not produce an ac current at harmonics of the applied frequency whereas on the other hand faradaic process generates an ac current at harmonics of applied frequency and behave non-linearly. It follows that measurement of higher harmonics, rather than of the fundamental frequency, can yield information about redox processes without interference from the double layer.

The interfacial region shows pseudo capacitive behavior and creates a phase difference between applied ac potential and ac current response. With the phase-selective techniques the ac current at different phase angles (second or higher harmonics) can be measured. This selective detection of the ac current using lock-in-amplifier only afford the information about the faradaic process and largely eliminates the double-layer

charging current contribution to the measured ac current. The instrumental setup of phase-selective second-harmonic ac voltammetry is shown in **Figure 4.1**.

The most important time scale of the second-harmonic ac voltammetric experiment is the period of the ac signal employed. Finally the amplitude and phase of second-harmonic current response is detected. The result of the detection is usually displayed as the variation of the second-harmonic current amplitude with the dc potential in phase and out of phase with the input sinusoidal potential, respectively. This is the basis of the analytical method proposed in this note.

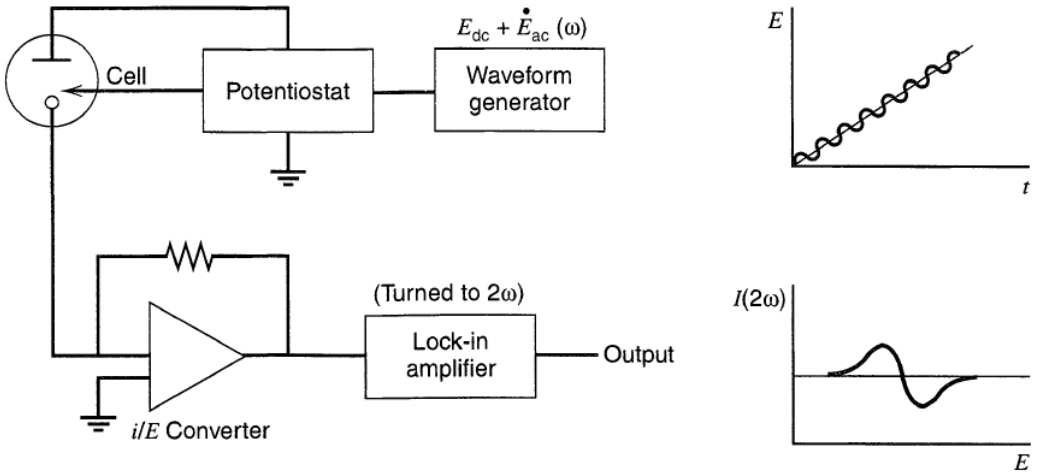

Figure 4.1: Block diagram for phase-selective second-harmonic ac voltammetry.[xiii]

Figure 4.2 represents the significant aspects of the phase-selective second-harmonic ac voltammogram of ac signal and display both positive and negative lobes. Actually the voltammogram is merely the second derivative of normal dc voltammogram. It is reported that for the rapid charge transfer and slow follow-up chemical reaction i.e., reversible system the difference between two peaks or between negative and positive lobes should be 68 mV/*n*, where *n* is the number of electron transfer.[12] Both positive and negative lobes are equal in current magnitudes, sharp, and symmetrical around the point of intersection with the dc potential axis and that this intersection point is located at the standard potential whatever the phase angle was applied.

[xiii] Figure 4.1 is taken from Bard & Faulkner 2001.

Simply, if this is the case the potential at which second-harmonic current is nulled is the thermodynamic half-wave potential. For the case when the product of the electrode reaction is very reactive, the second harmonic peak can lose intensity and symmetry, but the difference between the two peaks is still the same. More importantly, the null potential is still the thermodynamic half-wave potential.[12]

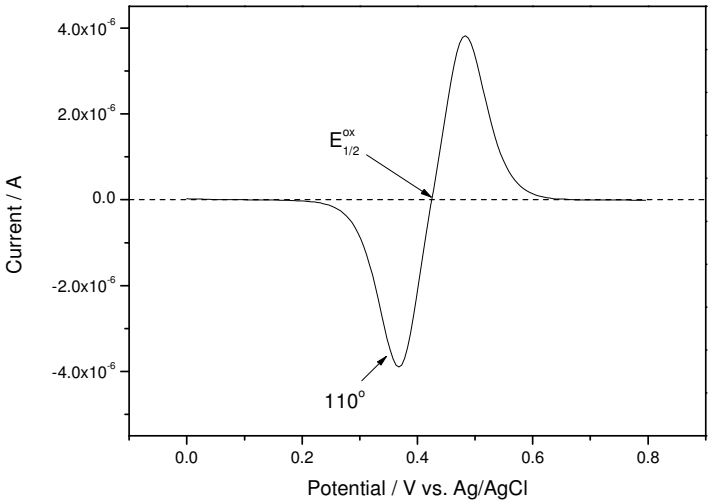

Figure 4.2: SHACV signals obtained for the oxidation of 3 mM ferrocene in acetonitrile containing 0.1 M TBAP as supporting electrolyte at a platinum electrode: frequency, 100 Hz, amplitude of the sinusoidal potential, 25 mV: temperature, 298 K.

Generally a recommended procedure for determining a half-wave potential for an electrode process is to record both I (in phase) and Q (quadrature) components[xiv] voltammograms.[10] So if the oxidized and reduced forms of the redox couple are stable in solution, both components will be symmetrical and appear as mirror images about the zero current point. The intersection point of I and Q components at the nulled current defines the half-wave reversible potential. This is one of the interesting and most important features of phase-selective second-harmonic ac voltammetric current amplitude voltammogram as shown in **Figure 4.3**.

[xiv] The phase shift between I and Q components is instrument dependent.

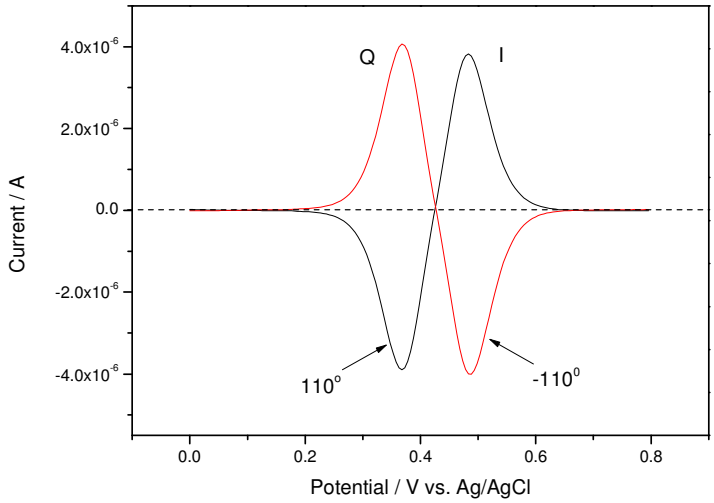

Figure 4.3: SHACV signals obtained for the oxidation of 3 mM ferrocene in acetonitrile containing 0.1 M TBAP as supporting electrolyte at a platinum electrode: frequency, 100 Hz, amplitude of the sinusoidal potential, 25 mV: temperature, 298 K.

On the other hand, if the product of the electrode reaction is not stable and undergoes a fast follow-up chemical reaction, then I and Q components loose their symmetry. The use of higher angular frequency relative to the rate constant for the fast follow-up chemical reaction ensure that the mirror image relationship still holds and also the I and Q components intersect at nulled current and provide the opportunity to have half-wave potentials. In the case when the follow-up chemical reaction is fast relative to the applied angular frequency, the mirror image relationship no longer is observed and the intersection of I and Q components does not occur at zero current and it is not possible to deduce half-wave potentials from the experiment.

Phase-selective second-harmonic ac voltammetry brings us two new dimensions, the frequency and the phase of the current relative to the applied ac potential, as compared to the conventional dc voltammetry. These two properties e.g., frequency and the phase can be used in the determination of the half-wave reversible potentials in cases where direct measurements are not possible from conventional dc techniques. The phase-selective second-harmonic ac voltammetry provides us following advantages such as:

- Low background current
- Zero double layer charging current

- High sensitivity to kinetic influences
- Quick and precise measurements of half-wave reversible potentials from the zero current crossing point of I and Q components even in the presence of rapid, irreversible follow-up chemical reactions.
- Also noteworthy is the independence of redox potential on electrode material

Chapter 5. Photomodulated Voltammetry

> It is a scientific fact that your body will not absorb cholesterol if you take it from another person's plate.
>
> (*Dave Barry*)

The half-wave oxidation and reduction potential of carbon center free radicals are significant quantities and can be combined with other thermodynamic data for the calculation of the hydrocarbon acidities, which from other ways are difficult to obtain.[16-17, 87-88] Free radicals are generally formed as intermediates during the reactions and knowledge of their oxidation and reduction potentials offer adequate understanding of the reaction mechanism.[89]

These transient species have short life times usually in milli-second range (i.e., chemically irreversible reaction) and cannot sustain for long period of time. Therefore, free radicals are not suitable as starting materials for standard electrochemical methods.[89]

In 1985 Wayner and Griller made an important advancement by employing modulated photochemical generation of free radicals with phase-sensitive detection of the electrochemical current resulting from oxidation or reduction of the radicals.[15-17, 89] The utilization of modulation principle in the determination increases the sensitivity by many orders of magnitude and permits the detection of radicals in non-aqueous solvents.[90]

Earlier studies showed the use of pulse radiolysis with voltammetric detection or with rotating photoelectrode but encountered many difficulties i.e., methods have been restricted to water as solvent which reacts rapidly with most ions, formed on reduction or oxidation of free radicals.[91]

The principle of photomodulated voltammetric operation is simple.[91] The acetonitrile solutions containing appropriate precursors (e.g., a ketone) and tetrabutylammonium tetraflouroborate (0.1 M) as the supporting electrolyte are exposed to the lamp. The light source is an Osram Hg lamp (500 W) which is capable of producing sufficient

amount of radicals in the range of 10^{-7}-10^{-8} M, i.e., well below the detection level of instrument. The instrumental block diagram is shown in **Figure 5.1**.[92] Samples are flowed through cell so as to avoid problems associated with sample depletion and/or product formation. The voltage at the working electrode was scanned between certain limits until the oxidation or reduction of the radicals may occur producing a small alternating current (ac). The phase-sensitive detector lock-in-amplifier is used for detecting the amplitude of the oscillating signals. As the potential is scanned a voltammogram of potentials vs. the alternating current can be constructed. The shape of the PMV voltammograms has a typically sigmoid shape as shown in **Figure 5.2**.

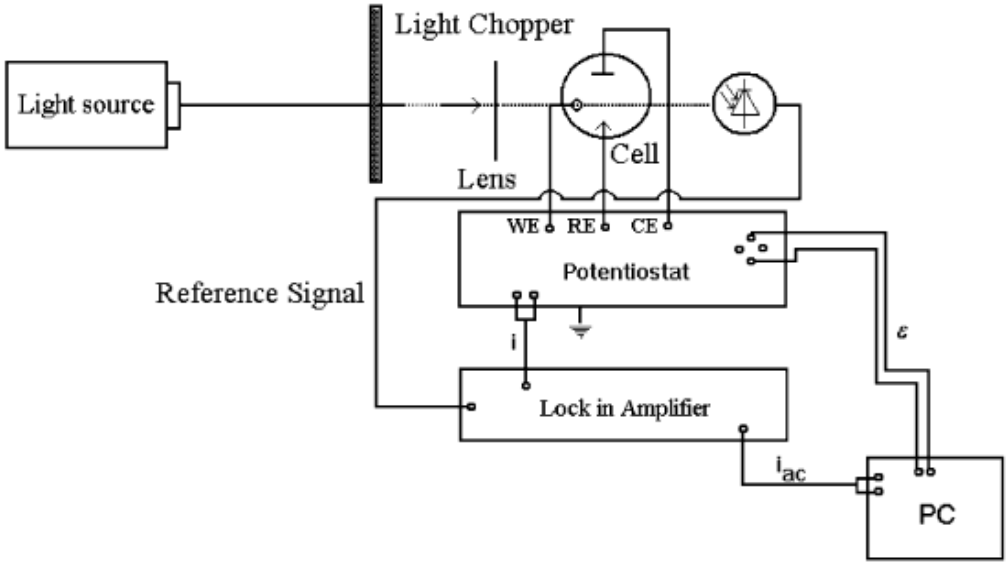

Figure 5.1: The apparatus for photomodulated voltammetry with appropriate setup.[xv]

From two different approaches radicals can be generated.[92] One is the direct method and utilizes the direct photolysis of i.e., diphenylacetone to generate the benzyl radical in MeCN solution

$$C_6H_5CH_2COCH_2C_6H_5 \xrightarrow{hv} 2C_6H_5{}^{\cdot}CH_2 + CO \qquad (5.1)$$

Second is an indirect method such as by photolyzing di-t-butylperoxide to tert-butoxyl radicals, which subsequently abstract a proton from diphenylacetone to generate benzyl radical

[xv] Figure 5.1 is taken from Grampp et al., 2008.

$$\text{t-BuOOBu-t} \xrightarrow{hv} 2\text{t-BuO}^{\cdot} \qquad (5.2)$$
$$\text{t-BuO}^{\cdot} + C_6H_5CH_3 \longrightarrow \text{t-BuOH} + C_6H_5{}^{\cdot}CH_2$$

Both ways lead to the same oxidation and reduction potentials.

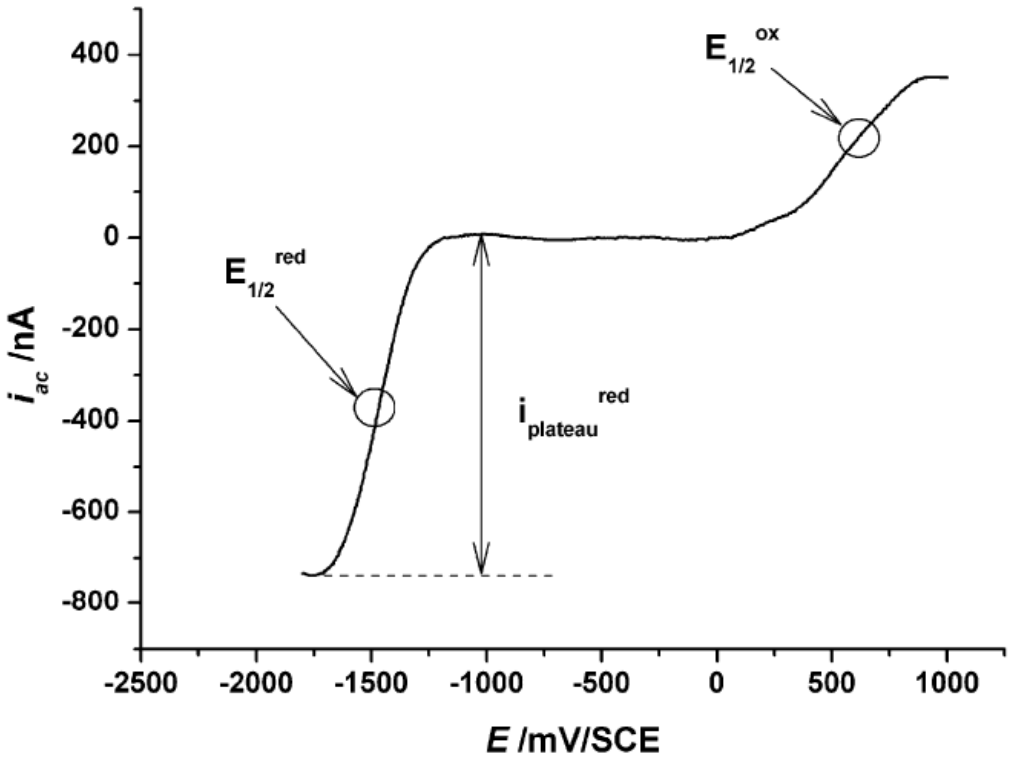

Figure 5.2: Photomodulated voltammogram of the benzyl radical; 9 mM diphenylacetone in acetonitrile with 0.08 M TBATFB, chopper frequency, 75 Hz; phase setting, 180°; v = 15 mVs^{-1}.[xvi]

The technique is employed to find the half-wave oxidation/reduction potentials of 1,3-diphenylacetone, 1,1,3,3-tetraphenylacetone, diphenyl disulfide, mixture of 0.5 M acetone and 1.0 M 2-propanol, glycine anhydride and alanine anhydride.[93-94] As discussed before the actual application of the technique demands sophistication and expertise in instrumental setup. These requirements lead us to encounter many problems during the measurements that will be described in results and discussions chapter.

[xvi] Figure 5.2 is taken from Grampp et al., 2008.

Chapter 6. General Experimental Procedure

> Every experiment proves something. If it doesn't prove what you wanted it to prove, it proves something else.
>
> (*Anonymous*)

6.1 Chemicals

1,3-Diphenylacetone purchased from Aldrich was recrystallized from hexane. Diphenyl disulfide obtained from Aldrich (HPLC grade, ≥97%). Some amount of purified 1,1,3,3-Tetraphenylacetone obtained from senior colleague. Other compounds are Glycine anhydride (Sigma, 99%), and Alanine anhydride (Aldrich, 99%). Acetonitrile (MeCN, Fluka) was dried over molecular sieve (3 A^o) and distilled under argon atmosphere. Dimethylsulfoxide (DMSO, Fluka) was recrystallized by freezing cycles. Aceton (Aldrich) and 2-Propanol (Aldrich) were purified according to standards methods. The supporting electrolyte, tetrabuylammonium tetrafluoroborate (Bu4NBF4, Fluka), and tetrabutylammonium perchlorate (TBAP, Fluka) salts were vacuum-dried at 80^o for 24 h before use. Ferrocene used as an internal standard in acetonitrile was purified by sublimation procedure. Potassium ferricyanide used as an internal standard in aqueous solution was purified by recrystalization method and dried under vacuum in desiccators. HCl and NaOH were purchased from Carl Roth Gmbh. Potassium nitrate (KNO_3, Aldrich, ≥99%) was used as supporting electrolyte in aqueous solutions. The details of all quencher compounds used in this work are given in **Table 6.1**.

Table 6.1: Used substances, their supplier, and purification method.

Substance	Supplier	Purification
Methoxybenzene (Anisole)	Fluka (≥ 99%)	as received
2-Methyanisole	Alfa Aesar (99%)	as received
3-Methylanisole	Alfa Aesar (99%)	as received
4-Methylanisole	Fluka (≥98%)	as received
2-Bromoanisole	Aldrich (≥97%)	as received
1,3-Dimethoxybenzene	Aldrich (≥98%)	as received
1,4-Dimethoxybenzene	Aldrich (≥99%)	as received
1,2,4-Trimethoxybenzene	Aldrich (≥97%)	recrystallization
N,N´-Dimethylaniline	Merck (≥99%)	fresh vacuum distillation
N,N´-Diethylaniline	Fluka (≥99.5%)	fresh vacuum distillation
Triphenylamine	Fluka (≥98%)	recrystallization
4,4´-bis-(dimethylamino) diphenylmethane (DMPM)	Aldrich (≥98%)	recrystallization
1,4-Diazabicyclo[2.2.2]octane (DABCO)	Aldrich (≥98%)	recrystallization
N-Methylpyrrole	Aldrich (≥99%)	as received
1,2,5-Trimethylpyrrole	Aldrich (≥99%)	as received
N-phenyl-tetrachloro-phthalimide (PTPA)	synthesized	synthesized
Adenine	Alfa Aesar (99%)	as received
Adenosine	Alfa Aesar (99%)	as received
Thymine	Alfa Aesar (99%)	as received
Thymidine	Alfa Aesar (99%)	as received
Alanine	Alfa Aesar (99%)	as received
Histidine	Fluka (≥ 99%)	as received
Methionine	Fluka (≥ 99%)	as received
2,2´-Bipyridine	Aldrich (≥99%)	as received
3,3´,4,4´-Benzophenone tetracarboxylic acid	Gift from Dr. Y. Lin, Chinese academy of science chemistry department, Beijing	as received

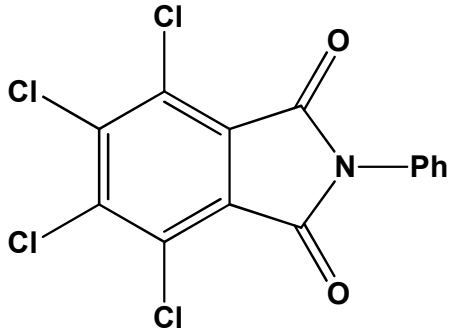

N-phenyl-tetrachloro-phthalimide

6.2 Instrumentations and Procedures

6.2.1 Cyclic Voltammetry

All cyclic voltammetric measurements were carried out using an Autolab/EAs 2 computer-controlled electrochemical system equipped with a potentiostat (model PGSTAT 302N). The software GPES (version 4.9.007) was used for the electrochemical measurements. Conventional three electrode assembly was used containing working electrodes platinum (2 mm) and glassy carbon (2 mm) imbedded in Teflon, a platinum wire counter electrode, a tungsten wire reference electrode, and Ag/AgCl wire reference electrode. The distance between the reference electrode and the working electrode was kept at a bare minimum which reduces the cell resistance. The three electrode assembly employed provides iR compensation.

Working electrodes were manually cleaned, before each scan, by mechanical polishing using diamond paste. The electrodes were then rinsed with deionized water, immersed in concentrated nitric acid for 5 second, rinsed second time and then dried in an air. The custom made electrochemical cell allows measurements with 20-25 mL of solutions. Ferrocenium/ferrocene couple was used as an internal standard. The concentration of 1-3 mM of ferrocenium/ferrocene was used.

Measurements were done in both aqueous and non-aqueous solvents. In non-aqueous solvents e.g., MeCN and DMSO, tetra-butylammonium perchlorate (TBAP, 0.1 M) was used as supporting electrolyte, respectively. The sweep rate varied from 10 to 1000 mVs^{-1}. A tungsten wire was always used as a reference electrode in non-aqueous systems. For each measurement, a small amount of ferrocene was added as an internal standard. All potentials are in volts and will be referred to the ferrocenium/ferrocene couple. The redox potentials recorded are sensitive to the presence of water in acetonitrile. For this reason dry acetonitrile was used. During the experiments the sample is kept under argon to ensure that the acetonitrile stays dry and exclude oxygen which might otherwise interfere with your analyte. The background recorded in acetonitrile solution is shown in **Figure 6.1**. The concentrations of compounds were kept between 1-5 mM when performing experiments in non-aqueous solvents.

All compounds listed above showed distinctive current maxima of the anodic wave but no cathodic wave on the reverse scan at various sweep rate used in the range of 10-1000 mVs^{-1}. The values of the peak potentials for these compounds were reproducible to

within ± 20 mV for different run, when the standard cleaning procedure of the working electrode mentioned above was applied. Our measured half-wave potentials are in good agreement with the literature values but some are not and the external factors responsible for the variations are not clear. No deterioration of the working electrode was observed.

Whereas in aqueous solutions, potassium nitrate (KNO_3, 0.1M) was used as supporting electrolyte along with buffers. Double distilled water was used for making all solutions. All experiments were performed at 298 K temperature.

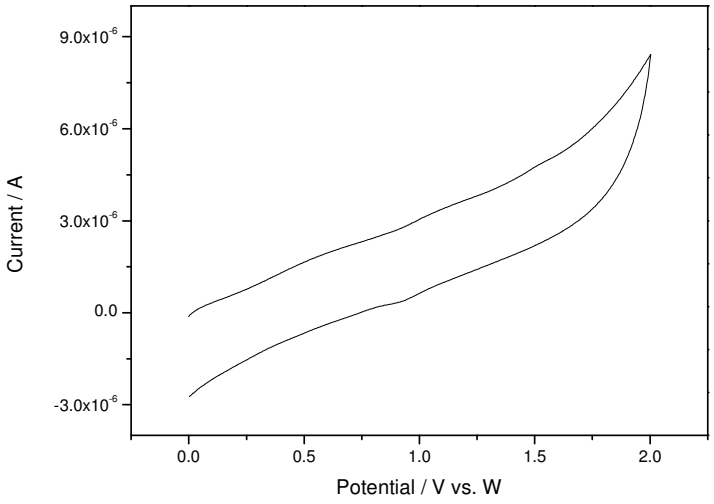

Figure 6.1: Cyclic voltammogram of acetonitrile solution containing 0.1 M TBAP obtained at 298 K and 100 mVs^{-1}.

The sweep rate varied from 10 to 500 mVs^{-1}. All buffer solutions were prepared as stock of concentration 6 M. The buffers solutions were used for maintaining the pH of the solutions and the details are given in **Table 6.2**. The typical concentrations of the compounds used were in the range of 1-5 mM. Ag/AgCl (0.1 M KNO_3; water) wire was used as a reference electrode. The reference electrode was made by inserting a silver wire into 0.1 M solution of potassium nitrate and separated from the electrolyte solution by a frit. A small amount of potassium ferricyanide was added to check the potential of Ag/AgCl reference electrode. All potentials are in volts and will be referred to the Ag/AgCl reference electrode. All compounds measured in aqueous solution showed

distinctive current maxima of the anodic wave but no cathodic wave on the reverse scan at various sweep rate used in the range of 10-500 mVs^{-1}. The values of the peak potentials for these compounds were reproducible to within ± 50 mV for different run, when the standard cleaning procedure of the working electrode mentioned above was applied. Our measured half-wave potentials are in good agreement with the literature values but some are not and the external factors responsible for the variations are not clear. No deterioration of the working electrode was observed. The backgrounds recorded in aqueous solutions for different pH values are given from **Figure 6.2** to **Figure 6.11**.

Table 6.2: Inorganic aqueous phosphate buffer solution for different pH[a]

Components	pH
HCl	2
HCl + KH_2PO_4	2.9
HCl + KH_2PO_4	4
KH_2PO_4 + Na_2HPO_4	5.2
KH_2PO_4 + Na_2HPO_4	6.1
KH_2PO_4 + Na_2HPO_4	7
KH_2PO_4 + Na_2HPO_4	7.9
Na_2HPO_4 + NaOH	10
Na_2HPO_4 + NaOH	11
NaOH	11.8

[a] Phosphate buffers of different composition were prepared in lab.

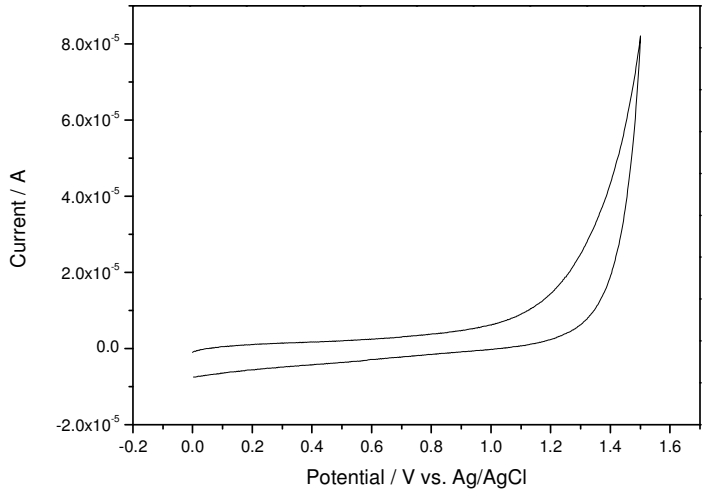

Figure 6.2: Cyclic voltammogram of aqueous solution containing 0.1 M KNO_3 and 0.01 M HCl buffer (pH 2) obtained at 298 K.

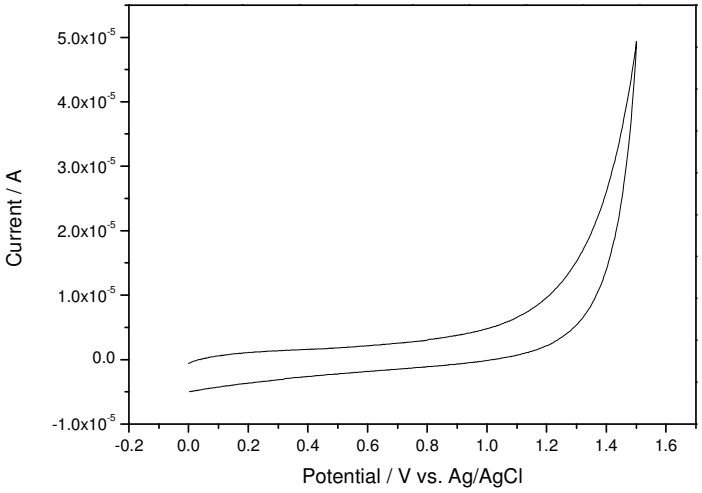

Figure 6.3: Cyclic voltammogram of aqueous solution containing 0.1 M KNO_3 and 0.01 M phosphate buffer (pH 2.9) obtained at 298 K.

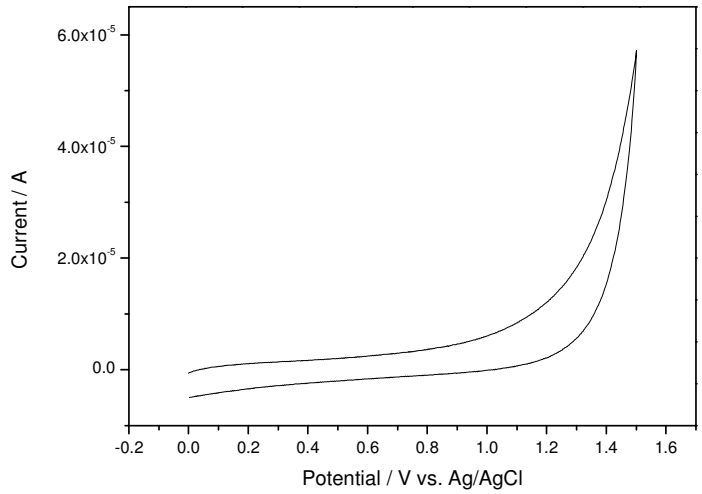

Figure 6.4: Cyclic voltammogram of aqueous solution containing 0.1 M KNO_3 and 0.01 M phosphate buffer (pH 4) obtained at 298 K.

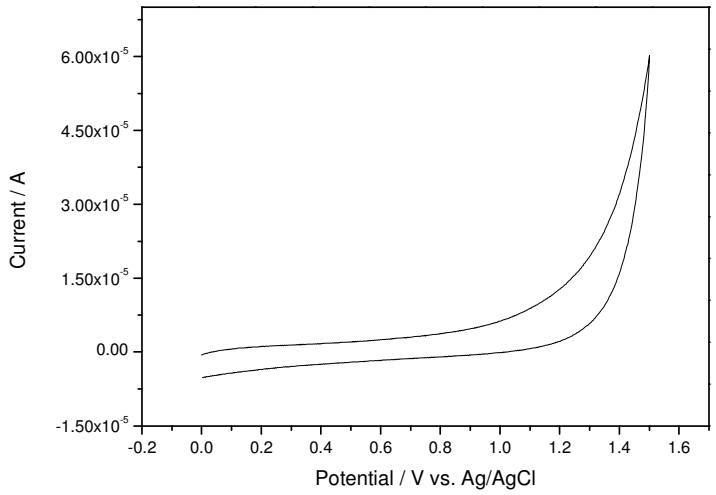

Figure 6.5: Cyclic voltammogram of aqueous solution containing 0.1 M KNO_3 and 0.01 M phosphate buffer (pH 5.2) obtained at 298 K.

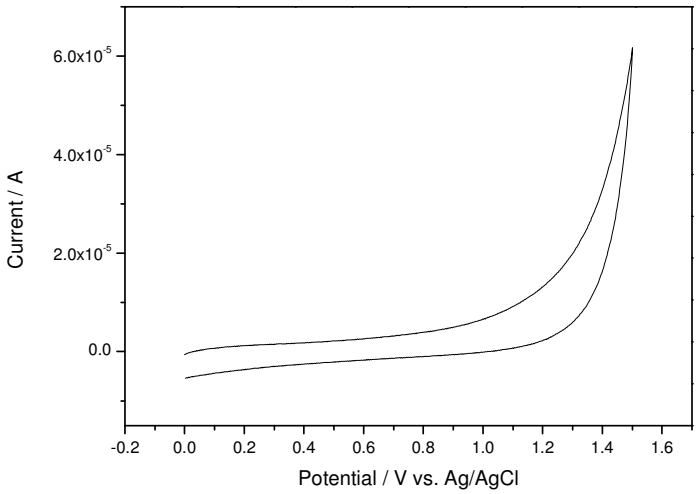

Figure 6.6: Cyclic voltammogram of aqueous solution containing 0.1 M KNO_3 and 0.01 M phosphate buffer (pH 6.1) obtained at 298 K.

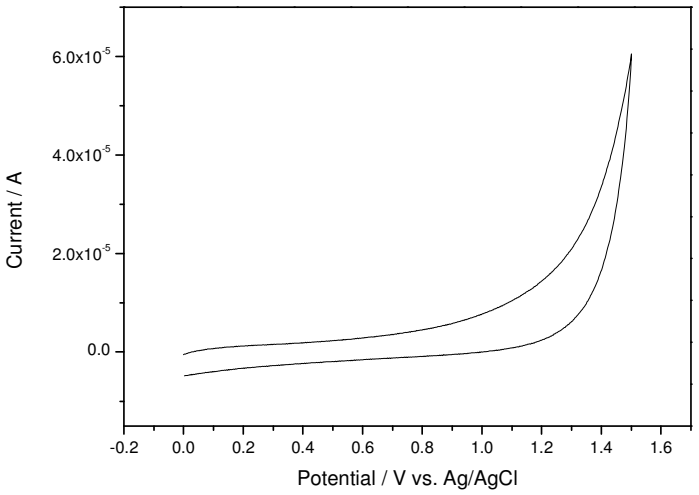

Figure 6.7: Cyclic voltammogram of aqueous solution containing 0.1 M KNO_3 and 0.01 M phosphate buffer (pH 7) obtained at 298 K.

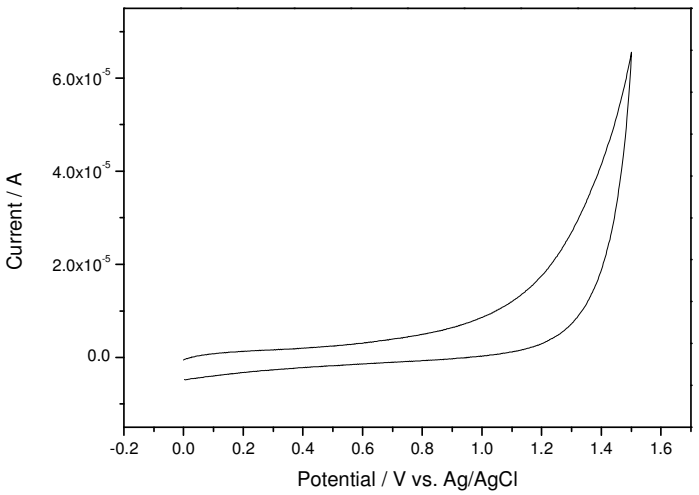

Figure 6.8: Cyclic voltammogram of aqueous solution containing 0.1 M KNO_3 and 0.01 M phosphate buffer (pH 7.9) obtained at 298 K.

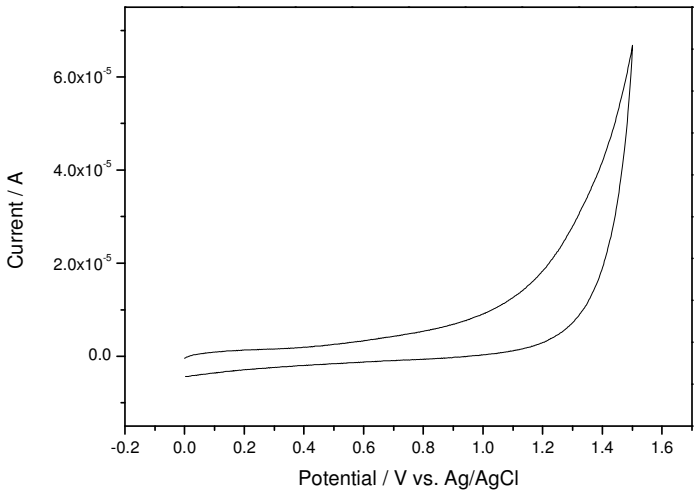

Figure 6.9: Cyclic voltammogram of aqueous solution containing 0.1 M KNO_3 and 0.01 M phosphate buffer (pH 10) obtained at 298 K.

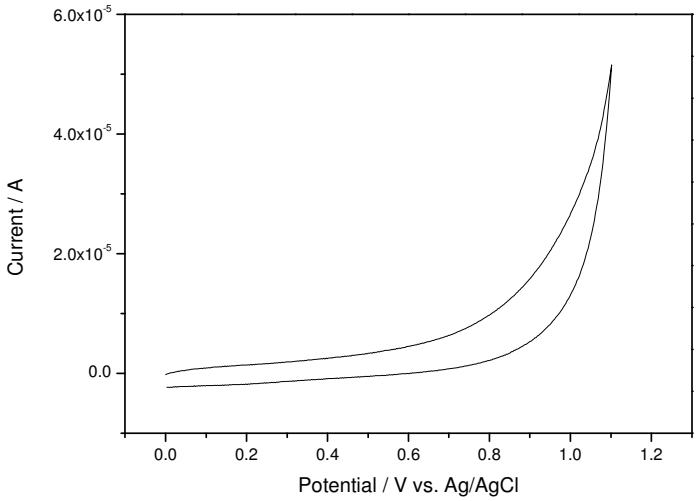

Figure 6.10: Cyclic voltammogram of aqueous solution containing 0.1 M KNO_3 and 0.01 M NaOH buffer (pH 11.8) obtained at 298 K.

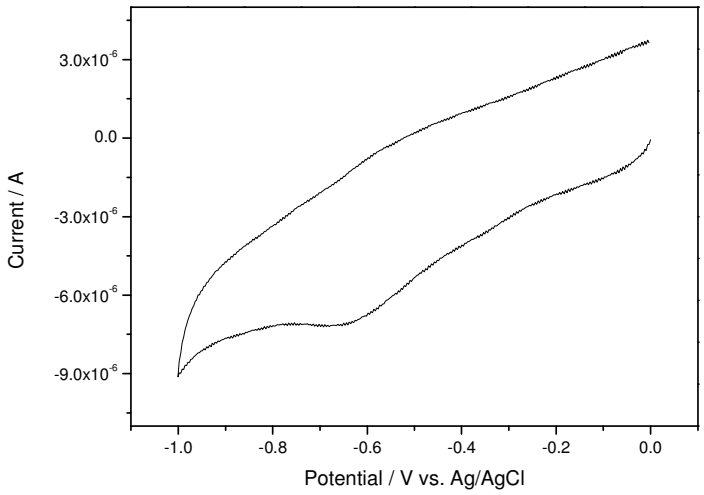

Figure 6.11: Cyclic voltammogram of aqueous solution containing 0.1 M KNO_3 and 0.01 M HCl buffer (pH 2) obtained at 298 K.

6.2.2 Phase-selective Second-harmonic AC Voltammetry

The phase-sensitive second-harmonic ac voltammetric experiments were performed using an Autolab/EAs 2 computer-controlled electrochemical system equipped with a potentiostat (model PGSTAT 302N). The instrument equipped with phase-sensitive detector lock-in-amplifier. The software GPES (version 4.9.007) was used for the electrochemical measurements. A three-electrode electrochemical cell was used with maximum capacity of 20-25 mL including gas bubbler and gas outlet ports. The platinum working electrode (2 mm) imbedded in Teflon was used. All solutions were prepared in 0.01 M solutions of tetrabutylammonium perchlorate in acetonitrile. The solutions were deaerated with argon at least 15 minutes before measurements. The typical concentrations of the compounds used were in the range of 1-5 mM. A reference electrode Ag/AgCl (0.1 M TBAP; acetonitrile) was made by inserting a silver wire into 0.1 M solution of tetrabutylammonium perchlorate and separated from the electrolyte solution by a frit. A platinum wire as the counter electrode was employed for all measurements. The sweep rate was used between 5-20 mVs^{-1}. The mechanical polish of the working electrode was employed with diamond paste before and after each measurement. The electrode is then rinsed with deionized water, immersed in concentrate nitric acid for 5 seconds and then rinsed again with deionized water and

then dried in air. The ferrocenium/ferrocene redox couple was used as an internal standard for all measurements and all the potentials were corrected against it. Two components of phase-selective second-harmonic ac voltammograms were recorded for each compound, in-phase (I) and quadrature (Q).

6.2.3 Photomodulated Voltammetry

The instrumentation for the photomodulated voltammetry (see **Figure 5.1**) is similar to that reported in literature and has been described previously.[87-88, 92] The flow through electrochemical cell, made from Teflon was designed and built at the University of Aarhus, Denmark and has a cylindrical chamber (Ø = 9 mm, L = 6 mm). The working electrode consists of a gold net (minigrid, 1000 mesh, Good-fellow) platinum net (minigrid, 250 mesh, Good-fellow) sealed in plastic foil and Teflon foil, which is provided with a hole (Ø = 7 mm) in order to ensure contact between net and solution. The area covered by the metal which forms the net is 0.218 cm^2. Electrical contact to the working electrode was realized with an insulated platinum wire.

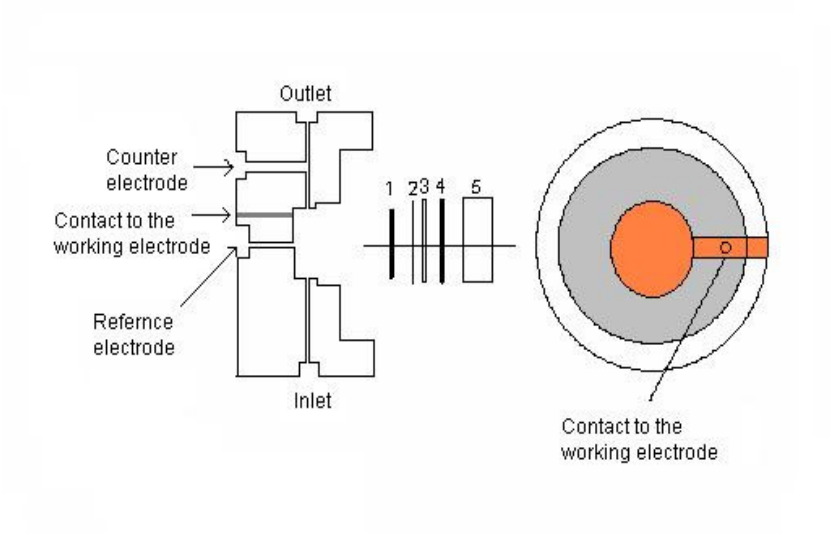

Figure 6.12: Construction of the cell and its parts (1) O-ring (2) working electrode (3) quartz window (4) O-ring (5) screw.

Solutions are allowed to flow slowly through cell (ca. 10 ml / min), after carefully degassing the solution with argon, in order to avoid depletion of the photochemical precursors. The gold minigrid is actually sandwiched between two quartz windows. The inner window contains a 5 mm diameter hole that defines the working area of the

electrode. **Figure 6.12** is described the construction of the cell.[xvii] The output from the lamp was modulated with a light chopper that was fitted with a specially designed iris so that the light intensity at the sample rose and fell approximately as a sine wave. A plot of the ac current versus the potential gave a voltammogram of the photogenerated free radical. The cell was held together by compression with seals between the Teflon and the quartz being made with Kalrex O-rings.

The light beam was focused on the working electrode through a quartz window that represents one of the walls of the chamber. A steel counter electrode was placed in the outlet of the cell, in order to avoid interference from products formed at the electrode. As a reference electrode we used a commercially available SCE (Flex-Ref electrode; World Precision Instruments) and Tungsten Wire (W), placed behind the working electrode and sufficiently close to it, to achieve a low ohmic drop. The light source (500 W Osram Hg lamp), a light chopper (home made), IR-water filter, a quartz lens and the electrochemical cell were placed in line on an optical bench. The reference signal coming from the lamp was taken from the electrochemical cell by a light guide placed the reference signal from the photodiode detector. The instrumentation also included a potentiostat (68FR0.5, Wenking), a lock-in-amplifier (186 Synchro-Het, PAR) for the detection of the ac component of the current as well as a computer for control of the electrochemical setup and for data acquisition. The instrumentation did not include any device for the compensation of ohmic drop. Light source generate a detectable amount of radicals. Water filter made of quartz so that uv light can pass unhindered. The radicals were generated by the direct photolysis. Solutions of 3, 6, and 9 mM were slowly flowed (1-2 ml/min) through the cell, after carefully degassing the solution with argon. The chopper frequency varied from 50 to 180 Hz at a potential scan rate was varied from 10 to 50 mV/s. Measured potentials are reported with respect to the aqueous saturated calomel electrode by employing the ferrocenium/ferrocene couple as an internal standard (0.41 V/SCE in MeCN). Three to four voltammograms were recorded for each set of experimental parameters

[xvii] Custom made.

Chapter 7. Results and Discussion

Theory helps us bear our
ignorance of facts.

(*George Santayana*)

Excited states molecules have their own chemical and physical properties and are showing distinctive features compared to ground states molecules. It has been reported that electron transfer can be a common reaction for excited states molecules.[95-97] This electron transfer reaction of the excited states molecules deactivate the excited states molecules to its ground state and simultaneously transfer the energy to other molecules usually quenchers. So the energy transfer experiment is basically the quenching of the excited states properties by the quenchers which further provides information's about excited states as well.[98-99] The important properties of the quenchers[36, 100-101] that determine the quenching ability of the molecules is its reduction and oxidation potential and here we are going to measure the oxidation/reduction potentials of quenchers.

The study carried out on different series of structurally related quenchers. This includes reductive quenchers such as aromatic amines, methoxybenzenes,[102] pyrroles, DNA bases, nucleosides, and amino acids and two oxidative quenchers 2-2´-bipyridine, and 3-3´,4-4´-benzophenone tetracarboxylic acid. Two different methodologies we have employed e.g., cyclic voltammetry, and phase-selective second-harmonic ac voltammetry for the determination of the ground states redox potential.

7.1 Cyclic Voltammetric Studies of Quenchers often used in Photoinduced Electron Transfer Reactions

The cyclic voltammetric data obtained for the various reductive quenchers e.g., aromatic amines, methoxybenzenes, pyrroles, and few other compounds are given in **Table 7.1**. All these quenchers, except TMP and DMPM, are showing well-defined single irreversible oxidation wave on forward scan but no cathodic wave on the reverse scan even at scan rate up to 1000 mVs^{-1}.[101] The cyclic voltammogram for methoxybenzene (anisole) taken at different scan rate is represented in **Figure 7.1**. The analysis of the

cyclic voltammogram reveals that the current in the foot of the anodic wave does not change even at different scan rate. This behavior confirms that the electron transfer from these quenchers is electrochemically unidirectional i.e., totally irreversible in nature. This was first suggested by Reinmuth in 1964.[52] Beside this, there are other number of criteria can also be employed to establish the totally irreversible nature of these quenchers but it is sufficient to mention here that the absence of the reverse electron-transfer step indicates that the oxidized cation is highly unstable

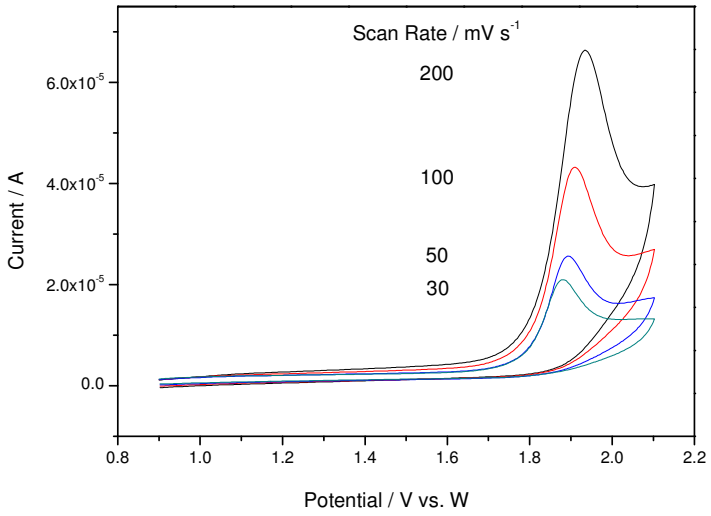

Figure 7.1. Cyclic voltammogram of 3.6 mM methoxybenzene in MeCN containing 0.1 M TBAP obtained at 298 K.

The measured widths $(E_p^{ox} - E_{1/2}^{ox})$ of the anodic waves are represented in **Table 7.1** column 3. The values are expectedly larger than the value for a reversible charge transfer step such as 59 mV. The E_p^{ox} values can be reproduced within the following range ± 20 mV at a constant scan rate but the peak currents decreased when repeating the scan. During the experiments no aging of the electrode was found on a week to week basis test and this suggested that the surface of the platinum electrode is not affected with these compounds. Sometimes we have found some complications arising from the deposition of the compound on the surface of the electrode when repeating the scans and this could change the response of the compounds. To avoid this problem after

each scan we have cleaned the electrode with mechanical polishing as described in experimental section.

The diffusion coefficients are also calculated just to confirm that the charge-transfer step is the diffusion rate limiting step. The values for diffusion coefficient are listed in **Table 7.1** column 5. The i_p in the cyclic voltammograms is proportional to the $v^{1/2}$, compare **Figure 7.1**, as well as to the concentration C of these compounds, both of which are consistent with diffusion as the rate limiting step.[39, 50, 103-104]

In the case of totally irreversible electrochemical processes the rate constant for electron transfer $k(E_p^{ox})$ can be related to the anodic peak potential E_p^{ox} as expressed in equation (2.33) and under this condition, the chare-transfer process is slow compared to the follow-up chemical reaction. The irreversible oxidation of quenchers is an EC mechanism described in equations (2.25) and (2.26), and for the reaction the heterogeneous rate constants independent of potential can be calculated using equation (2.31) and are given in **Table 7.1** column 6.

For checking the reversibility of the electrochemical processes the plot between E_p^{ox} *or* $E_{p/2}^{ox}$ vs. $\log v$ based on equations (2.35) and (2.37) can also be utilized. The plots furnish a straight line with slope between 0-30 mV for reversible electron transfer process and for the irreversible electron transfer processes the slope should be greater than 30 mV. **Figure 7.2** and **Figure 7.3** are representing the linear plot between E_p^{ox} *or* $E_{p/2}^{ox}$ and $\log v$ for methoxybenzene. For all other compounds such kind of plots are given in appendix B. Similar observation has been done by plotting E_p^{ox} vs. $\log i_p$ for methoxybenzene, see **Figure 7.4**. The plot between E_p^{ox} and $\log i_p$ also provides information about electrochemical reversibility/irreversibility; further plots for other are compounds in appendix B. The values of transfer coefficient β obtained from above three methods and also from the width of the anodic wave are listed in **Table 7.2**. The results provide strong evidence that the process is a totally irreversible electron transfer process. The potential dependence of the transfer coefficient is also checked and the plot between transfer coefficient β and the potential E is given in **Figure 7.5**.

We have first time used tungsten wire as a reference electrode because it's relatively cheap and easy to employ. During the experiments we have observed the potential of

the tungsten was not fixed and vary on day to day basis. Keeping this in mind, we have employed ferrocenium/ferrocene redox couple as an internal standard and all the potentials were calibrated against ferrocenium/ferrocene redox couple.

Table 7.1: Cyclic voltammetric data for various quenchers[a]

Compd	E_p^{ox} [b]/ V	$E_p^{ox} - E_{p/2}^{ox}$ [c]/ mV	β [c]	D [d]/ 10^5 $cm^2\ s^{-1}$	$-\log k(E_p^{ox})$ [e]/ $cm\ s^{-1}$
Methoxybenzene (Anisole)	1.32	63	0.76	7.8	1.48
2-Methylanisole	1.26	79	0.61	1.3	1.42
3-Methylanisole	1.27	75	0.64	4.4	1.96
4-Methylanisole	1.27	92	0.52	2.8	1.79
2-Bromoanisole	1.55	147	0.32	1.9	1.48
1,3-Dimethoxy-Benzene	1.15	96	0.50	4.3	1.61
1,4-Dimethoxy-Benzene	0.94	73	0.65	2.5	1.77
1,2,4-Trimethoxy-benzene	0.65	63	0.76	1.8	1.47
N,N´-Dimethyl-aniline	0.34	76	0.71	4.4	1.62
N,N´-Diethyl-aniline	0.33	77	0.62	2.7	1.75
Triphenylamine	0.61	76	0.63	3.0	1.72
4,4´-Bis-(dimethylamino) diphenylmethane	0.47	73	0.65	4.4	1.55
DABCO	0.33	68	0.70	3.1	1.69
N-Methylpyrrole	1.01	96	0.50	4.8	1.10
1,2,5-Trimethyl-pyrrole	0.55	63	0.76	8.5	1.39
N-Phenyl-tetrachloro-phthalimide	1.89	98	0.49	4.0	1.72

[a] CV measurements at 100 mVs^{-1} with stationary platinum electrode in acetonitrile solution containing 0.1 M TBAP as supporting electrolyte at 298 K. [b] Potential relative to ferrocenium/ferrocene couple. [c] Calculated according to equation (2.34). [d] Calculated from equation (2.39). [e] Obtained from equation (2.31).

Table 7.2: Transfer coefficient determine by several independent methods[a]

compd	transfer coefficient				
	E_p^{ox} *vs.* $\log \upsilon$	$E_{p/2}^{ox}$ *vs.* $\log \upsilon$	E_p^{ox} *vs.* $\log i_p$	$E_p^{ox} - E_{p/2}^{ox}$	a.v.
Methoxybenzene (Anisole)	0.63	0.64	0.89	0.68	0.71±0.12
2-Methylanisole	0.49	0.78	0.40	0.56	0.56±0.16
3-Methylanisole	0.47	0.79	0.42	0.60	0.57±0.16
4-Methylanisole	0.33	0.46	0.37	0.53	0.42±0.08
2-Bromoanisole	0.28	0.53	0.23	0.31	0.34±0.13
1,3-Dimethoxy-benzene	0.56	0.70	0.52	0.45	0.56±0.10
1,4-Dimethoxy-benzene	0.66	0.69	0.74	0.63	0.68±0.05
1,2,4-Trimethoxy-benzene	0.45	0.68	0.43	0.71	0.57±0.15
N,N´-Dimethyl-aniline	0.46	0.72	0.42	0.65	0.56±0.14
N,N´-Diethyl-aniline	0.29	0.39	0.23	0.57	0.37±0.15
Triphenylamine	0.68	0.79	0.45	0.59	0.63±0.14
4,4´-Bis-(dimethylamino) diphenylmethane	0.31	0.63	0.24	0.54	0.43±0.18
DABCO	0.39	0.69	0.38	0.62	0.52±0.15
N-Methylpyrrole	0.25	0.37	0.31	0.44	0.47±0.08
1,2,5-Trimethyl-pyrrole	0.41	0.73	0.37	0.61	0.53±0.17
N-Phenyl-tetrachloro-phthalimide	0.38	0.78	0.34	0.45	0.49±0.20

[a] See chapter 2.

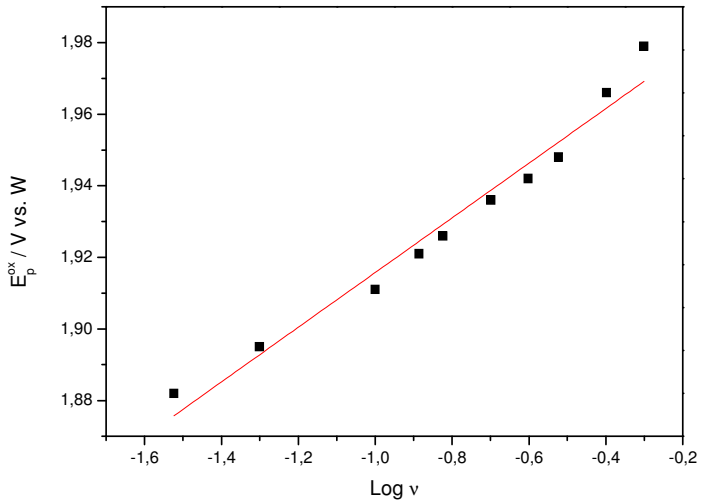

Figure 7.2: Variation of anodic peak potential E_p^{ox} with CV sweep rate at a platinum electrode at 298 K in acetonitrile solution containing 0.1 M TBAP and 3.6 mM methoxybenzene.

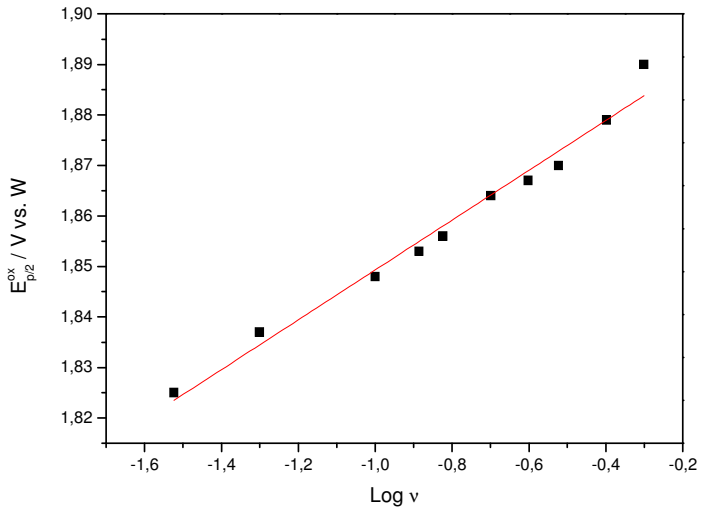

Figure 7.3: Variation of anodic peak potential $E_{p/2}^{ox}$ with CV sweep rate at a platinum electrode at 298 K in acetonitrile solution containing 0.1 M TBAP and 3.6 mM methoxybenzene.

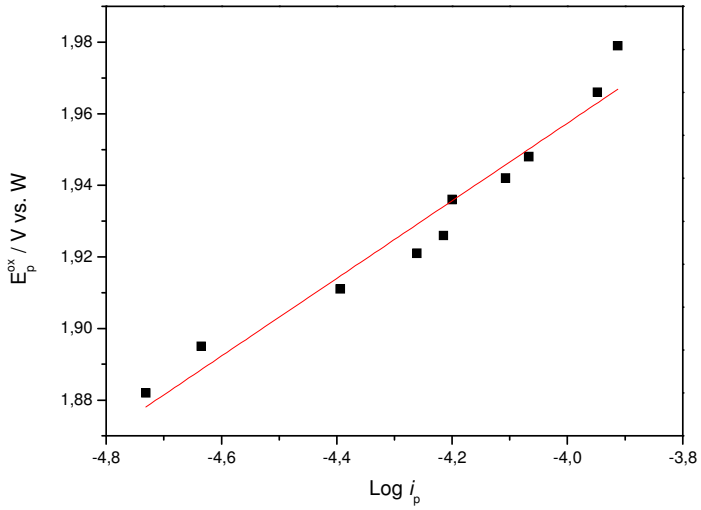

Figure 7.4: Variation of anodic peak potential E_p^{ox} with peak current at a platinum electrode at 298 K in acetonitrile solution containing 0.1 M TBAP and 3.6 mM methoxybenzene.

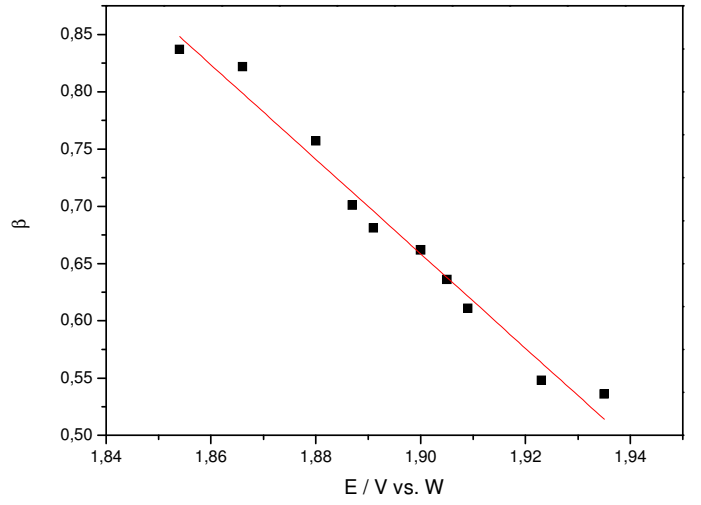

Figure 7.5: Dependence of the heterogeneous electron transfer beta with the applied electrode potential E for the methoxybenzene.[xviii]

[xviii] The transfer coefficient is plotted at the average potential of the CV wave, given by $E = \frac{E_p^{ox} + E_{p/2}^{ox}}{2}$.

The half-wave oxidation potential, $E_{1/2}^{ox}$, is readily obtained from the analysis of the cyclic voltammograms.[19, 105-106] The cyclic voltammograms for all compounds recorded at various scan rate. **Figure 7.1** is representing the cyclic voltammogram for methoxybenzene taken at different scan rate. For all other compounds the voltammograms are given in appendix A. The sweep dependence values for the width of the CV wave, $(E_p^{ox} - E_{1/2}^{ox})$, calculated as discussed before and are given in **Table 7.1** column 3. From the width of the CV wave the electron transfer coefficient β has been calculated using equation (2.34). The $E_{1/2}^{ox}$ can be evaluated from the intercept of the linear plots based on the free energy relationships given in chapter 2 and the equations are (2.43), (2.45), and (2.46). The same $E_{1/2}^{ox}$ values of compounds are obtained irrespective of the use of different free energy relationships for electron transfer reactions.[19] The data obtained are given in **Table 7.3**. The linear plots obtained for oxidation peak potential E_p^{ox} as a function of electron transfer coefficient β based on the following three free energy relationships, Marcus, Rehm-Weller and Marcus-Levine free energy relationships are given in **Figure 7.6**, **Figure 7.7**, and **Figure 7.8**. The values for intrinsic barrier $\Delta G^{\neq}(0)$ obtained from the slope of the linear plots and are given in **Table 7.4**.

It has been noted that the values obtained for $E_{1/2}^{ox}$ are not in much difference from the values reported in various literature for some of the quenchers. The comparison is given in **Table 7.5**.

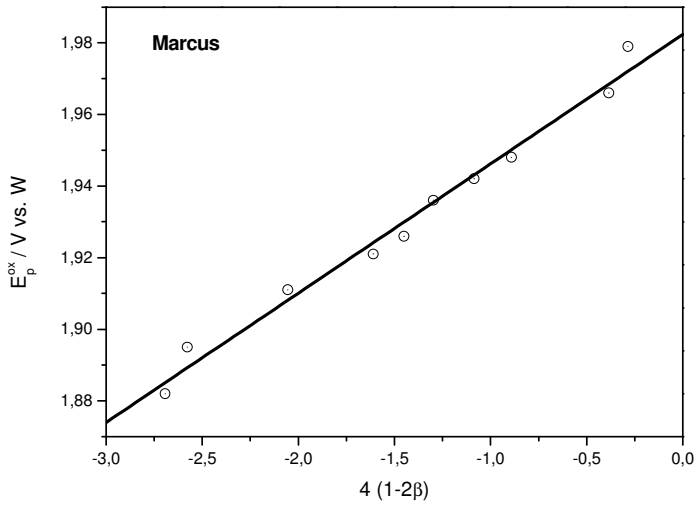

Figure 7.6: The oxidation peak potential E_p^{ox} of methoxybenzene plotted as a function of the transfer coefficient β based on the Marcus free energy relationship, see equation (2.45).

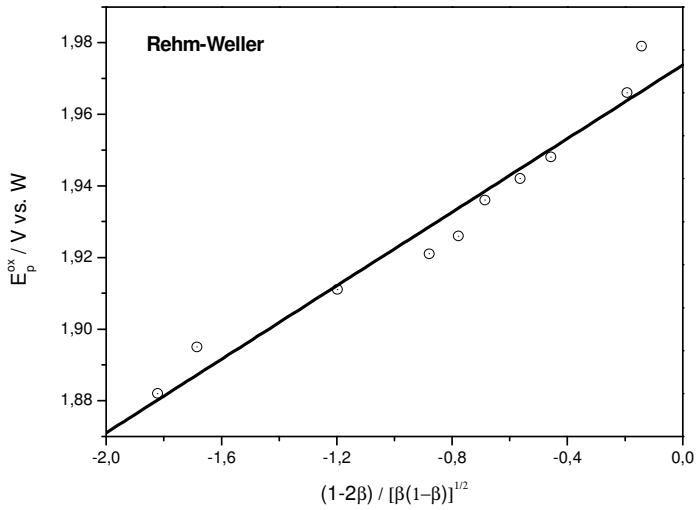

Figure 7.7: The oxidation peak potential E_p^{ox} of methoxybenzene plotted as a function of the transfer coefficient β based on the Rehm-Weller free energy relationship, see equation (2.43).

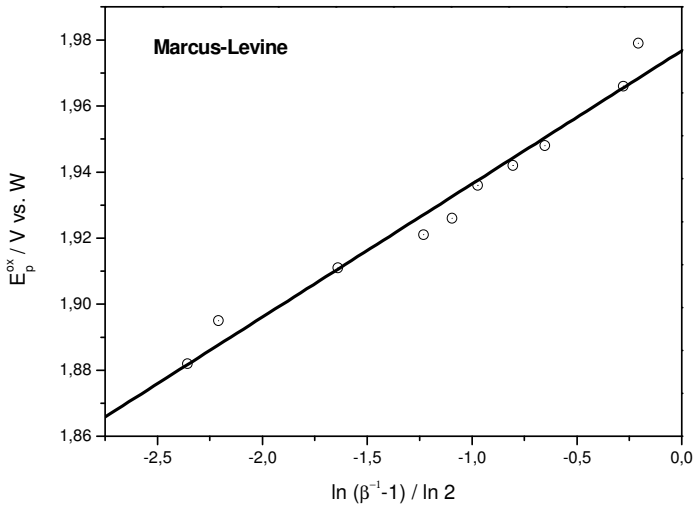

Figure 7.8: The oxidation peak potential E_p^{ox} of methoxybenzene plotted as a function of the transfer coefficient β based on the Marcus-Levine free energy relationship, see equation (2.46).

Table 7.3: Half-wave oxidation potential for various quenchers[a]

compd	$E_{1/2}^{ox}$ / V vs. Fc/Fc$^+$			
	Marcus	Rehm-Weller	Marcus-Levine	a.v.
Methoxybenzene (Anisole)	1.370	1.365	1.367	1.367±0.002
2-Methylanisole	1.299	1.299	1.299	1.299±0
3-Methylanisole	1.315	1.314	1.313	1.315±0.001
4-Methylanisole	1.306	1.306	1.306	1.306±0
2-Bromoanisole	1.372	1.400	1.391	1.388±0.014
1,3-Dimethoxy-benzene	1.151	1.151	1.151	1.151±0
1,4-Dimethoxy-benzene	0.961	0.960	0.960	0.961±0
1,2,4-Trimethoxy-benzene	0.728	0.718	0.721	0.722±0.003
N,N´-Dimethyl-aniline	0.400	0.396	0.398	0.398±0.002
N,N´-Diethyl-aniline	0.394	0.392	0.393	0.393±0.001
Triphenylamine	0.634	0.633	0.633	0.633±0
4,4´-Bis-(dimethylamino) diphenylmethane	0.508	0.508	0.508	0.508±0
DABCO	0.384	0.381	0.382	0.382±0.001
N-Methylpyrrole	0.998	0.998	0.998	0.998±0
1,2,5-Trimethyl-pyrrole	0.588	0.587	0.587	0.587±0
N-Phenyl-tetrachloro-phthalimide	1.900	1.900	1.900	1.900±0

[a] Obtained in acetonitrile solution at 298 K, mathematical description found in chapter 2.

Table 7.4: The values for intrinsic barrier obtained for various quenchers[a]

compd	$(\Delta G^{\neq}(0)/F)/V$			
	Marcus	Rehm-Weller	Marcus-Levine	a.v.
Methoxybenzene (Anisole)	0.022	0.031	0.025	0.026±0.004
2-Methylanisole	0.050	0.098	0.068	0.072±0.024
3-Methylanisole	0.039	0.069	0.050	0.053±0.015
4-Methylanisole	0.041	0.074	0.053	0.056±0.016
2-Bromoanisole	0.133	0.211	0.158	0.168±0.039
1,3-Dimethoxy-benzene	0.066	0.129	0.096	0.097±0.031
1,4-Dimethoxy-benzene	0.019	0.034	0.024	0.026±0.007
1,2,4-Trimethoxy-benzene	0.035	0.048	0.038	0.040±0.006
N,N´-Dimethyl-aniline	0.038	0.064	0.047	0.049±0.013
N,N´-Diethyl-aniline	0.060	0.109	0.079	0.082±0.024
Triphenylamine	0.023	0.039	0.028	0.030±0.017
4,4´-Bis-(dimethylamino) diphenylmethane	0.032	0.061	0.043	0.045±0.016
DABCO	0.035	0.058	0.043	0.045±0.016
N-Methylpyrrole	0.093	0.181	0.126	0.133±0.044
1,2,5-Trimethyl-pyrrole	0.020	0.035	0.025	0.027±0.007
N-Phenyl-tetrachloro-phthalimide	0.053	0.104	0.072	0.076±0.025

[a] Obtained in acetonitrile solution at 298 K, mathematical description found in chapter 2.

Table 7.5: Comparisons from the literature values (in MeCN at 298 K)

	$E_{1/2}^{ox}$		
compd	V vs. Fc/Fc^{+}[a]	V vs. SCE[b]	V vs. SCE
Methoxybenzene (Anisole)	1.367	1.767	1.76[c]
2-Methylanisole	1.299	1.699	-
3-Methylanisole	1.315	1.715	1.77[d]
4-Methylanisole	1.306	1.706	1.68[d]
2-Bromoanisole	1.388	1.788	-
1,3-Dimethoxy-benzene	1.151	1.551	-
1,4-Dimethoxy-benzene	0.961	1.361	1.34[c]
1,2,4-Trimethoxy-benzene	0.722	1.122	1.12
N,N´-Dimethyl-aniline	0.398	0.798	0.81[e]
N,N´-Diethyl-aniline	0.393	0.793	0.76[e]
Triphenylamine	0.633	1.033	1.06[e]
4,4´-Bis-(dimethylamino) diphenylmethane	0.508	0.908	-
DABCO	0.382	0.782	-
N-Methylpyrrole	0.998	1.398	-
1,2,5-Trimethyl-pyrrole	0.587	0.987	-
N-Phenyl-tetrachloro-phthalimide	1.900	2.300	-

[a] From **Table 7.3**. [b] Measured potential for Fc^{+}/Fc vs. SCE is = + 0.400 V.
[c] From reference[102]
[d] From reference[36]
[e] From reference[1]

As discussed before for all compounds except DMPM and TMP, well defined anodic wave obtained. In the case of DMPM three peaks observed for oxidation, see **Figure 7.9**. The first and the third oxidation are irreversible in nature as seen from the cyclic voltammogram whereas the second oxidation is reversible. The explanation for such behavior is beyond the scope of this work. We are interested only in the first oxidation and the $E_{1/2}^{ox}$ calculated are given in **Table 7.3**.

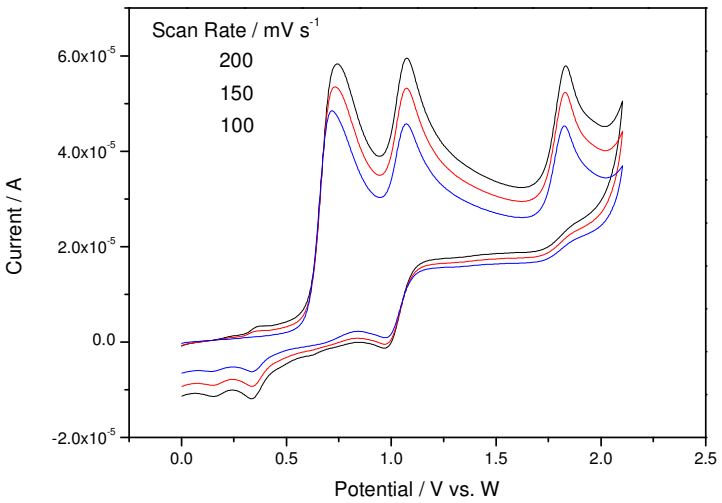

Figure 7.9: Cyclic Voltammogram of 3 mM 4,4´-bis(dimethylamino)diphenylmethane in MeCN containing 0.1 M TBAP obtained at 298 K.

On the other hand the cyclic voltammogram of TMP showed two irreversible oxidations waves. **Figure 7.10** represent the cyclic voltammogram for TMP. The half-wave oxidation potential calculated is given in **Table 7.3**.

Detailed studies have already been done on the oxidations of aromatic amines such as N,N´-dimethylaniline, N,N´-diethylaniline, 1,4-Diazabicyclo[2.2.2]octane and Triphenylamine.[107-115] Adams and co-workers showed that the anodic oxidation of aniline and its derivatives in non-aqueous solutions usually occurs via a number of reactions and leads to a large number of products, depending upon the reaction condition.

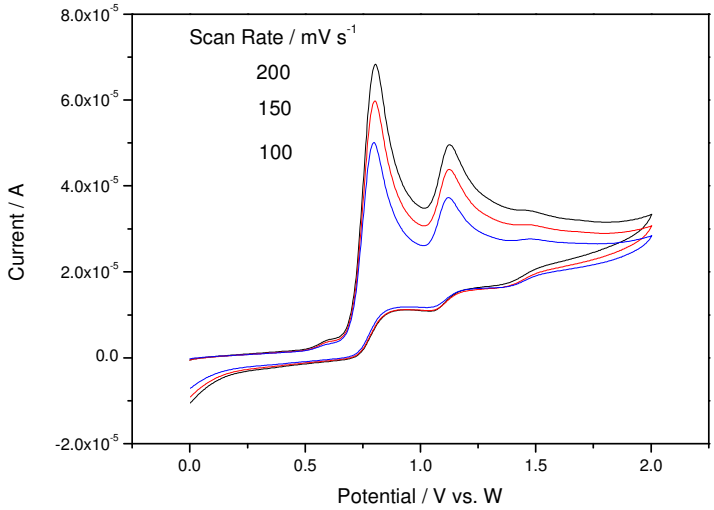

Figure 7.10: Cyclic Voltammogram of 3 mM 1,2,5-trimethylpyrrole in MeCN containing 0.1 M TBAP obtained at 298 K.

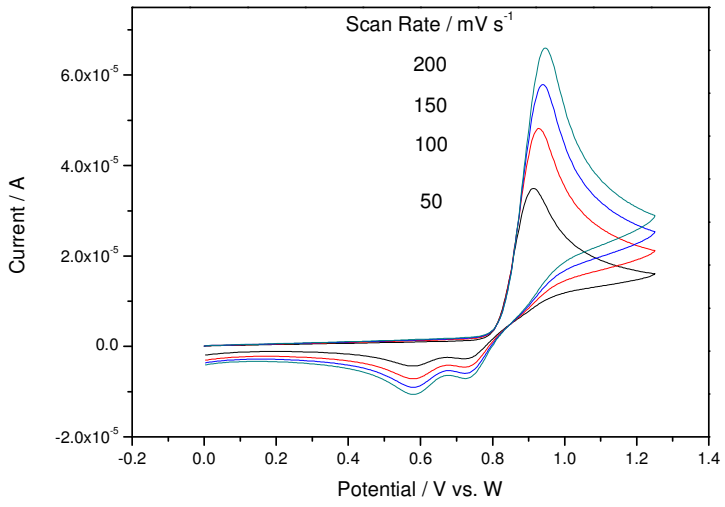

Figure 7.11: Cyclic Voltammogram of 3.1 mM N,N´-dimethylaniline in MeCN containing 0.1 M TBAP obtained at 298 K.

.

For example N,N´-dimethylaniline and N,N´-diethylaniline showed a single anodic wave on forward scan and when reverse two small peaks are present for the reduction where Triphenylamine showed three reduction peaks. Earlier studies reveal that the major product from DMA oxidation in non-aqueous solutions was N,N,N´,N´-tetramethylbenzidine (TMB). TMB is more easily oxidized than DMA and forms stable dication. The oxidation of TPA was similar to the anodic oxidation of amomatic amines, such as N,N´-dimethylaniline, where tetrphenylbenzidine formation was observed due to the dimerization of the $TPA^{\bullet+}$ cation radical. The cyclic voltammogram obtained for N,N´-dimethylaniline is given in **Figure 7.11**. The cyclic voltammograms for N,N´-diethylaniline and triphenylamine are given in appendix B.

7.2 Cyclic Voltammetric Studies of Biologically Relevant Substances

Electrochemical technique such as cyclic voltammetry has been used for the study and for the detection of biologically relevant compounds. Donor compounds (reductive quenchers) such as adenine, adenosine, thymine, thymidine, alanine, histidine, and methionine was analysed for their $E_{1/2}^{ox}$ whereas oxidative quenchers i.e., 2,2´-Bipyridine, and 3,3´,4,4´-benzophenone tetracarboxylic acid was analysed for their $E_{1/2}^{red}$. For all compounds the pH range 2-12 was used during the study.

The electrochemical approach, through nondestructive techniques such as cyclic voltammetry offers several distinct advantages: scanning the electrode potential is equivalent to scanning a continuous set of electron acceptors; the current flowing through the electrode is a direct measure of the overall kinetics, which includes the diffusion of the various species toward or from the electrode. Once diffusion has been taken into account, the current is thus a reflection of the mechanism and kinetics of the set of reactions under investigation. An additional attractive feature of this approach is that the forward and reverse reactions may be simultaneously characterized.

We could not find any response for the oxidation of adenine, thymidine and alanine on glassy carbon electrode. All other 4 compounds gave electrochemically irreversible oxidation wave at positive potentials, indicating the formation of reaction products upon oxidation (i.e., an EC reaction).[54, 65, 68, 116] Whereas other two compounds gave well defined irreversible cathodic wave on reduction. Electrochemical reversibility has been checked by dependence of peak potential on scan rate. Both the peak current and potentials depended on pH values of solution and vary with change of scan rate. This indicates that the electrode process was controlled simultaneously by diffusion and adsorption. With increasing scan rate, anodic peak potentials shifted to more positive values.

Typical cyclic voltammogram for thymine using phosphate buffer system obtained at different scan rate is shown in **Figure 7.12**. The oxidation signals are well resolved from the background response. Cyclic voltammograms for other compounds e.g., adenosine, histidine and methionine are given in appendix A.

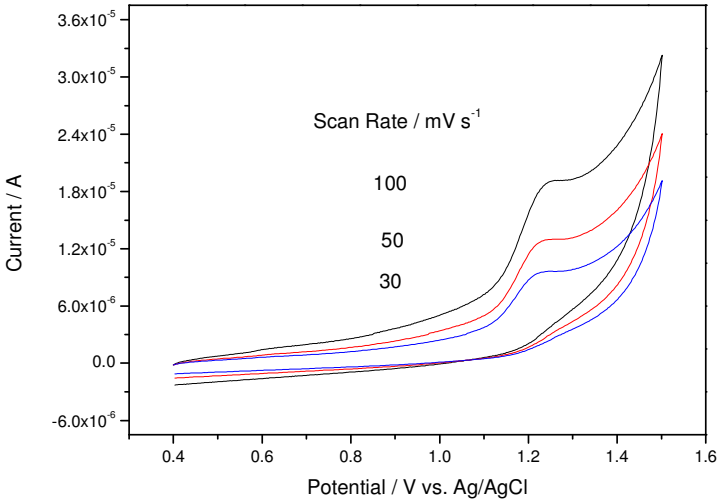

Figure 7.12: Cyclic voltammogram of 1 mM aqueous solution of thymine containing 0.1 M KNO_3 and 0.01 M Phosphate Buffer (pH 4) obtained at 298 K.

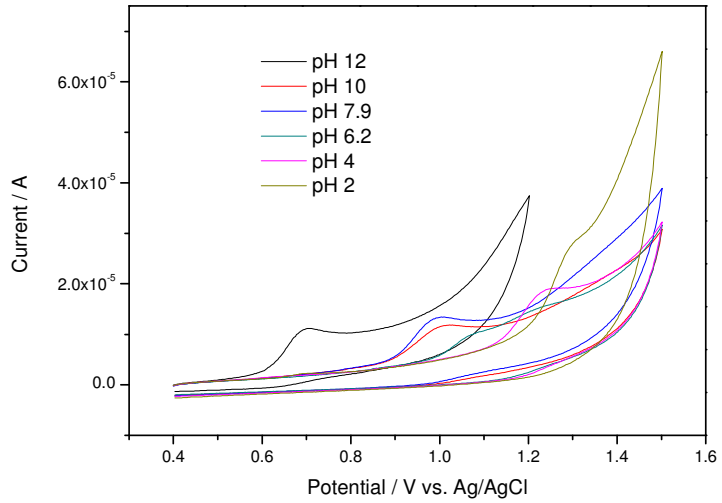

Figure 7.13: Cyclic voltammogram of 1 mM aqueous solution of thymine containing 0.1 M KNO_3 obtained at 298 K, 100 mVs^{-1}, and at different pH.[xix]

[xix] The details for buffer systems used in this work are given in experimental section.

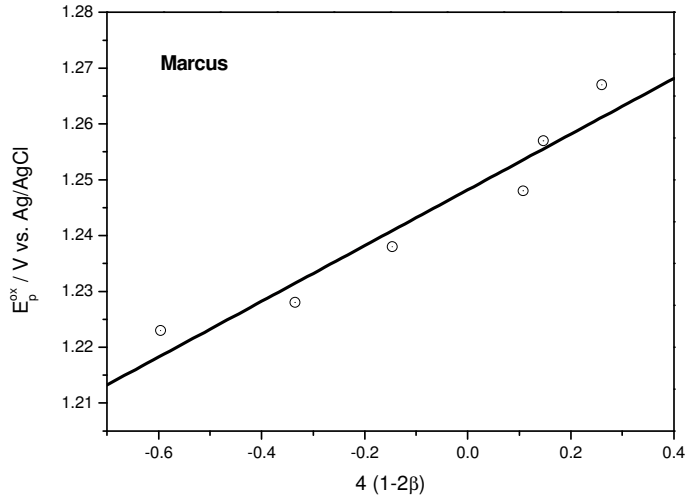

Figure 7.14: The oxidation peak potential E_p^{ox} of thymine plotted as a function of the transfer coefficient β based on the Marcus free energy relationship; see equation (2.45), at pH 4.

The oxidation of thymine and other compounds have also been observed at different pH values. The shift in peak potential, E_p^{ox}, toward less positive value with higher pH (acidic to alkaline) is recorded for thymine, adenosine, histidine and methionine. The pH dependence oxidation of thymine in the pH range 2-12 is given in **Figure 7.13**. The pH dependence cyclic voltammogram for oxidation of other compounds are given in appendix A. To establish the variation of peak potential or half-wave potential on pH, the peak potential E_p^{ox} or half-wave potential $E_{1/2}^{ox}$ are plotted against pH. The plots are given in **Figure 7.15** and **Figure 7.16**. For single proton transfer reaction the slope value should be 59 mV or less.

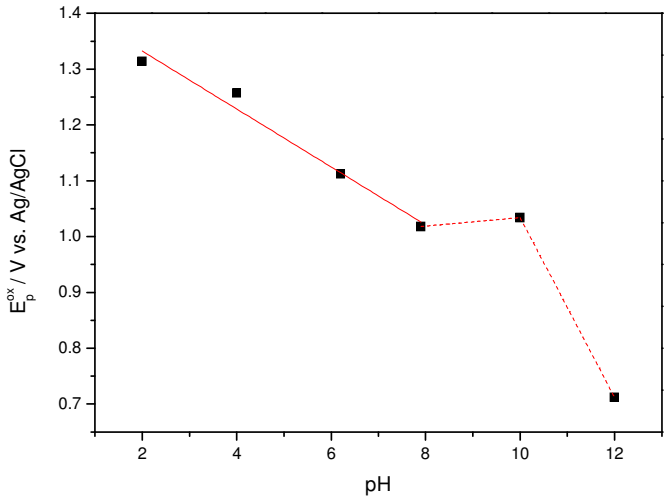

Figure 7.15: The oxidation peak potential E_p^{ox} of thymine plotted as a function pH obtained at 298 K, 100 mVs^{-1}

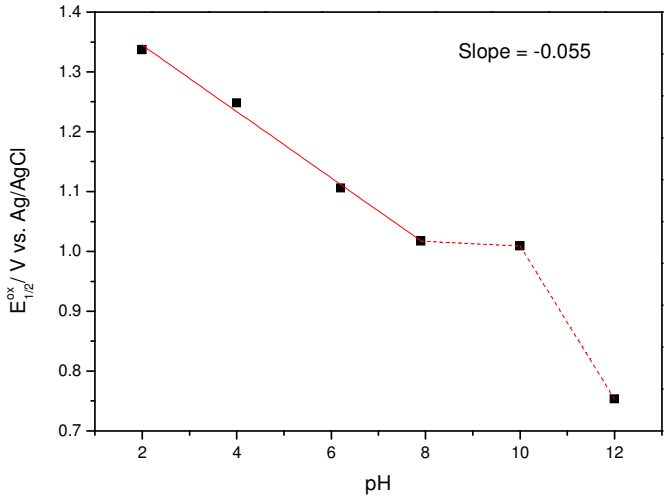

Figure 7.16: The oxidation half-wave potential $E_{1/2}^{ox}$ of thymine plotted as a function pH obtained at 298 K, 100 mVs^{-1}

During the experiment we have realized that the available potential range or window for oxidation/reduction in water is simply too narrow because the oxidation/reduction of water obscure the response from the compounds. The potential range in aqueous solution also depends on the electrode material and electrolyte system as well. Of the available electrodes we have found that only the glassy carbon has by far the widest oxidative window from 0 to +1.5 V. On the other hand because platinum is a good catalyst for oxidation of water, the potential range for platinum is found smaller than glassy carbon such as from -0.8 to + 0.8. In our case all compounds oxidized at higher positive potential so platinum does not facilitate the detection of these compounds.

For obtaining the half-wave oxidation potential, $E_{1/2}^{ox}$, similar methodology has been applied as discussed in previous section. Because all three free energy relationships provide relatively similar values for $E_{1/2}^{ox}$ so here we are going to utilize only the Marcus free energy relationship for calculation of $E_{1/2}^{ox}$. The cyclic voltammogram for thymine at different sweep rate and at pH 4 is already given in **Figure 7.12**. The values for the width of the CV wave, $(E_p^{ox} - E_{1/2}^{ox})$, and for the electron transfer coefficient have been calculated. The $E_{1/2}^{ox}$ can be evaluated from the intercept of the linear plot based on the Marcus free energy relationship equation (2.45). The plot for oxidation peak potential as a function of electron transfer coefficient β is given in **Figure 7.14**. By similar treatment the half-wave oxidation potential for thymine at different pH values have been calculated and are representing in **Table 7.6**. The linear plot based on Marcus free energy relationship equation (2.45) for other compounds are given in appendix B. The $E_{1/2}^{ox}$ values for adenosine, histidine, and methionine at different pH values are given in **Table 7.7**, **Table 7.8**, and **Table 7.9**.

Table 7.6: Half-wave oxidation potential for thymine at different pH values[a]

pH[b]	E_p^{ox} / V vs. Ag/AgCl	$E_{1/2}^{ox}$ / V vs. Ag/AgCl
2	1.314	1.337
4	1.257	1.248
6.2	1.112	1.106
7.9	1.018	1.017
10	1.034	1.009
12	0.712	0.753

[a] CV measurements at 100 mVs^{-1} with stationary glassy carbon electrode in aqueous solution containing 0.1 M KNO_3 as supporting electrolyte and buffer solutions at 298 K.
[b] The details of the buffer systems used are given in experimental section.

Table 7.7: Half-wave oxidation potential for adenosine at different pH values[a]

pH[b]	E_p^{ox} / V vs. Ag/AgCl	$E_{1/2}^{ox}$ / V vs. Ag/AgCl
2	1.363	1.424
4	1.325	1.308
6.2	1.302	1.304
7	1.347	1.296
7.9	1.275	1.136
10	1.302	1.005

[a] CV measurements at 100 mVs^{-1} with stationary glassy carbon electrode in aqueous solution containing 0.1 M KNO_3 as supporting electrolyte and buffer solutions at 298 K.
[b] The details of the buffer systems used are given in experimental section.

Table 7.8: Half-wave oxidation potential for histidine at different pH values[a]

pH[b]	E_p^{ox} / V vs. Ag/AgCl	$E_{1/2}^{ox}$ / V vs. Ag/AgCl
6.1	1.084	0.976
7.9	0.844	0.953
10	0.804	0.916
11	0.721	0.694
12	0.623	0.658

[a] CV measurements at 100 mVs^{-1} with stationary glassy carbon electrode in aqueous solution containing 0.1 M KNO_3 as supporting electrolyte and buffer solutions at 298 K.
[b] The details of the buffer systems used are given in experimental section.

Table 7.9: Half-wave oxidation potential for methionine at different pH values[a]

pH[b]	E_p^{ox} / V vs. Ag/AgCl	$E_{1/2}^{ox}$ / V vs. Ag/AgCl
2	1.075	0.902
4	1.031	0.903
6.2	1.040	0.650
10	0.949	0.877
11	0.989	0.694

[a] CV measurements at 100 mVs^{-1} with stationary glassy carbon electrode in aqueous solution containing 0.1 M KNO_3 as supporting electrolyte and buffer solutions at 298 K.
[b] The details of the buffer systems used are given in experimental section.

Two oxidative quenchers i.e., 2,2´-Bipyridine, and 3,3´,4,4´-benzophenone tetracarboxylic acid were analysed for their half-wave reduction potential, $E_{1/2}^{red}$. Both compounds showed well defined cathodic wave on reduction and no anodic wave when oxidized at the glassy carbon electrode thus the reduction of these compound are entirely irreversible electrode reaction. The typical cyclic voltammogram for 3,3´,4,4´-benzophenone tetracarboxylic acid shown in **Figure 7.17** was taken at different sweep rate. Cyclic voltammogram for 2,2´-Bipyridine is given in appendix A. The reduction of 3,3´,4,4`-benzophenone tetracarboxylic acid was studied at different pH values and found that negative shift in peak potential, E_p^{red}, at higher pH values. Both compounds gave reduction peak only in acidic medium and no peak was observed in alkaline medium. The pH dependence reduction of 3,3´,4,4´-benzophenone tetracarboxylic acid is given in **Figure 7.18**. The dependence of peak potential of half-wave potential on pH are given in **Figure 7.20** and **Figure 7.21**. For 2,2´-Bipyridine the pH dependence voltammogram is given in appendix A.

The half-wave reduction potential, $E_{1/2}^{red}$, evaluated by using the Marcus free energy relationship equation (2.54).[19, 105-106] The plot for reduction peak potential as a function of electron transfer coefficient β is given in **Figure 7.19**. The $E_{1/2}^{red}$ for 3,3´,4,4´-benzophenone tetracarboxylic acid and 2,2´-Bipyridine are given in **Table 7.10**, and **Table 7.11**.

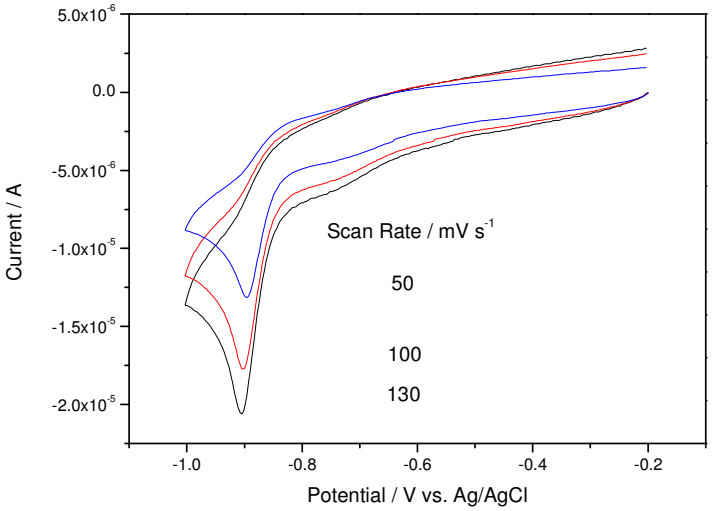

Figure 7.17: Cyclic voltammogram of 1 mM aqueous solution of 3,3´,4,4´-benzophenone tetracarboxylic acid containing 0.1 M KNO_3 and 0.01 M phosphate buffer (pH 2.9) obtained at 293K.

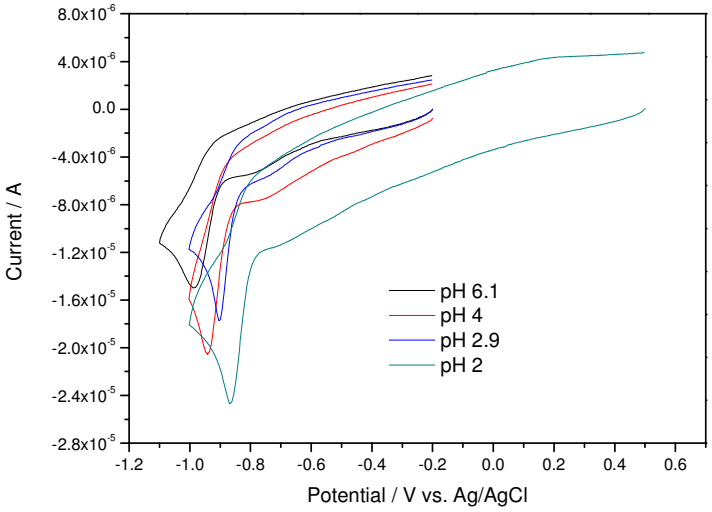

Figure 7.18: Cyclic voltammogram of 1 mM aqueous solution of 3,3´,4,4´-benzophenone tetracarboxylic acid containing 0.1 M KNO_3 obtained at 293K, 100 mVs^{-1}, and at different pH.[xx]

[xx] The details for buffer systems used in this work are given in experimental section.

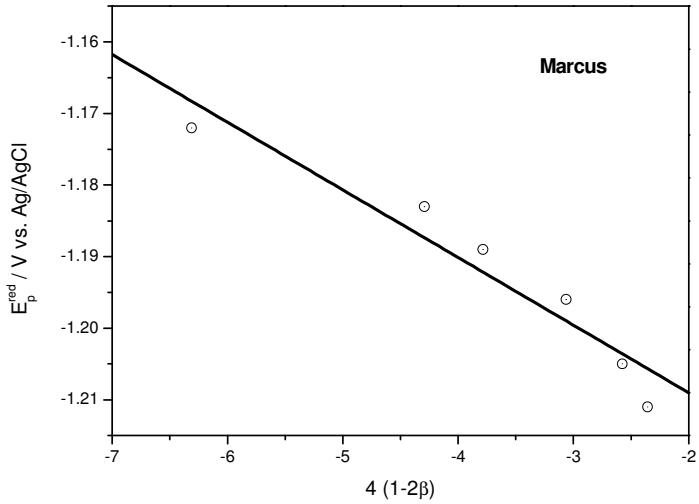

Figure 7.19: The reduction peak potential E_p^{red} of 3,3´,4,4´-benzophenone tetracarboxylic acid plotted as a function of the transfer coefficient β based on the Marcus free energy relationship, see equation(2.54), at pH 2.9.

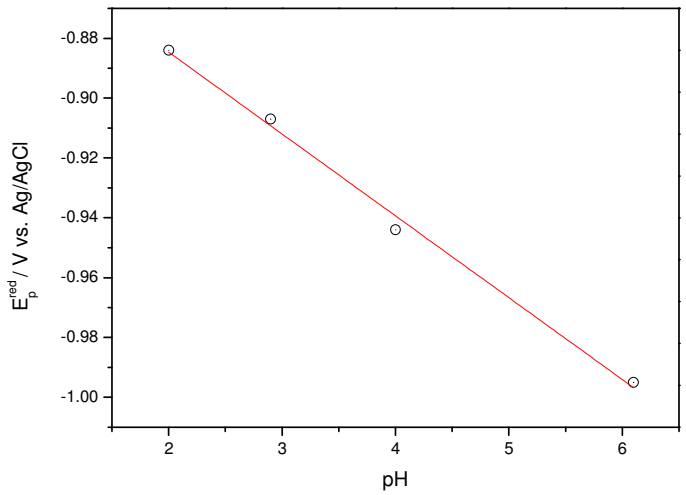

Figure 7.20: The reduction peak potential E_p^{red} of 3,3´,4,4´-benzophenone tetracarboxylic acid plotted as a function pH obtained at 298 K, 100 mVs^{-1}

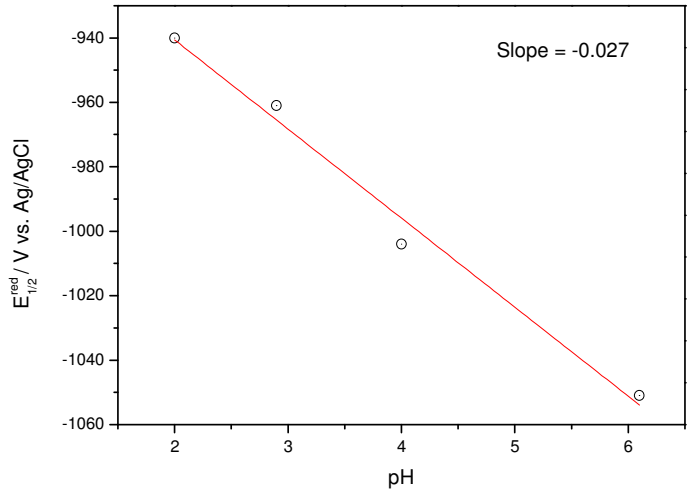

Figure 7.21: The reduction half-wave potential $E_{1/2}^{red}$ of 3,3´,4,4´-benzophenone tetracarboxylic acid plotted as a function pH obtained at 298 K, 100 mVs^{-1}

Table 7.10: Half-wave reduction potential for 3,3´,4,4´-benzophenone tetracarboxylic acid at different pH values[a]

pH[b]	E_p^{red} / V vs. Ag/AgCl	$E_{1/2}^{red}$ / V vs. Ag/AgCl
2	-0.884	-0.940
2.9	-0.907	-0.961
4	-0.944	-1.004
6.1	-0.995	-1.051

[a] CV measurements at 100 mVs^{-1} with stationary glassy carbon electrode in aqueous solution containing 0.1 M KNO_3 as supporting electrolyte and buffer solutions at 298 K.

[b] The details of the buffer systems used are given in experimental section.

Table 7.11: Half-wave reduction potential for 2,2´-Bipyridine at different pH values[a]

pH[b]	E_p^{red} / V vs. Ag/AgCl	$E_{1/2}^{red}$ / V vs. Ag/AgCl
2	-1.151	-1.252
2.9	-1.189	-1.228
4	-1.385	-1.407
6.1	-1.433	-1.424

[a] CV measurements at 100 mVs^{-1} with stationary glassy carbon electrode in aqueous solution containing 0.1 M KNO_3 as supporting electrolyte and buffer solutions at 298 K.

[b] The details of the buffer systems used are given in experimental section.

7.3 Second Harmonic AC Voltammetric Studies of Quenchers

For compounds that show irreversible electrochemical behavior on the time scale of simple cyclic voltammetry, it is not possible to have directly their thermodynamic half-wave oxidation/reduction using cyclic voltammetry. We have attacked this problem by employing an alternative technique, phase-selective second-harmonic ac voltammetry, which allows us to have the reversible electrode potential for highly unstable and rapid follow-up chemical reactions. In our study the method apparently is very successful for every compound that we have tested. The technique is not very simple like cyclic voltammetry and its application requires considerable effort and patience in order to obtain the symmetrical second harmonic ac voltammograms.

For strictly diffusion controlled processes the second harmonic current amplitude voltammograms are characterized by two symmetrical positive and negative lobes separated by a zero current minimum. The resolution is also excellent[117-118] and this technique would therefore appear to be more attractive than with the fundamental harmonic and dc methods. The half-wave potential can be measured directly from the minimum of the second harmonic voltammograms as long as the irreversible follow-up chemical reactions are characterized by rate constant as large as 10^{-5} s.[10-13] This ability to ascertain conveniently and quickly the E-half value in the presence of rapid, irreversible follow-up chemical reactions represents an important advantage of second harmonic ac voltammetry for the study of such systems.

The thermodynamically reversible potentials for rapidly reacting redox systems, taken from symmetrical or nearly symmetrical phase-selective second-harmonic ac voltammograms are reported here. The phase-selective second-harmonic ac voltammogram for the oxidation of the methoxybenzene at a platinum electrode is illustrated in **Figure 7.22**. The voltammogram represents the second derivative of normal dc voltammogram and exhibits both positive and negative lobes due to phase-sensitive detection of ac signal. As discussed before for rapid charge transfer with slow follow-up chemical reaction the current magnitudes of each lobe of the second harmonic response are equal and also the peak to peak separation should be 68 mV/n, where n is the number of electron transferred.[12] But this is not the case for compounds that we have measured by phase-selective second-harmonic ac voltammetry, even not a single

compound showed such type of behavior exactly. Still we are able to find the thermodynamic half-wave oxidation potentials for such compounds.

The second harmonic ac polargraphs show a good crossing point, invariant with frequency. Thus the potentials obtained are electrochemically reversible. Second harmonic ac voltammetry was used to determine the radical reduction potentials reversibly. Good reversible behaviour was observed with a well defined crossing point.

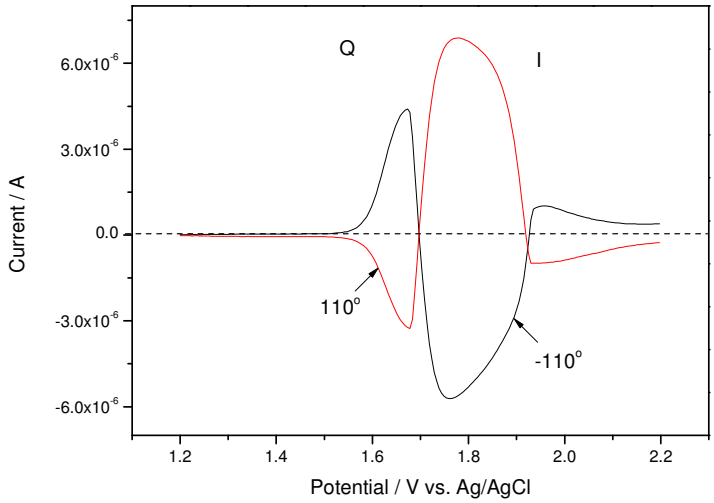

Figure 7.22: SHACV signals obtained for the oxidation of 3 mM methoxybenzene in acetonitrile containing 0.1 M TBAP as supporting electrolyte at a platinum electrode: frequency, 100 Hz, amplitude of the sinusoidal potential, 25 mV: temperature, 298 K.

Under the experimental conditions, for all our compounds we found that the follow-up chemical reactions are faster relative to the linear sweep and slow compared with the ac modulation technique. Consequently the second harmonic peaks lose their symmetry and intensity both, but the peak to peak separation is still approximately 68 mV/n. More importantly, the null potential is still the thermodynamic half-wave potential. Literature survey revealed that for redox system with irreversible chemical reactions following charge transfer as in equations (2.25) and (2.26) as long as the pseudo first order rate constant behavior does not exceed about $2x10^{-4}$ the thermodynamic half-wave oxidation/reduction potential will be measurable from the crossing points of the I and Q component voltammograms.[10-11] For these reason we have recorded both in phase (I)

and quadrature (Q) components for all the compounds. The half-wave oxidation potentials were measured where both components intersect usually at zero or nearly zero.

The use of phase-selective second-harmonic ac voltammetry increases the sensitivity by two or more orders of magnitude over conventional dc voltammetry. **Figure 7.22** shows the in-phase and quadrature components of the second harmonic ac voltammograms. The responses obtained obviously have 180^{o} phase difference. However, in contrast to the fundamental harmonic, there is no evidence of significant charging current in either component. That is, as in second harmonic ac voltammetry, the double layer charging current is extremely small. The use of phase-sensitive detection with the second harmonic technique, while not necessary for minimizing the charging current, does offer advantages in the nature of the wave shape.

The main characteristics of a chemically reversible system are the symmetry of the positive and negative lobes around zero crossing point or intersection point with the dc potential axis this is located at the standard potential whatever the phase angle. Sometimes it is possible that the response obtained at a given phase angle and at the same phase angle plus 180^{o} are not always symmetrical around the horizontal axis.[10] It can be seen that one phase angle (and the same plus 180) exists for which the two lobes are symmetrical around the intersection point but, unlike the reversible case, the symmetry disappears as soon as the phase angle deviates from this value.

With cyclic voltammetry, we never found perfect reversibility for these compounds though second harmonic response still not the reversible in true sense but we can interpret it as nearly reversible behavior. Furthermore, we didn't find traces of double layer charging current when examining the base line of the second harmonic voltammograms. The power of the second harmonic ac technique is evident in the determination of the reduction potentials of the following compounds such as methoxybenzenes, aromatic amines, and pyrroles.

We have employed higher frequency range from 50-250 Hz and we found that 110 Hz are suitable for our measurements. At higher frequency wave retained its shape and exhibited a linear relationship with the applied frequency. Under these criteria, the oxidation waves of our compounds indicate that the processes are rapid one-electron

oxidation processes. Higher frequency used to overcome the perturbation caused by the follow-up chemical reactions otherwise zero current intersection is difficult to observe.

Usually with higher frequency, the ac signal leads to greater broadening and distortion of the wave but we didn't find such type of behavior and the reason behind is that the charge transfer from the electrode to the substrate is rapid compared with the ac frequency. For each oxidation/reduction process we have studied a kinetic window in which good reversible electrochemical behavior is observed. The ac frequency must be rapid compared with the rate of the following chemistry, but it must be kept small enough to prevent distortion of the wave due to competition with the rate of the charge-transfer process. Fortunately, with all of our compounds a sufficiently broad window exists for each process to permit determination of the thermodynamic half-wave potentials. The results obtained from second-harmonic ac voltammetry for various quenchers are given in **Table 7.12**.

Table 7.12: The reversible half-wave oxidation potential obtained from SHACV[a] (in MeCN at 298 K)

	$E_{1/2}^{ox}$ / V	
compd	vs. Ag/AgCl	vs. Fc/Fc^+
Methoxybenzene (Anisole)	1.696	1.271
2-Methylanisole	1.589	1.164
3-Methylanisole	1.580	1.155
4-Methylanisole	1.525	1.100
2-Bromoanisole	1.799	1.374
1,3-Dimethoxy-benzene	1.464	1.039
1,4-Dimethoxy-benzene	1.288	0.863
1,2,4-Trimethoxy-benzene	1.011	0.586
N,N´-Dimethyl-aniline	0.728	0.303
N,N´-Diethyl-aniline	0.726	0.301
Triphenylamine	0.979	0.554
4,4´-Bis-(dimethylamino) diphenylmethane	0.827	0.402
DABCO	0.719	0.294
N-Methylpyrrole	not observed	not observed
1,2,5-Trimethyl-pyrrole	0.890	0.465

[a] Measured potential Fc/Fc^+ vs Ag/AgCl is 0.425 V. For the phase-selective second-harmonic response for ferrocene see chapter 4.

Table 7.13: Comparison of the results obtained from SHACV and CV methds measured in MeCN at 298 K.

	$E_{1/2}^{ox}$ / V	
	SHACV	CV
compd	vs. Fc/Fc^+	vs. Fc/Fc^+
Methoxybenzene (Anisole)	1.271	1.367
2-Methylanisole	1.164	1.299
3-Methylanisole	1.155	1.315
4-Methylanisole	1.100	1.306
2-Bromoanisole	1.374	1.388
1,3-Dimethoxy-benzene	1.039	1.151
1,4-Dimethoxy-benzene	0.863	0.961
1,2,4-Trimethoxy-benzene	0.586	0.722
N,N´-Dimethyl-aniline	0.303	0.398
N,N´-Diethyl-aniline	0.301	0.393
Triphenylamine	0.554	0.633
4,4´-Bis-(dimethylamino) diphenylmethane	0.402	0.508
DABCO	0.294	0.382
N-Methylpyrrole	not observed	0.998
1,2,5-Trimethyl-pyrrole	0.465	0.587

At frequency 100 Hz the oxidation waves do not exhibit the shape and symmetry but still indicating good reversibility on the time scale of experiments. The processes remain reversible over the frequency range 50-250 Hz. It is also important to note that in this work the null crossing point of these voltammograms does not shift as the frequency is changed in this reversible region. This demonstrates clearly that these potentials are not in any way being displaced by chemical processes with a time scale competitive with the ac frequency. It is also reported that the potentials are essentially unaffected of the choice of the electrode material used. At this moment we can not support this point as we have used only platinum electrode for all oxidation measurements by second harmonic ac voltammetry.

We conclude that the agreement between results obtained from cyclic voltammetry and second-harmonic ac voltammetry are in close agreement (**Table 7.13**), although it would be unwise to make a general claim for the validity of the methods. Our results

indicate that the second-harmonic ac voltammetry seems to be the method of choice for obtaining precise thermodynamic data in systems in which the products of the electrode reaction are kinetically very unstable. Consideration of the theory for reversible charge transfer with a follow-up irreversible first order chemical reaction leads to the conclusion given below. All compounds undergo very fast subsequent reaction after one electron oxidation thus higher frequency is needed to bring about reversibility for observing oxidations processes but we can not observe broadening of the wave. The work also points out that care must be taken in the interpretation of the measurements and that the observation of zero current crossing potential is not always sufficient for establishing the reversible potential for a reaction.

The most important advantage of using the second harmonic approach is derived from the previously mentioned fact that the minimum on the second harmonic voltammogram is relatively much less sensitive to the effects of the follow-up chemical reaction than the corresponding dc and fundamental harmonic techniques. Finally, within experimental error, our data are in gratifying agreement.

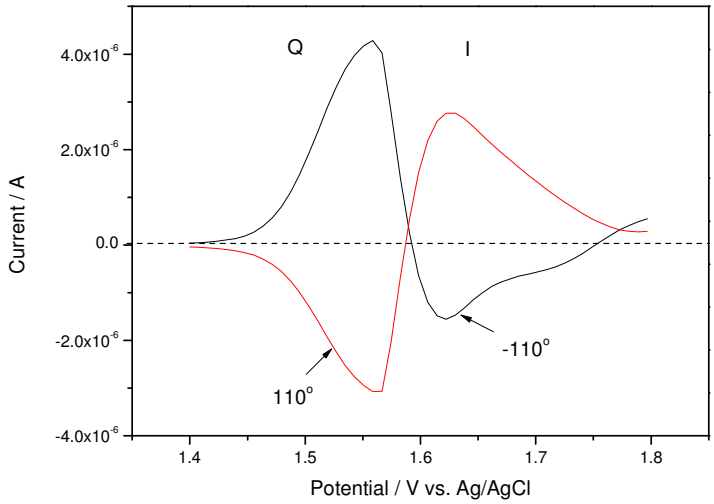

Figure 7.23: SHACV signals obtained for the oxidation of 3 mM 2-methylanisole in acetonitrile containing 0.1 M TBAP as supporting electrolyte at a platinum electrode: frequency, 100 Hz, amplitude of the sinusoidal potential, 25 mV: temperature, 298 K.

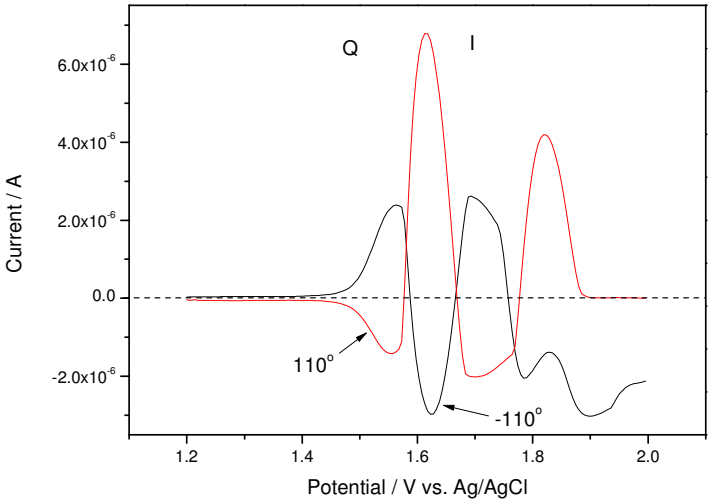

Figure 7.24: SHACV signals obtained for the oxidation of 3 mM 3-methylanisole in acetonitrile containing 0.1 M TBAP as supporting electrolyte at a platinum electrode: frequency, 100 Hz, amplitude of the sinusoidal potential, 25 mV: temperature, 298 K.

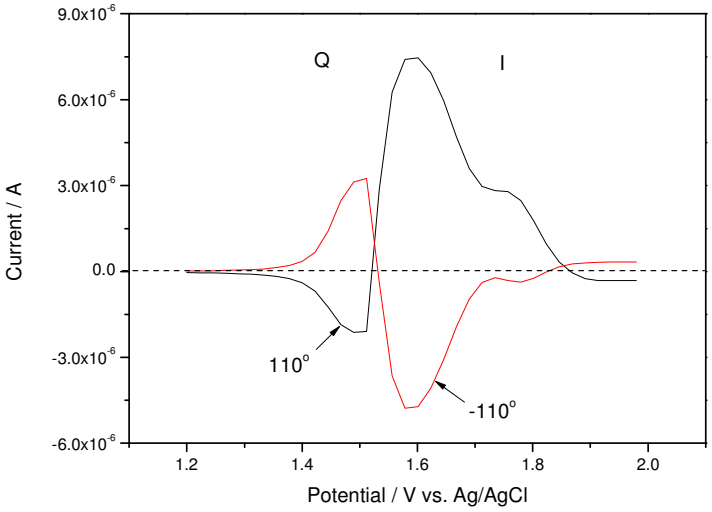

Figure 7.25: SHACV signals obtained for the oxidation of 3 mM 4-methylanisole in acetonitrile containing 0.1 M TBAP as supporting electrolyte at a platinum electrode: frequency, 100 Hz, amplitude of the sinusoidal potential, 25 mV: temperature, 298 K.

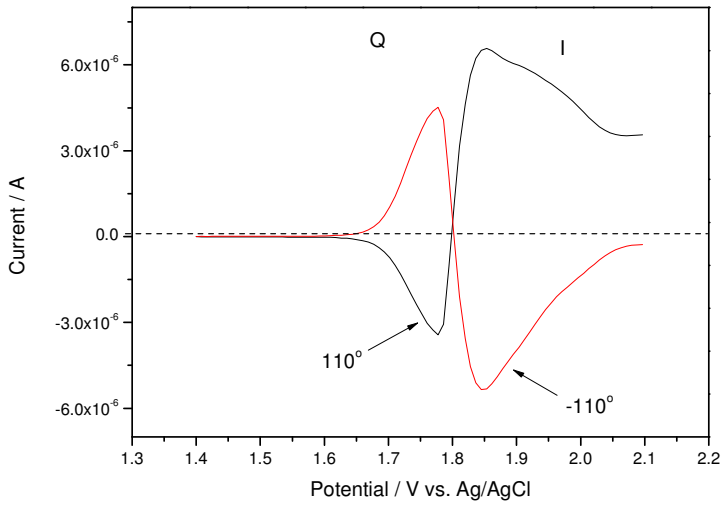

Figure 7.26: SHACV signals obtained for the oxidation of 3 mM 2-bromoanisole in acetonitrile containing 0.1 M TBAP as supporting electrolyte at a platinum electrode: frequency, 100 Hz, amplitude of the sinusoidal potential, 25 mV: temperature, 298 K.

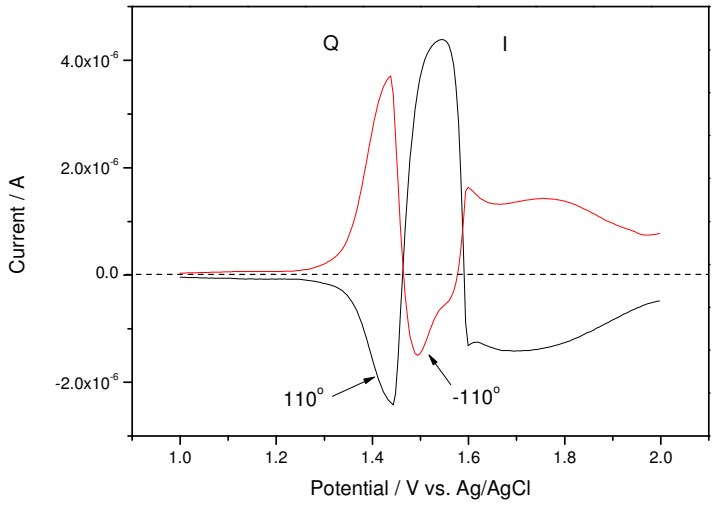

Figure 7.27: SHACV signals obtained for the oxidation of 3 mM 1,3-dimethoxybenzene in acetonitrile containing 0.1 M TBAP as supporting electrolyte at a platinum electrode: frequency, 100 Hz, amplitude of the sinusoidal potential, 25 mV: temperature, 298 K.

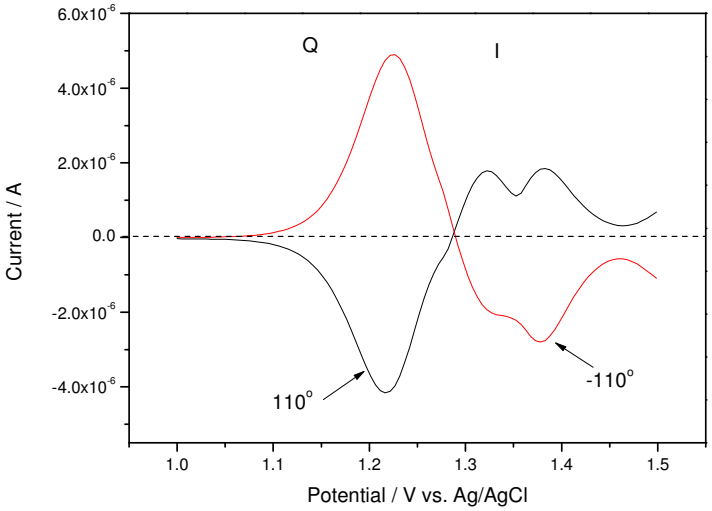

Figure 7.28: SHACV signals obtained for the oxidation of 3 mM 1,4-dimethoxybenzene in acetonitrile containing 0.1 M TBAP as supporting electrolyte at a platinum electrode: frequency, 100 Hz, amplitude of the sinusoidal potential, 25 mV: temperature, 298 K.

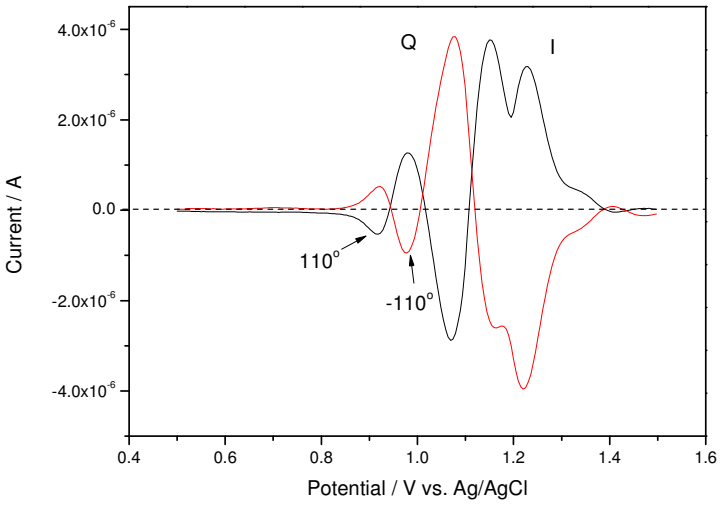

Figure 7.29: SHACV signals obtained for the oxidation of 3 mM 1,2,4-trimethoxybenzene in acetonitrile containing 0.1 M TBAP as supporting electrolyte at a platinum electrode: frequency, 100 Hz, amplitude of the sinusoidal potential, 25 mV: temperature, 298 K.

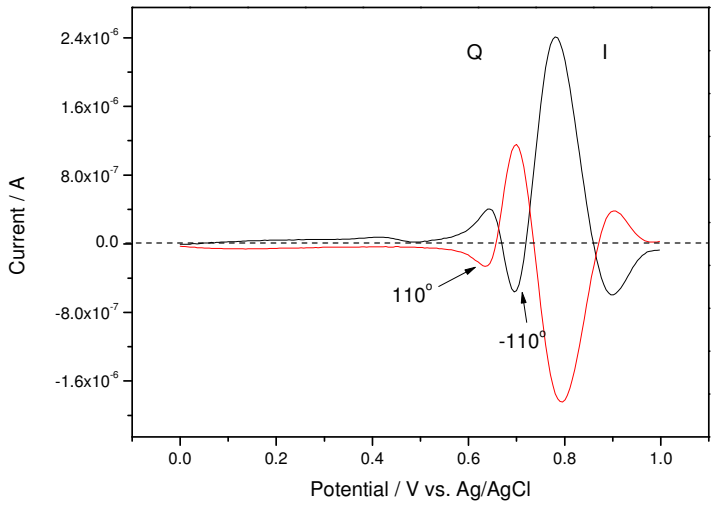

Figure 7.30: SHACV signals obtained for the oxidation of 3 mM N,N´-dimethylaniline in acetonitrile containing 0.1 M TBAP as supporting electrolyte at a platinum electrode: frequency, 100 Hz, amplitude of the sinusoidal potential, 25 mV: temperature, 298 K.

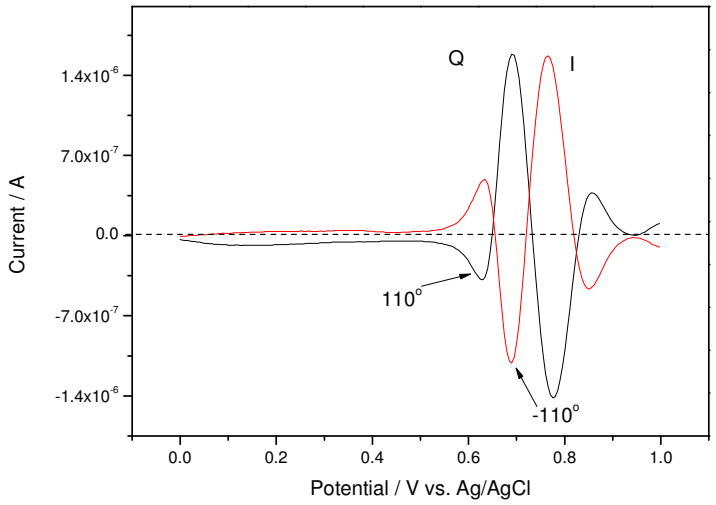

Figure 7.31: SHACV signals obtained for the oxidation of 3 mM N,N´-diethylaniline in acetonitrile containing 0.1 M TBAP as supporting electrolyte at a platinum electrode: frequency, 100 Hz, amplitude of the sinusoidal potential, 25 mV: temperature, 298 K.

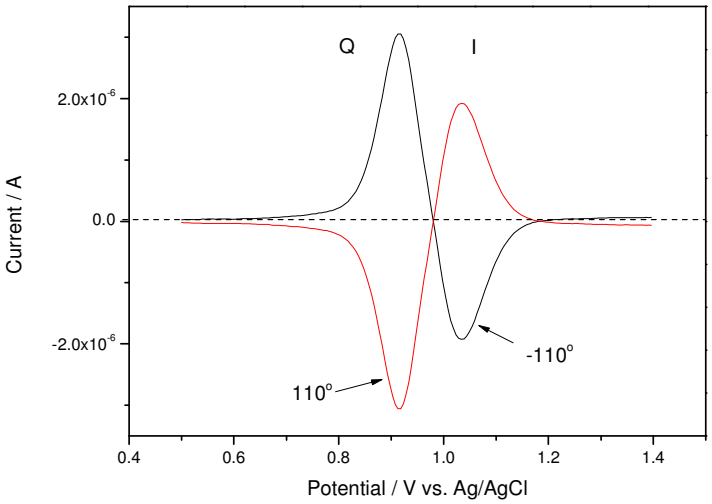

Figure 7.32: SHACV signals obtained for the oxidation of 3 mM triphenylamine in acetonitrile containing 0.1 M TBAP as supporting electrolyte at a platinum electrode: frequency, 100 Hz, amplitude of the sinusoidal potential, 25 mV: temperature, 298 K.

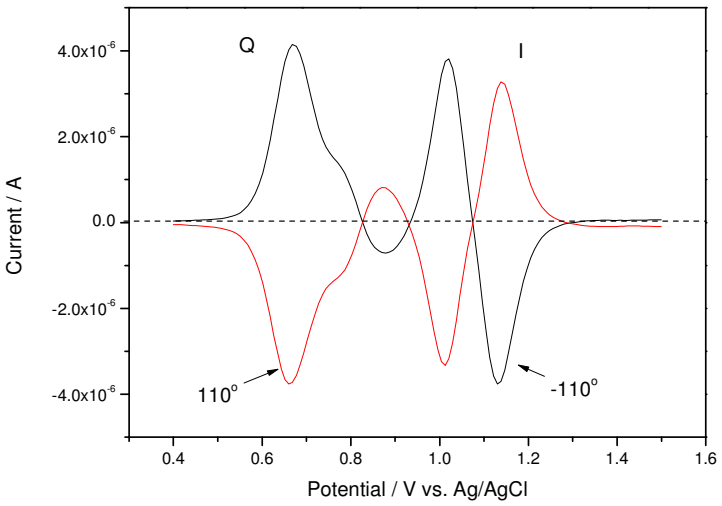

Figure 7.33: SHACV signals obtained for the oxidation of 3 mM DMPM in acetonitrile containing 0.1 M TBAP as supporting electrolyte at a platinum electrode: frequency, 100 Hz, amplitude of the sinusoidal potential, 25 mV: temperature, 298 K.

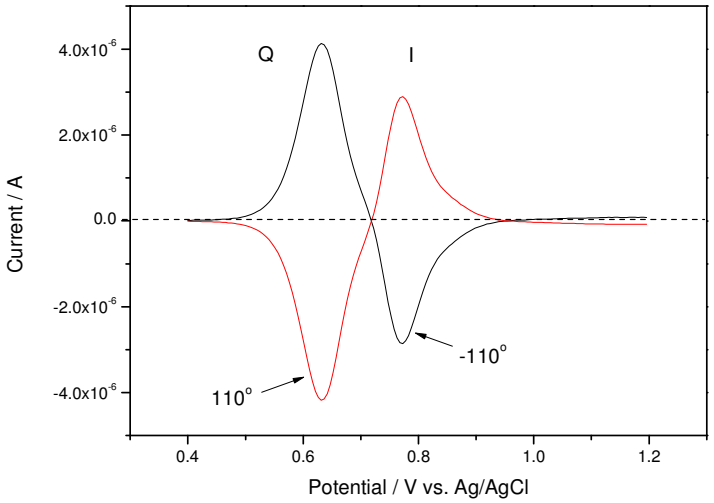

Figure 7.34: SHACV signals obtained for the oxidation of 3 mM DABCO in acetonitrile containing 0.1 M TBAP as supporting electrolyte at a platinum electrode: frequency, 100 Hz, amplitude of the sinusoidal potential, 25 mV: temperature, 298 K.

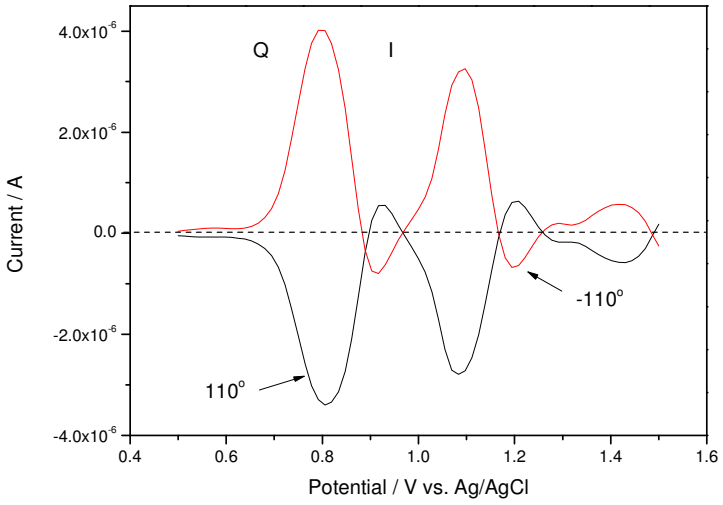

Figure 7.35: SHACV signals obtained for the oxidation of 3 mM 1,2,5-trimethylpyrrole in acetonitrile containing 0.1 M TBAP as supporting electrolyte at a platinum electrode: frequency, 100 Hz, amplitude of the sinusoidal potential, 25 mV: temperature, 298 K.

7.4 Photomodulated Voltammetry

PMV is usually employed to determine the half-wave potentials for the oxidation and reduction of the radicals, especially transient species having lifetime in milli-second range. The voltammogram obtained in PMV experiment very much resembles with steady state voltammogram with S-shaped reduction and oxidation signal and with characteristic diffusion limiting plateaus.

We have recorded a normal cyclic voltammogram just to check whether direct oxidation and reduction of precursors, solvent impurities occur, which can limit the possibility of extracting the modulated signal. Fortunately most compounds are harder to reduce and oxidize than their corresponding radicals; in cases where this is reversed PMV cannot be used. No polarogams were detected by the phase-sensitive method, in the absence of photolysis or of the radical precursors. When the lock-in-amplifier has locked on to the target signal a scan is performed in the desired potential range usually at sweep rates in the range of 0.05-0.2V. The concentration of the radicals generated by modulated photolysis in the PMV experiment oscillates at the same frequency as the light beam. While the potential is scanned between certain limits, oxidation or reduction of the radicals may occur producing a small alternating current (ac) detected by the lock-in-amplifier. The resulting PMV voltammogram has a typically sigmoid shape like shown in **Figure 5.2**.

The measurements can be separated from other contributions by the use of phase-sensitive detector which only detects signals that oscillate at the modulation frequency. Driving an experiment at a fixed frequency coupled with phase-sensitive detection can lead to enhancement in signal to noise of several orders of magnitude, and in this instance it allowed the detection of free radicals under conditions where their average concentration was ca. 10^{-7}-10^{-8} M and the average lifetime ca. 10^{-3}s. However, in practice these systems are slightly more complicated that this simple analysis would suggest.

Photomodulated voltammograms of the reduction and oxidation of the following compounds, 1,3-diphenylacetone, 1,1,3,3-tetraphenylacetone, diphenyl disulfide, mixture of 0.5 M acetone and 1.0 M 2-propanol, glycine anhydride and alanine anhydride were recorded.

Unfortunately we have not succeeded in getting half-wave potentials of above mentioned compound using photomodulated voltammetry. We have some results but we are not sure about their accurateness. One of the photomodulated voltammogram obtained for triphenylacetone is represented in **Figure 7.36**. We are working on the problems and hopefully we will do some more experiments in near future.

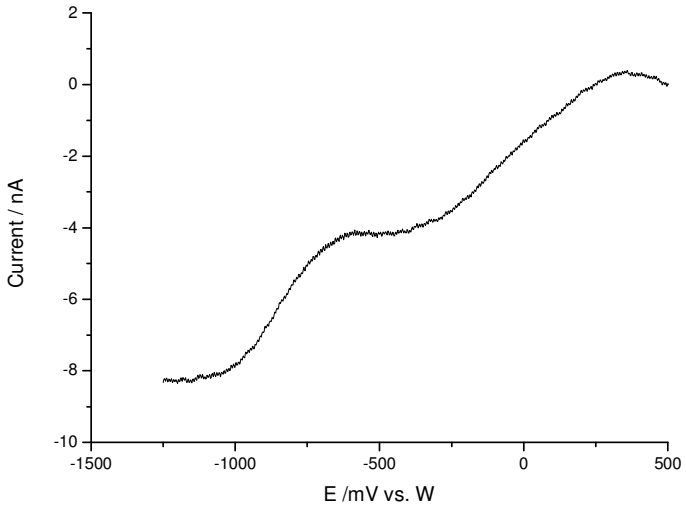

Figure 7.36: Photomodulated voltammogram of the triphenylacetone; 10 mM in acetonitrile with 0.1 M TBATFB, chopper frequency, 120 Hz; phase setting, 180^{o}; v = 15 mVs^{-1}.

Chapter 8. Conclusion and Outlook

Bad times have a scientific value.
There are occasions a good
learner would not miss.

(*Ralph Waldo Emerson*)

8.1 Conclusion

We have shown that the free energy relationships can be utilized to determine the half-wave oxidation/reduction potential of irreversible electrochemical systems. In the context of the free energy relationships, the relation between oxidation peak potential and half-wave oxidation potential has been established. From the analysis of cyclic voltammogram obtained for a compound at different sweep rate, values such as peak potentials and electron transfer coefficient have been extracted. These values were plotted e.g., peak potential vs. electron transfer coefficient. The half-wave potentials were obtained from the intercept of the plot between peak potential vs. electron transfer coefficient.

In summary, 16 compounds of various classes including methoxybenzenes, aromatic amines, and pyrroles have been measured with this methodology. Reliable values of redox potentials in irreversible systems were obtained for these compounds based on the free energy relationships.

Cyclic voltammetry indeed is the most widely used electrochemical technique. The technique is mainly used in fundamental and applied research. In the foregoing section, we have shown that how cyclic voltammetry can be used to study and detect biologically relevant compounds. Based on the free energy relationships (as mentioned above), the study was conducted to obtain half-wave potentials at different pH values. No such type of study was reported previously. Following biologically relevant reductive quenchers e.g., adenine, adenosine, thymine, thymidine, alanine, histidine, and methionine have been measured for their thermodynamic half-wave potentials. No oxidation peaks were observed for adenine, thymidine and alanine at glassy carbon electrode in the whole range of pH such as 2-12. Other four compounds gave well-

defined anodic wave in the positive potential. In addition, two oxidative quenchers such as 2,2`-Bipyridine, and 4,4`-benzophenone tetracarboxylic acid have also been studied. Both compounds have shown well-defined reduction wave. Thus we conclude that cyclic voltammetric analysis of these compounds at glassy carbon electrode offers the possibility of rapid and easy determination of half-wave reversible potential at different pH values.

From the results obtained using phase-selective second harmonic ac voltammetry it is infer that the technique provide a superior approach of directly measuring the reversible half-wave potentials relative to the well known dc and fundamental harmonic ac methods. For the systems in which the products of the electrode reaction are kinetically very unstable phase-selective second-harmonic ac voltammetry is the method of choice for obtaining precise thermodynamic potentials. The work also suggests that care must be taken when evaluate the redox potentials from the zero current crossing point if not you will end with wrong values. The next point which is of interest to us is that the potentials obtained from phase-selective second-harmonic ac voltammetry are in good agreement with the data derived from cyclic voltammetry within the error limits.

Finally a custom made photomodulated voltammetry has also been employed for determining the half-wave potentials of transient species. We have tried to find electrochemical oxidation and reduction potentials of 5-6 carbon-centerd free radicals by modulated photochemical generation. But we were not successful in implementation of the instrument correctly due to some unknown circumstances. Photomodulated voltammetry is still a relatively new technique for the detection of transient species with lifetime in milli-second and we need to understand the potential it has.

8.2 Outlook

The work described in this thesis prompts us to focus our attentions to one of the very interesting and fascinating idea. We have derived the relations for the experimental determination of half-wave potential for irreversible electrochemical systems using cyclic voltammetry. We have also utilized the phase-selective second-harmonic ac voltammetery for the same purpose. In the end we made an attempt for having redox potentials of transient species by photomodulated voltammetry. In principle the half-

wave redox potential can be measured by utilizing all three above mentioned techniques.

On the other hand instead of employing three different methodologies separately, one can apply phase-selective second-harmonic ac voltammetry.[xxi] Certain advantages it can offer over others are

- Low background current
- Zero double layer charging current
- High sensitivity to kinetic influences
- Quick and precise measurements of half-wave reversible potentials from the zero current crossing point of I and Q components even in the presence of rapid, irreversible follow-up chemical reactions.
- Also noteworthy is the independence of redox potential on electrode material
- Reactive intermediates having half-life in the order of 10^{-4}s can easily be determined.
- Less perturbed by the follow-up chemical reaction than the normal dc and fundamental ac voltammetry.

And this amazing opportunity left spaces for many more interesting experiments in future.

[xxi] Radicals generated by photolysis can be detected using second-harmonic ac voltammetry.

Chapter 9. Appendix A

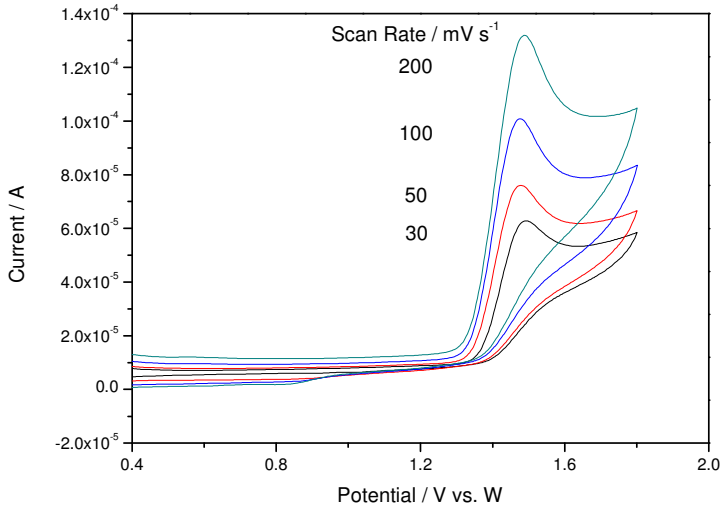

Figure 9.1: Cyclic voltammogram of 3.2 mM 2-methylanisole in MeCN containing 0.1 M TBAP obtained at 298 K.

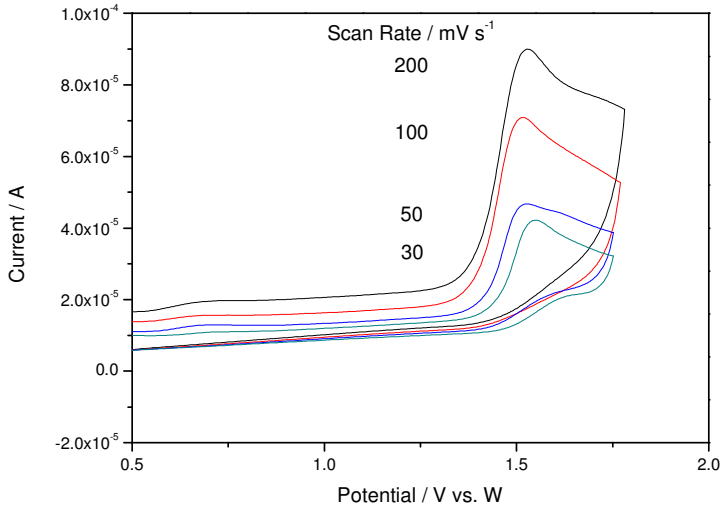

Figure 9.2: Cyclic voltammogram of 3.14 mM 3-methylanisole in MeCN containing 0.1 M TBAP obtained at 298 K.

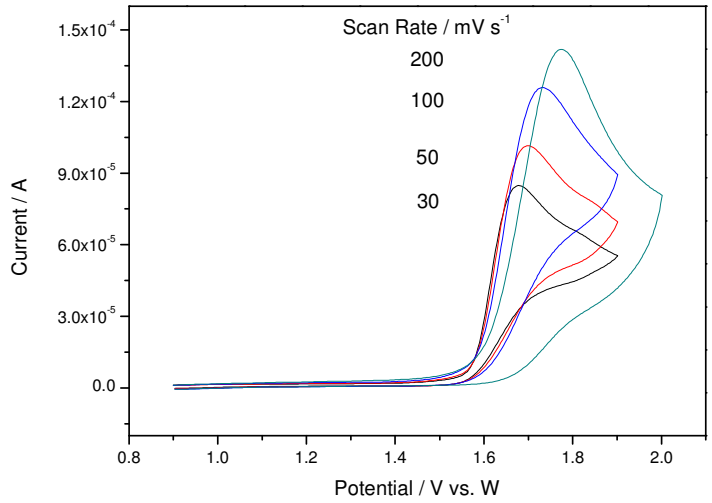

Figure 9.3: Cyclic voltammogram of 3.1 mM 4-methylanisole in MeCN containing 0.1 M TBAP obtained at 298 K.

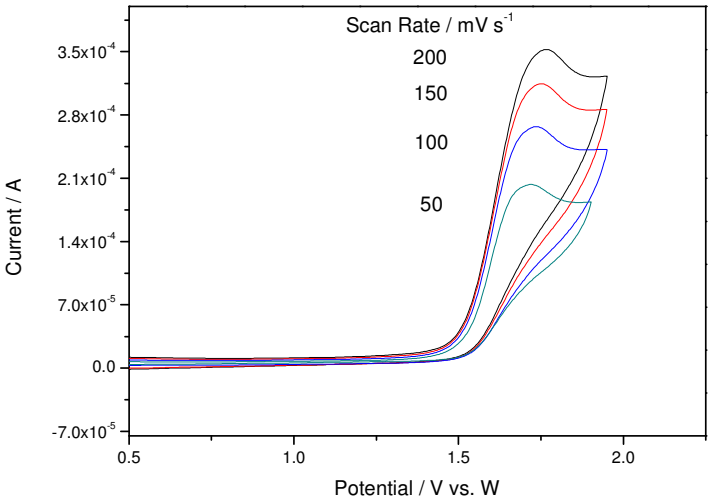

Figure 9.4: Cyclic voltammogram of 3.14 mM 2-bromoanisole in MeCN containing 0.1 M TBAP obtained at 298 K.

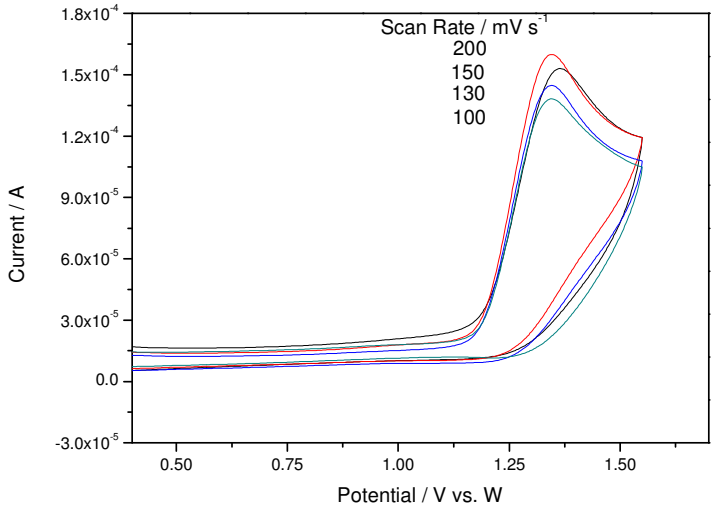

Figure 9.5: Cyclic voltammogram of 3.0 mM 1,3-dimethoxybenzene in MeCN containing 0.1 M TBAP obtained at 298 K.

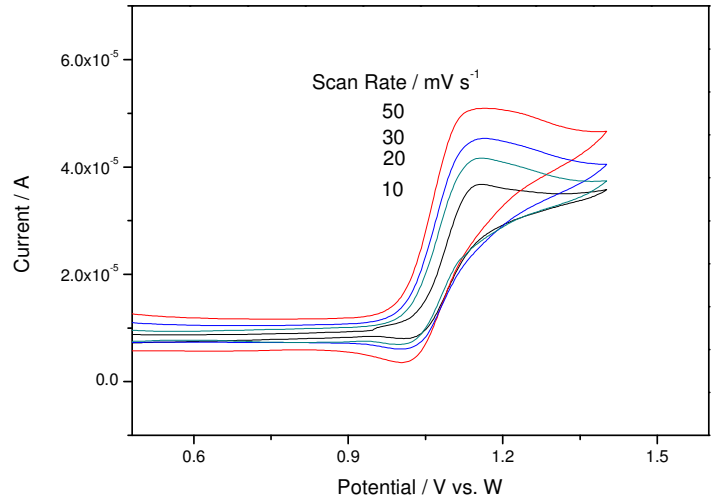

Figure 9.6: Cyclic voltammogram of 3.0 mM 1,4-dimethoxybenzene in MeCN containing 0.1 M TBAP obtained at 298 K.

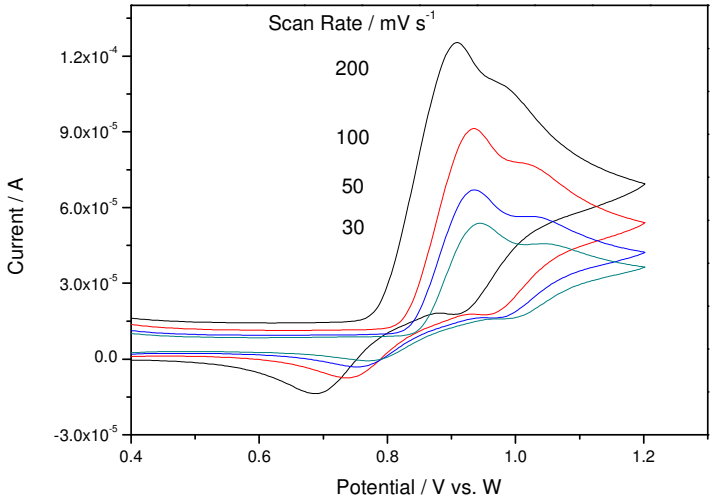

Figure 9.7: Cyclic voltammogram of 2.6 mM 1,2,4-trimethoxybenzene in MeCN containing 0.1 M TBAP obtained at 298 K.

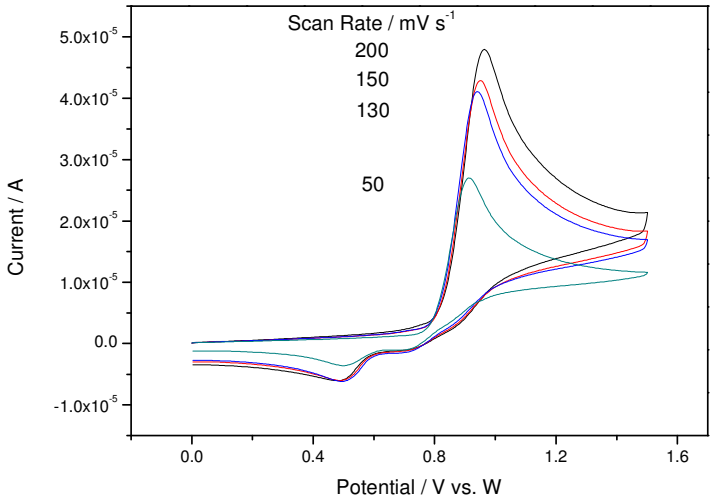

Figure 9.8: Cyclic voltammogram of 2.5 mM N,N´-diethylaniline in MeCN containing 0.1 M TBAP obtained at 298 K.

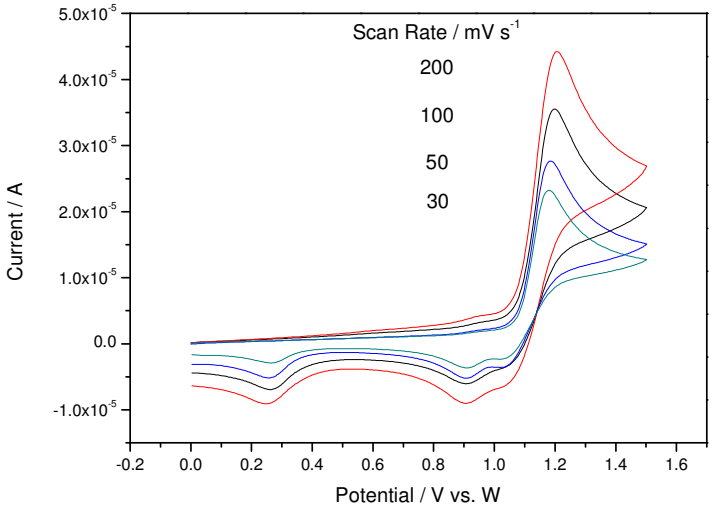

Figure 9.9: Cyclic voltammogram of 2 mM triphenylamine in MeCN containing 0.1 M TBAP obtained at 298 K.

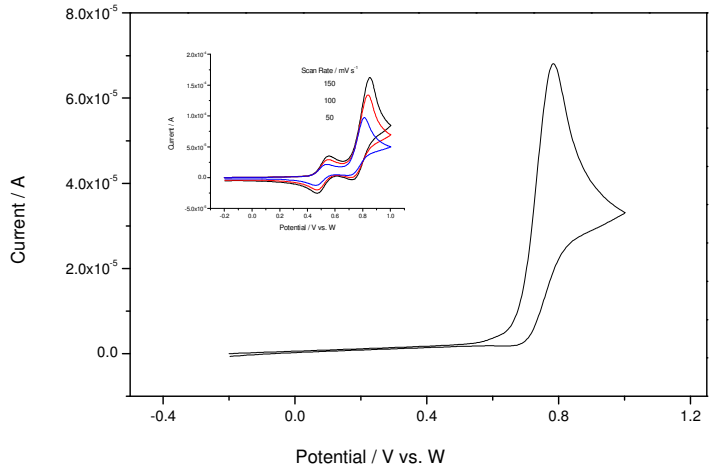

Figure 9.10: Cyclic voltammogram of 3 mM DABCO in MeCN containing 0.1 M TBAP obtained at 298 K.

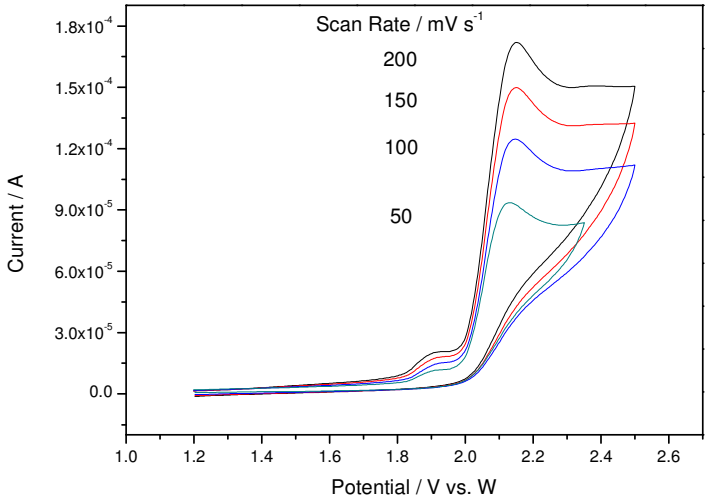

Figure 9.11: Cyclic voltammogram of 1 mM PTPA in MeCN containing 0.1 M TBAP obtained at 298 K.

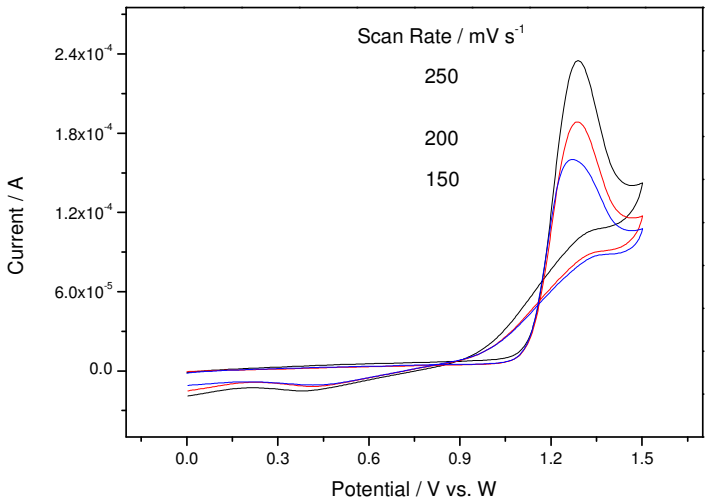

Figure 9.12: Cyclic voltammogram of 3.5 mM N-methylpyrrole in MeCN containing 0.1 M TBAP obtained at 298 K.

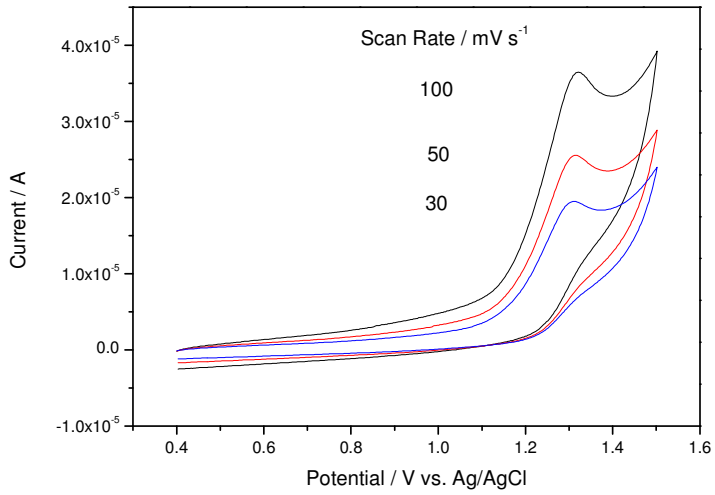

Figure 9.13: Cyclic voltammogram of 1 mM aqueous solution of adenosine containing 0.1 M KNO_3 and 0.01 M phosphate buffer (pH 4) obtained at 298 K.

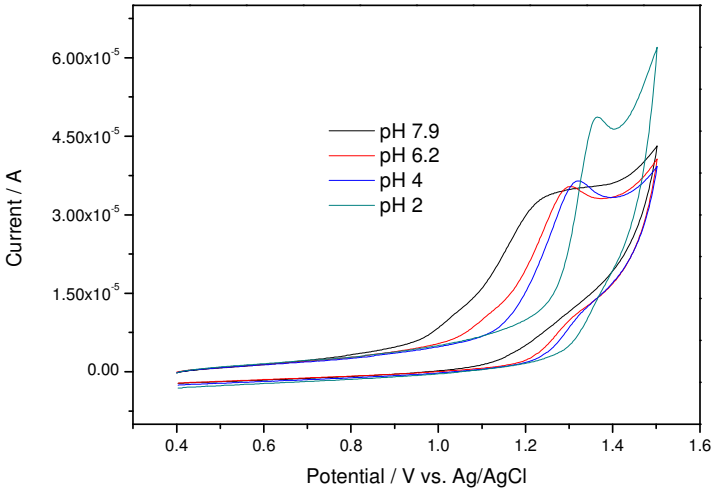

Figure 9.14: Cyclic voltammogram of 1 mM aqueous solution of adenosine containing 0.1 M KNO_3 obtained at 298 K, 100 mVs^{-1}, and at different pH.

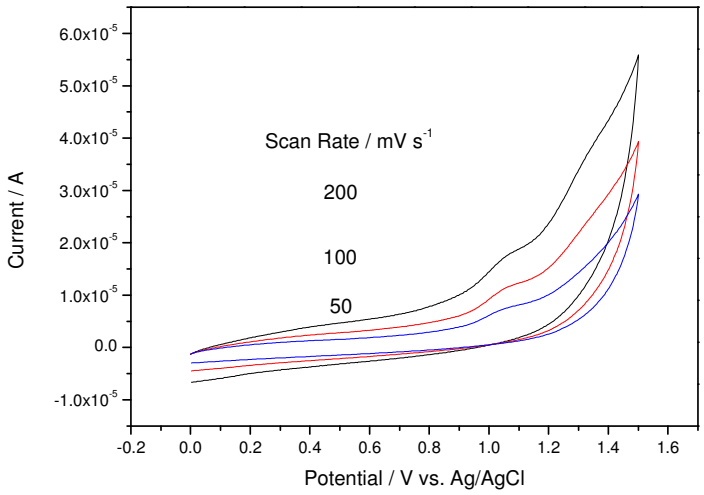

Figure 9.15: Cyclic voltammogram of 1 mM aqueous solution of histidine containing 0.1 M KNO_3 and 0.01 M phosphate buffer (pH 6.1) obtained at 298 K.

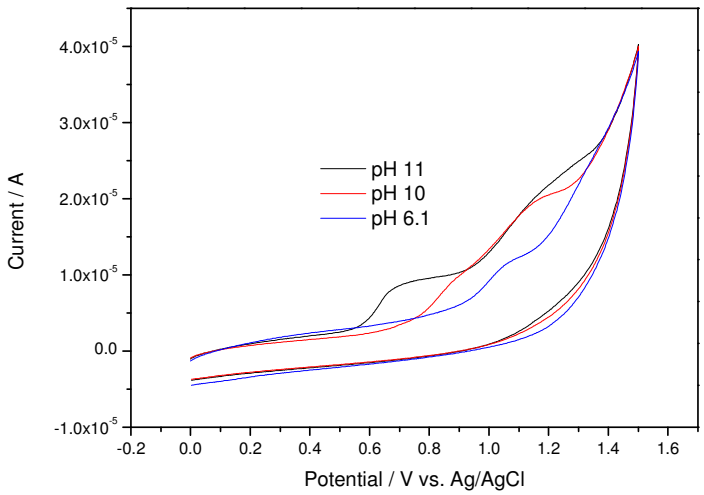

Figure 9.16: Cyclic voltammogram of 1 mM aqueous solution of histidine containing 0.1 M KNO_3 obtained at 298 K, 100 mVs^{-1}, and at different pH.

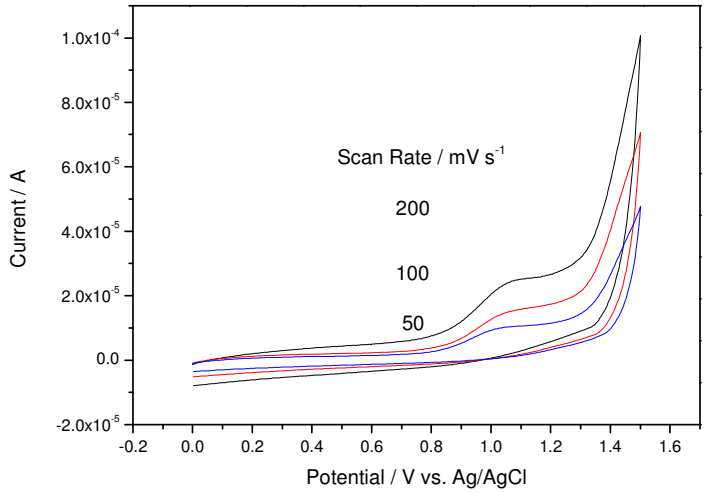

Figure 9.17: Cyclic voltammogram of 1 mM aqueous solution of methionine containing 0.1 M KNO_3 and 0.01 M phosphate buffer (pH 2) obtained at 298 K.

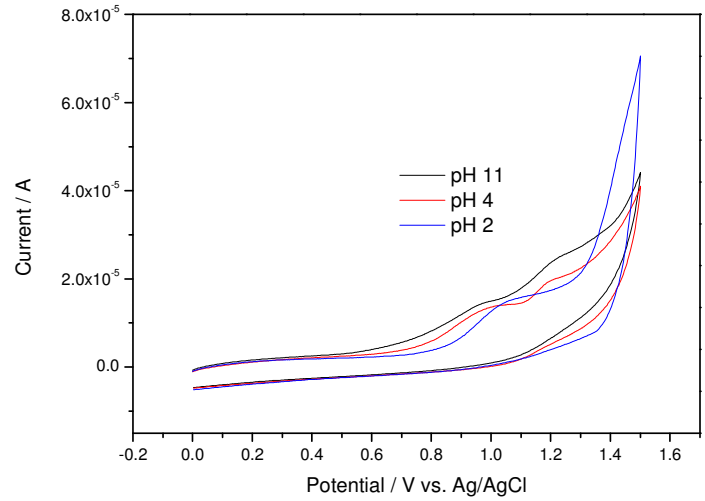

Figure 9.18: Cyclic voltammogram of 1 mM aqueous solution of methionine containing 0.1 M KNO_3 obtained at 298 K, 100 mVs^{-1}, and at different pH.

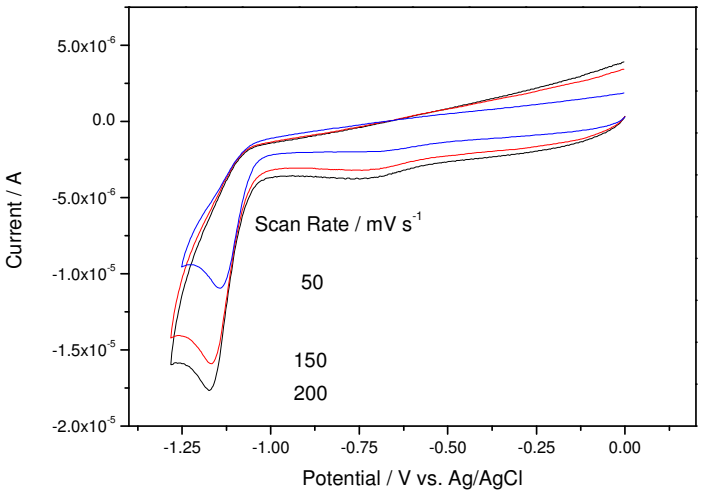

Figure 9.19: Cyclic voltammogram of 1 mM aqueous solution of 2,2´-bipyridine containing 0.1 M KNO_3 and 0.01 M phosphate buffer (pH 2) obtained at 298K.

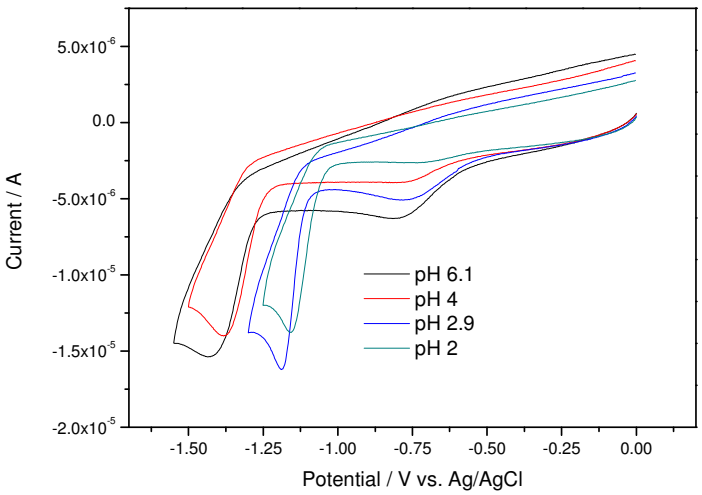

Figure 9.20: Cyclic voltammogram of 1 mM aqueous solution of 2,2´-bipyridine containing 0.1 M KNO_3 obtained at 298K, 100 mVs^{-1}, and at different pH.

Chapter 10. Appendix B

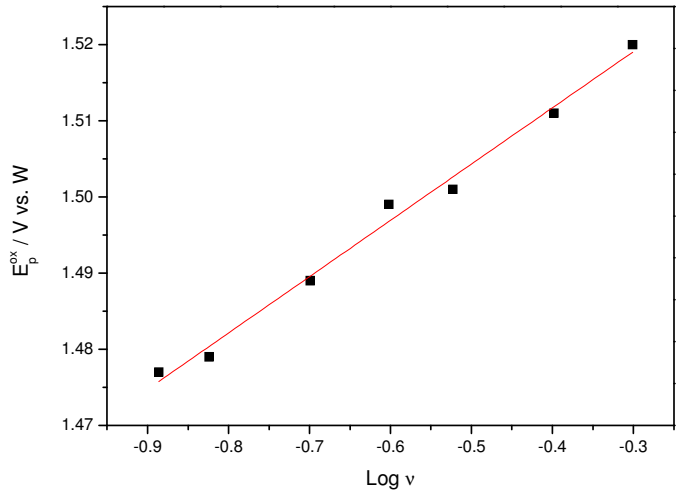

Figure 10.1: Variation of anodic peak potential E_p^{ox} with CV sweep rate at a platinum electrode at 298 K in acetonitrile solution containing 0.1 M TBAP and 3.2 mM 2-methylanisole.

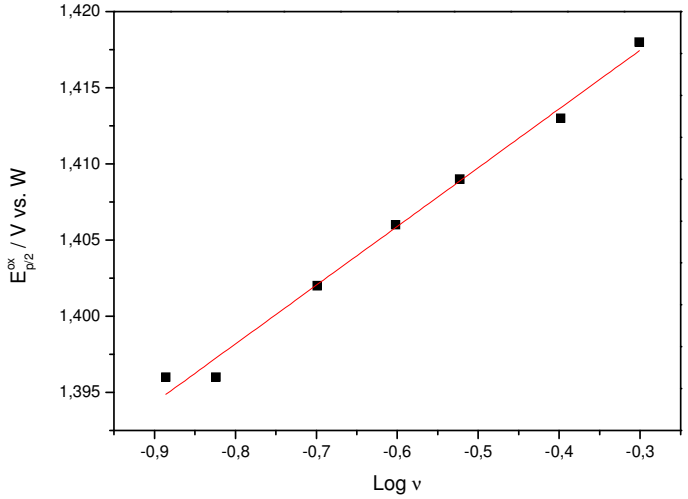

Figure 10.2: Variation of anodic peak potential $E_{p/2}^{ox}$ with CV sweep rate at a platinum electrode at 298 K in acetonitrile solution containing 0.1 M TBAP and 3.2 mM 2-methylanisole.

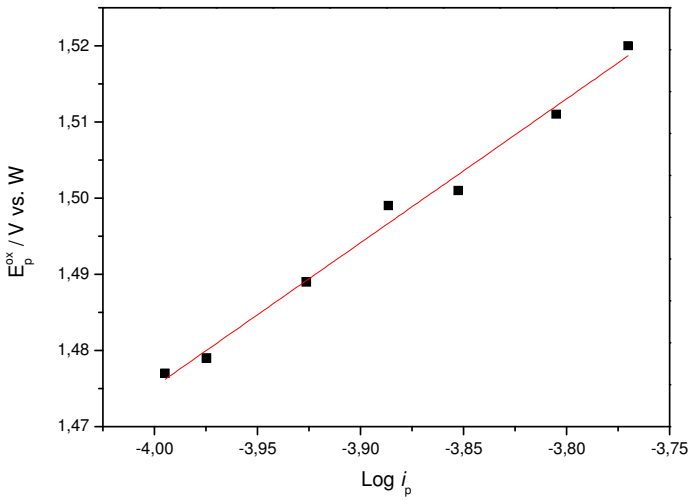

Figure 10.3: Variation of anodic peak potential E_p^{ox} with peak current at a platinum electrode at 298 K in acetonitrile solution containing 0.1 M TBAP and 3.2 mM 2-methylanisole.

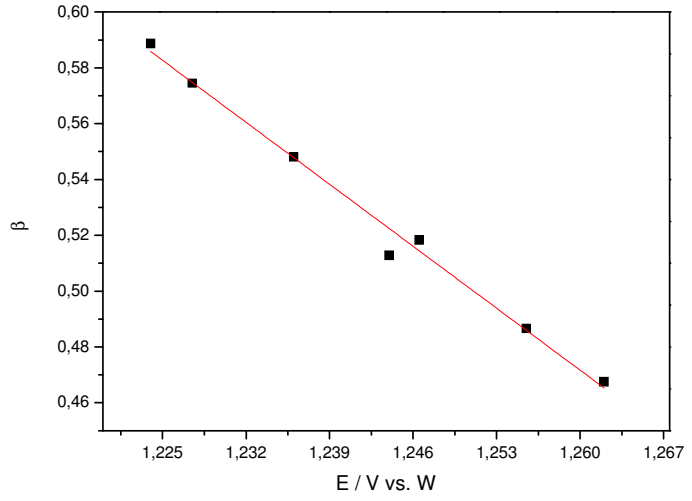

Figure 10.4: Dependence of the heterogeneous electron transfer beta with the applied electrode potential E for the 2-methylanisole.

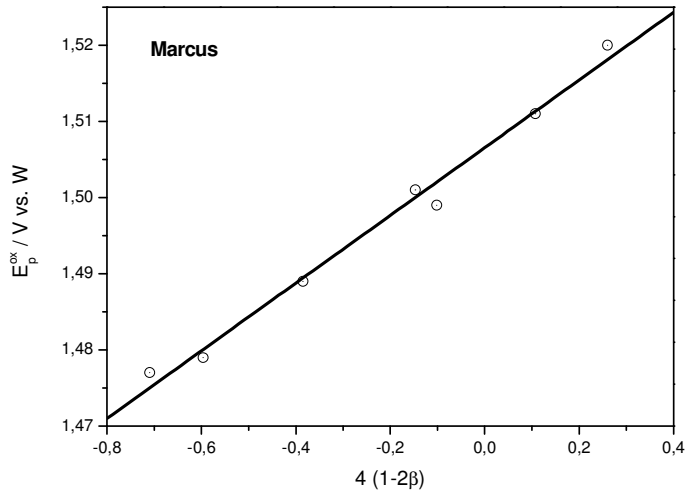

Figure 10.5: The oxidation peak potential E_p^{ox} of 2-methylanisole plotted as a function of the transfer coefficient β based on the Marcus free energy relationship, see equation (2.45).

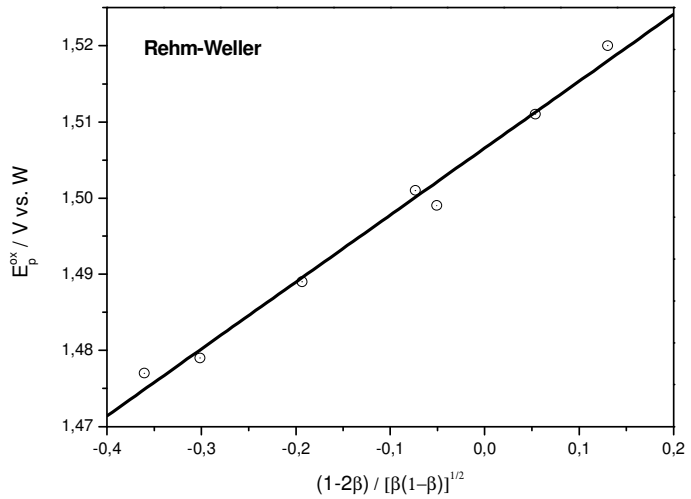

Figure 10.6: The oxidation peak potential E_p^{ox} of 2-methylanisole plotted as a function of the transfer coefficient β based on the Rehm-Weller free energy relationship, see equation (2.43).

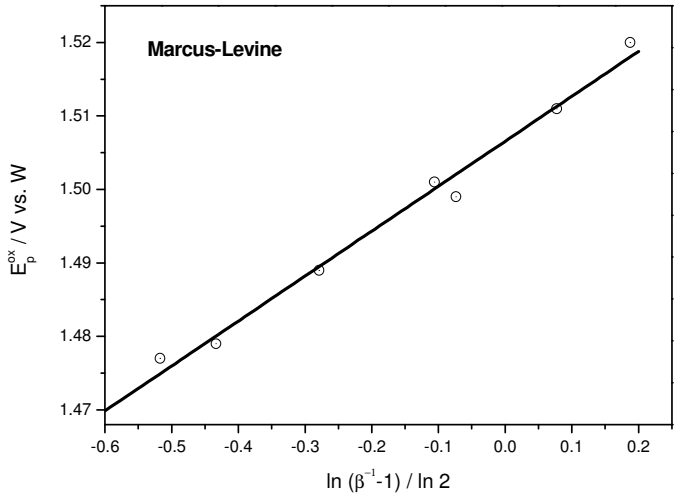

Figure 10.7: The oxidation peak potential E_p^{ox} of 2-methylanisole plotted as a function of the transfer coefficient β based on the Marcus-Levine free energy relationship, see equation (2.46).

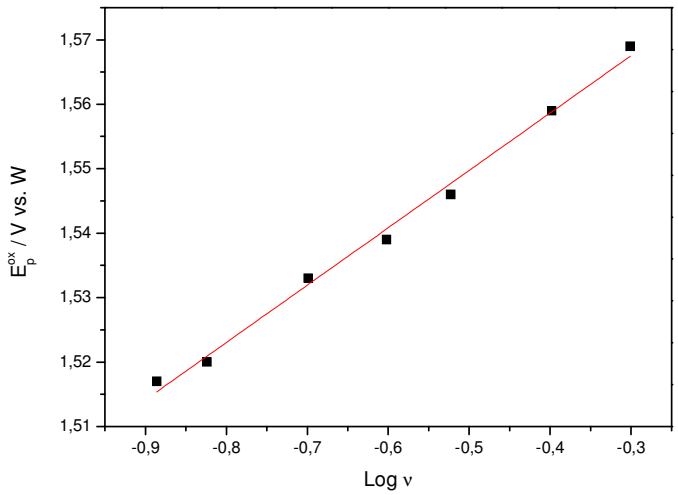

Figure 10.8: Variation of anodic peak potential E_p^{ox} with CV sweep rate at a platinum electrode at 298 K in acetonitrile solution containing 0.1 M TBAP and 3.1 mM 3-methylanisole.

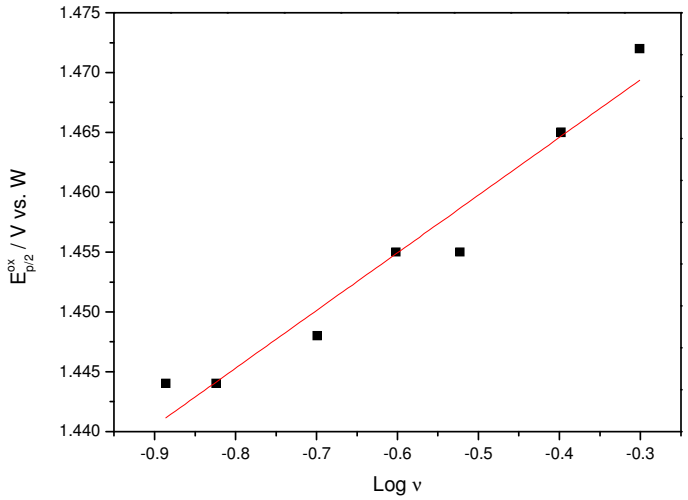

Figure 10.9: Variation of anodic peak potential $E^{ox}_{p/2}$ with CV sweep rate at a platinum electrode at 298 K in acetonitrile solution containing 0.1 M TBAP and 3.1 mM 3-methylanisole.

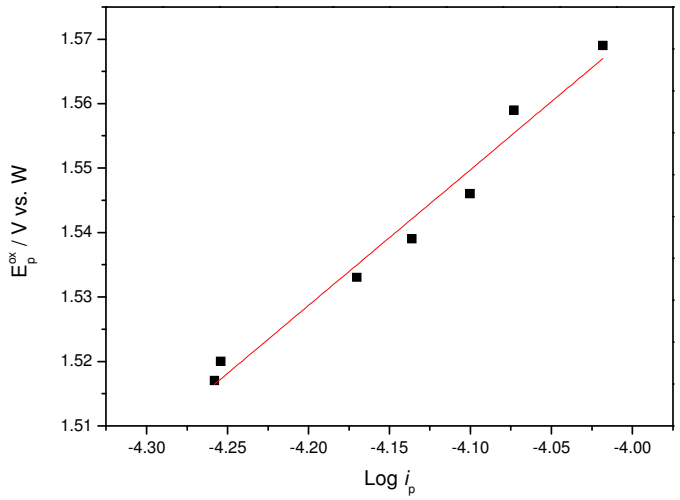

Figure 10.10: Variation of anodic peak potential E^{ox}_{p} with peak current at a platinum electrode at 298 K in acetonitrile solution containing 0.1 M TBAP and 3.1 mM 3-methylanisole.

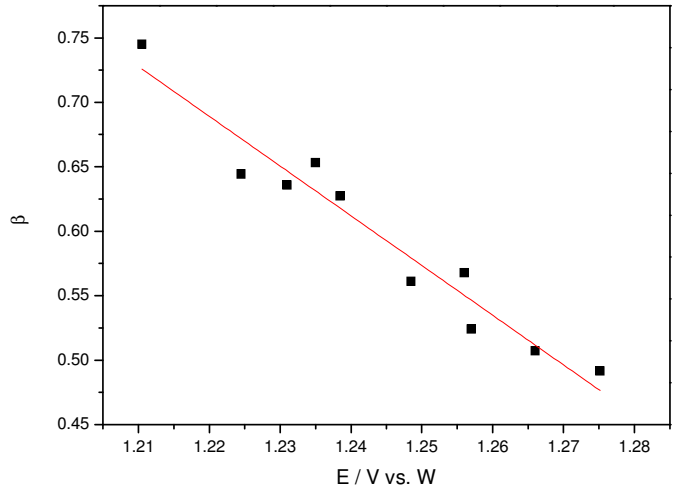

Figure 10.11: Dependence of the heterogeneous electron transfer beta with the applied electrode potential E for the 3-methylanisole.

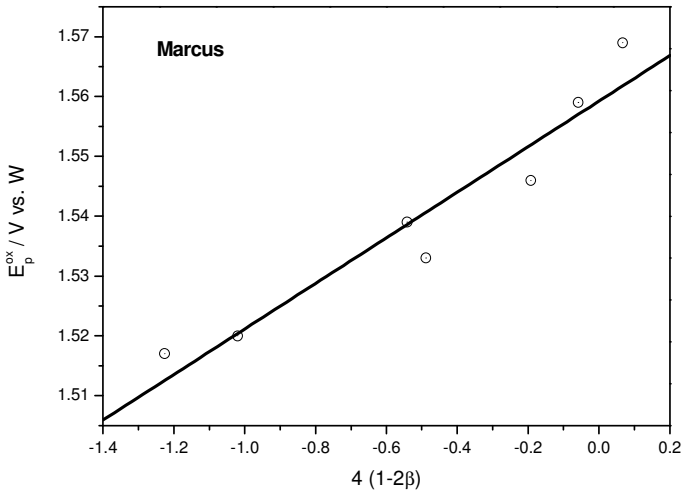

Figure 10.12: The oxidation peak potential E_p^{ox} of 3-methylanisole plotted as a function of the transfer coefficient β based on the Marcus free energy relationship, see equation (2.45).

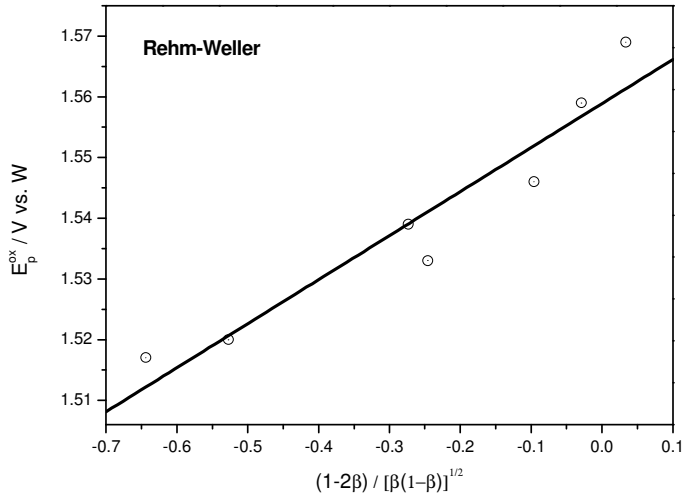

Figure 10.13: The oxidation peak potential E_p^{ox} of 3-methylanisole plotted as a function of the transfer coefficient β based on the Rehm-Weller free energy relationship, see equation (2.43).

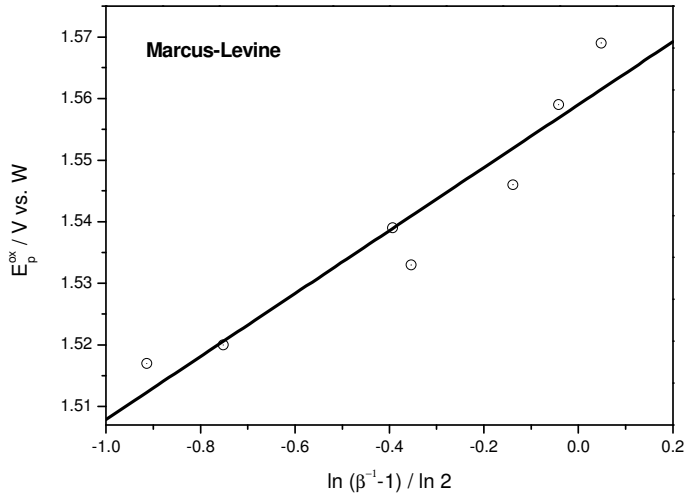

Figure 10.14: The oxidation peak potential E_p^{ox} of 3-methylanisole plotted as a function of the transfer coefficient β based on the Marcus-Levine free energy relationship, see equation (2.46).

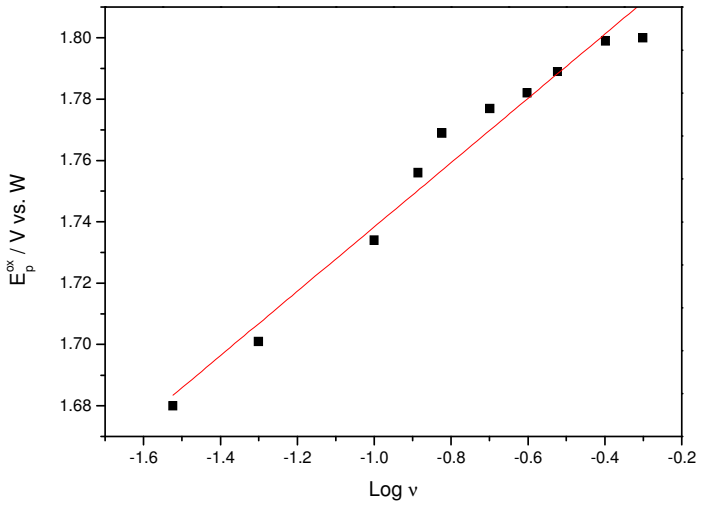

Figure 10.15: Variation of anodic peak potential E_p^{ox} with CV sweep rate at a platinum electrode at 298 K in acetonitrile solution containing 0.1 M TBAP and 3.1 mM 4-methylanisole.

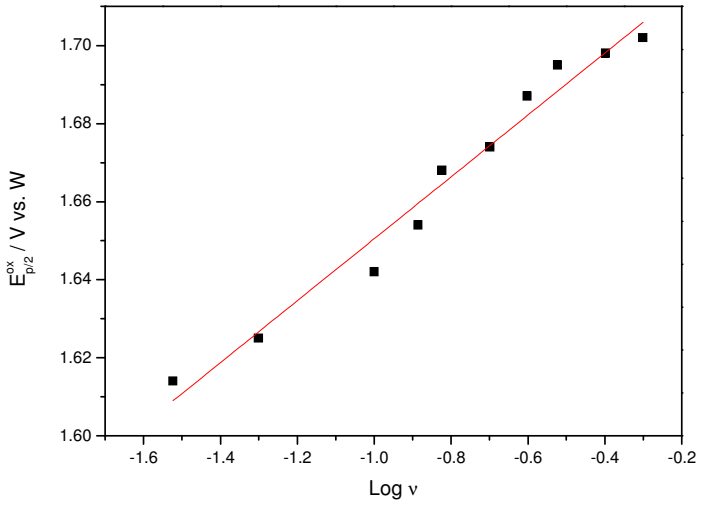

Figure 10.16: Variation of anodic peak potential $E_{p/2}^{ox}$ with CV sweep rate at a platinum electrode at 298 K in acetonitrile solution containing 0.1 M TBAP and 3.1 mM 4-methylanisole.

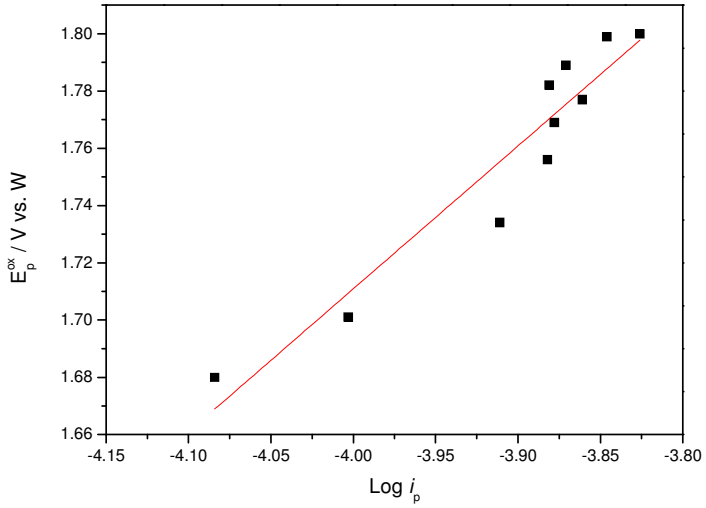

Figure 10.17: Variation of anodic peak potential E_p^{ox} with peak current at a platinum electrode at 298 K in acetonitrile solution containing 0.1 M TBAP and 3.1 mM 4-methylanisole.

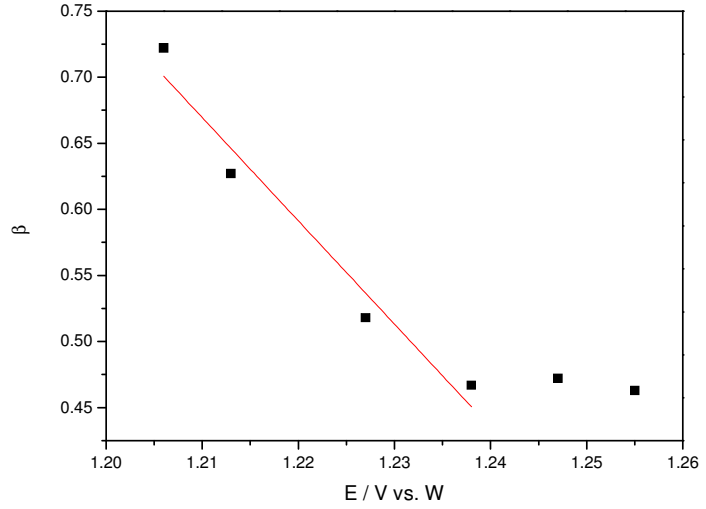

Figure 10.18: Dependence of the heterogeneous electron transfer beta with the applied electrode potential E for the 4-methylanisole.

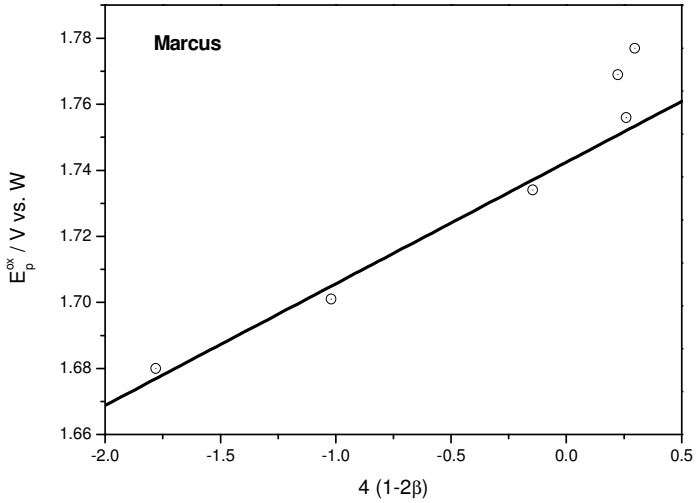

Figure 10.19: The oxidation peak potential E_p^{ox} of 4-methylanisole plotted as a function of the transfer coefficient β based on the Marcus free energy relationship, see equation (2.45).

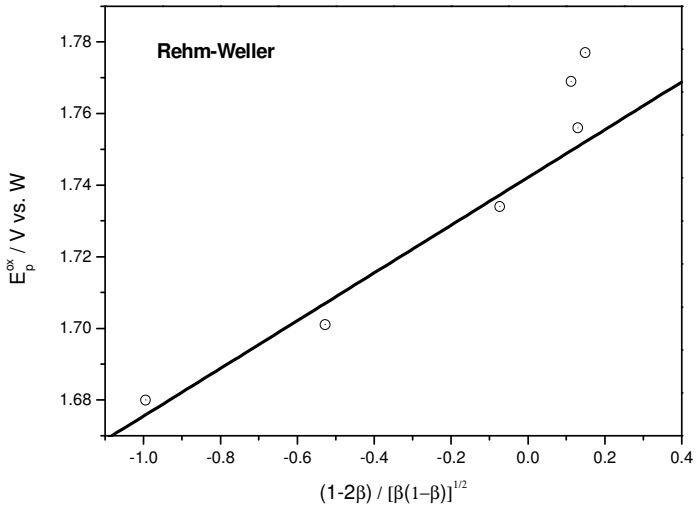

Figure 10.20: The oxidation peak potential E_p^{ox} of 4-methylanisole plotted as a function of the transfer coefficient β based on the Rehm-Weller free energy relationship, see equation (2.43).

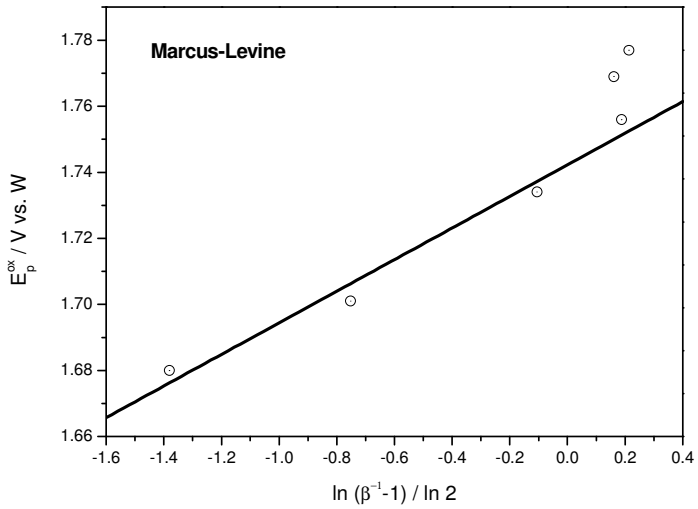

Figure 10.21: The oxidation peak potential E_p^{ox} of 4-methylanisole plotted as a function of the transfer coefficient β based on the Marcus-Levine free energy relationship, see equation (2.46).

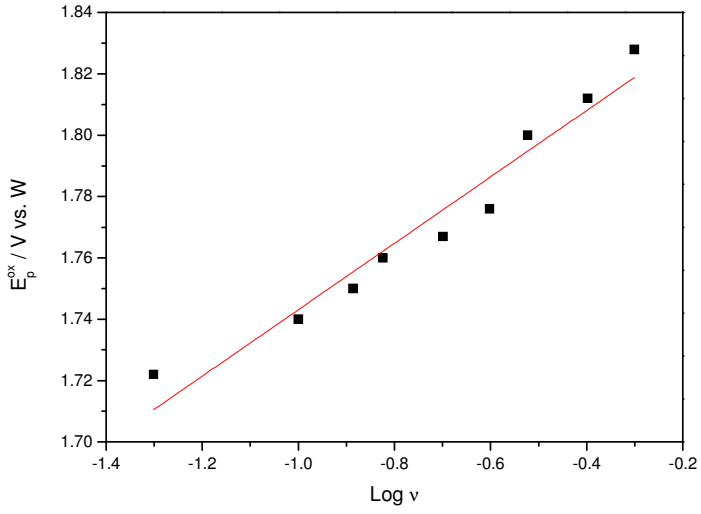

Figure 10.22: Variation of anodic peak potential E_p^{ox} with CV sweep rate at a platinum electrode at 298 K in acetonitrile solution containing 0.1 M TBAP and 3.1 mM 2-bromoanisole.

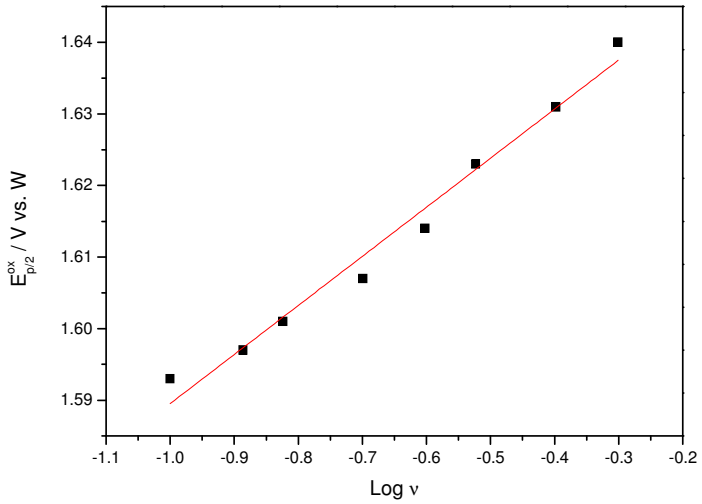

Figure 10.23: Variation of anodic peak potential $E^{ox}_{p/2}$ with CV sweep rate at a platinum electrode at 298 K in acetonitrile solution containing 0.1 M TBAP and 3.1 mM 2-bromoanisole.

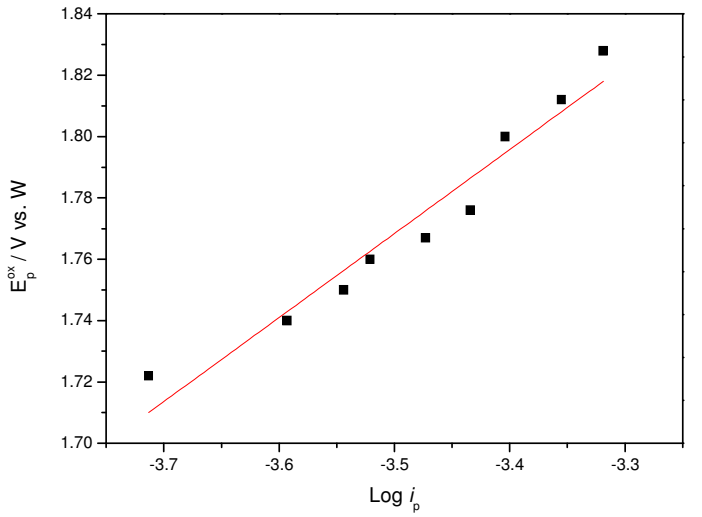

Figure 10.24: Variation of anodic peak potential E^{ox}_{p} with peak current at a platinum electrode at 298 K in acetonitrile solution containing 0.1 M TBAP and 3.1 mM 2-bromoanisole.

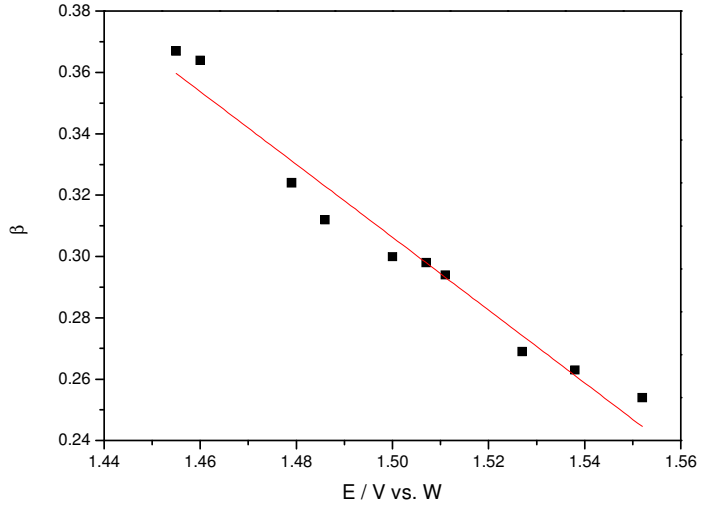

Figure 10.25: Dependence of the heterogeneous electron transfer beta with the applied electrode potential E for the 2-bromoanisole.

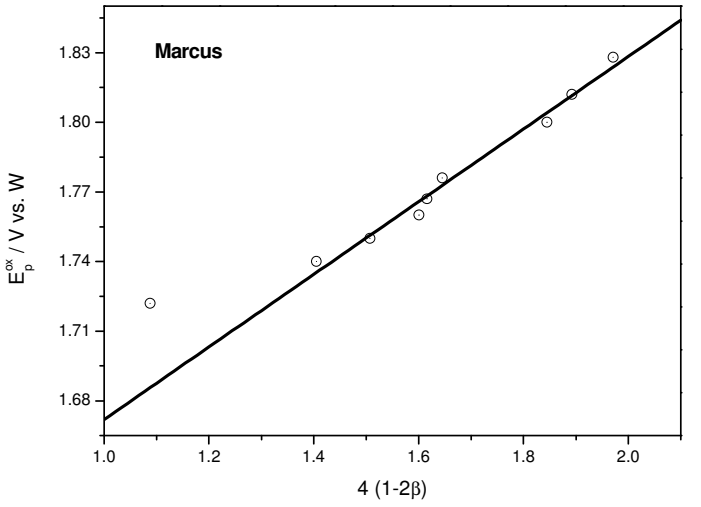

Figure 10.26: The oxidation peak potential E_p^{ox} of 2-bromoanisole plotted as a function of the transfer coefficient β based on the Marcus free energy relationship, see equation (2.45).

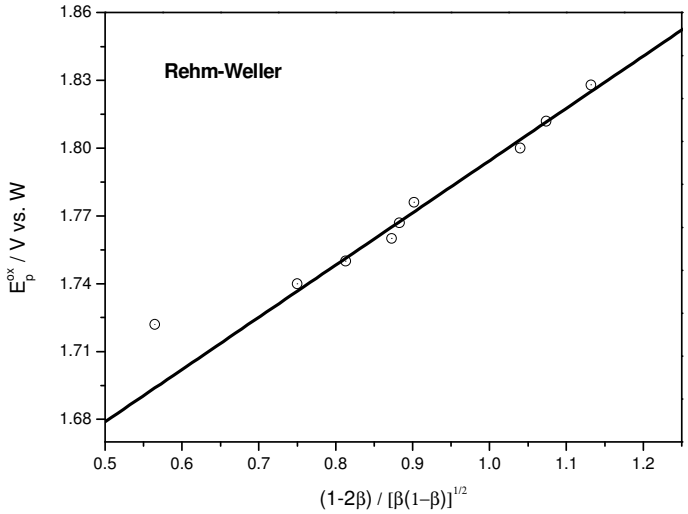

Figure 10.27: The oxidation peak potential E_p^{ox} of 2-bromoanisole plotted as a function of the transfer coefficient β based on the Rehm-Weller free energy relationship, see equation (2.43).

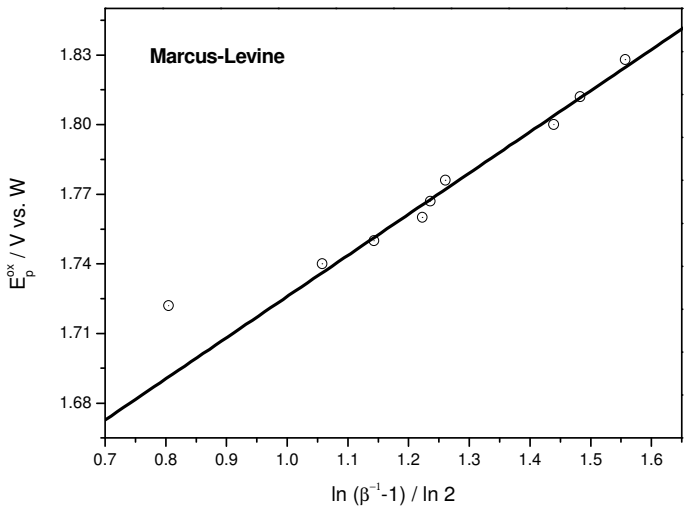

Figure 10.28: The oxidation peak potential E_p^{ox} of 2-bromoanisole plotted as a function of the transfer coefficient β based on the Marcus-Levine free energy relationship, see equation (2.46).

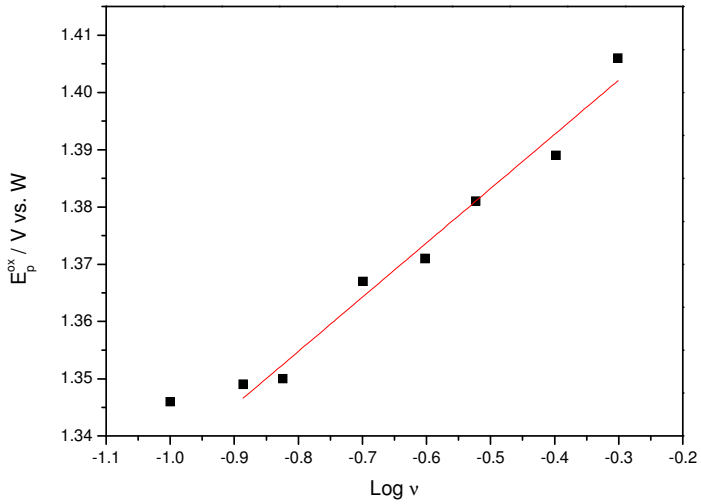

Figure 10.29: Variation of anodic peak potential E_p^{ox} with CV sweep rate at a platinum electrode at 298 K in acetonitrile solution containing 0.1 M TBAP and 3 mM 1,3-dimethoxybenzene.

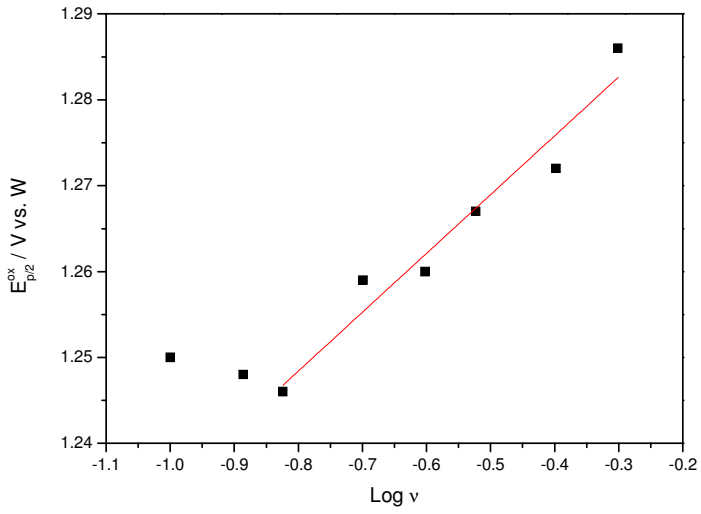

Figure 10.30: Variation of anodic peak potential $E_{p/2}^{ox}$ with CV sweep rate at a platinum electrode at 298 K in acetonitrile solution containing 0.1 M TBAP and 3 mM 1,3-dimethoxybenzene.

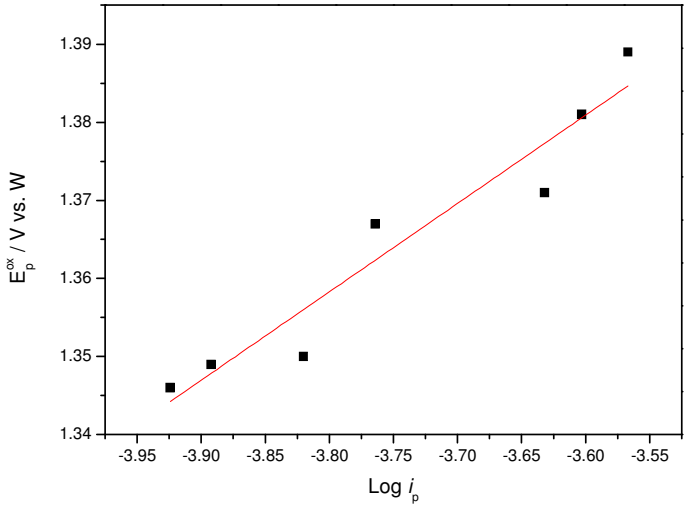

Figure 10.31: Variation of anodic peak potential E_p^{ox} with peak current at a platinum electrode at 298 K in acetonitrile solution containing 0.1 M TBAP and 3 mM 1,3-dimethoxybenzene.

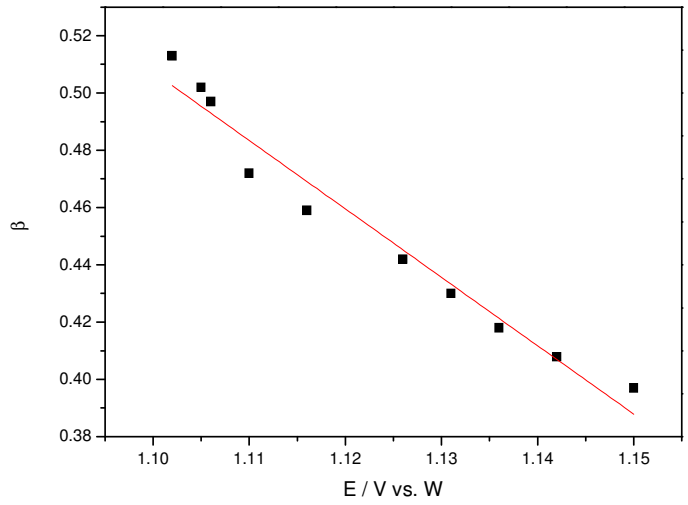

Figure 10.32: Dependence of the heterogeneous electron transfer beta with the applied electrode potential E for the 1,3-dimethoxybenzene.

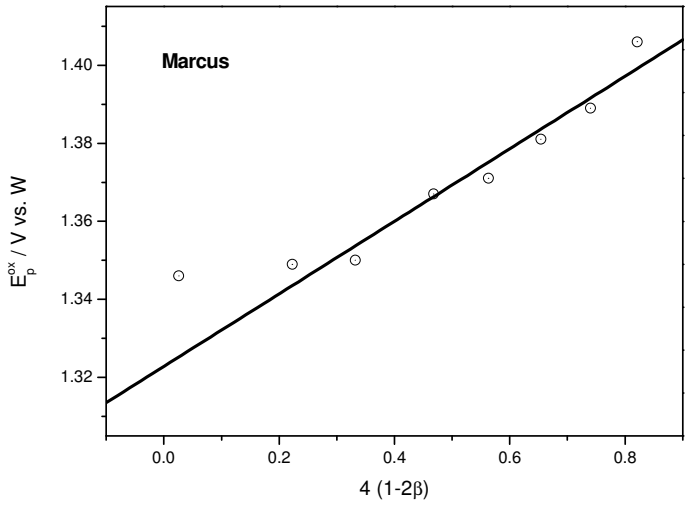

Figure 10.33: The oxidation peak potential E_p^{ox} of 1,3-dimethoxybenzene plotted as a function of the transfer coefficient β based on the Marcus free energy relationship, see equation (2.45).

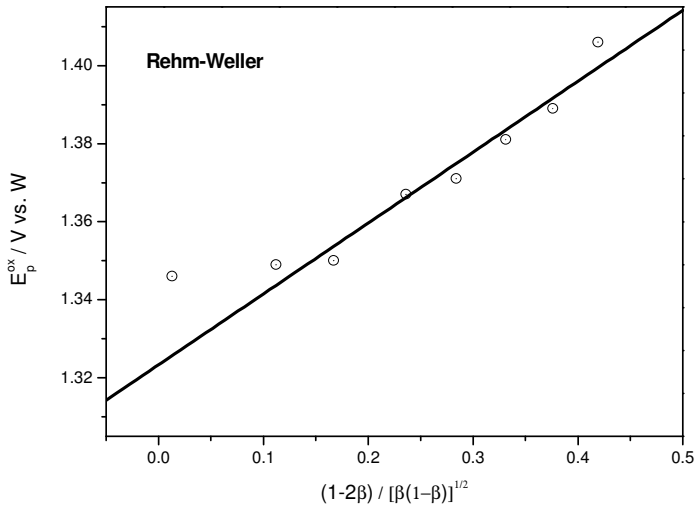

Figure 10.34: The oxidation peak potential E_p^{ox} of 1,3-dimethoxybenzene plotted as a function of the transfer coefficient β based on the Rehm-Weller free energy relationship, see equation (2.43).

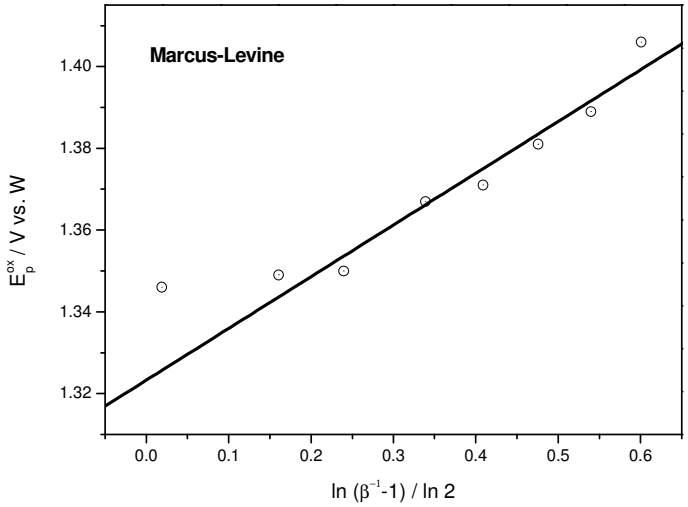

Figure 10.35: The oxidation peak potential E_p^{ox} of 1,3-dimethoxybenzene plotted as a function of the transfer coefficient β based on the Marcus-Levine free energy relationship, see equation (2.46).

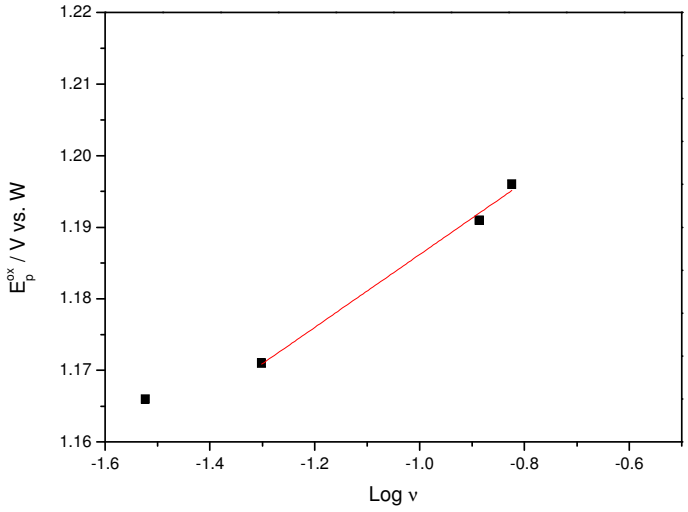

Figure 10.36: Variation of anodic peak potential E_p^{ox} with CV sweep rate at a platinum electrode at 298 K in acetonitrile solution containing 0.1 M TBAP and 3 mM 1,4-dimethoxybenzene.

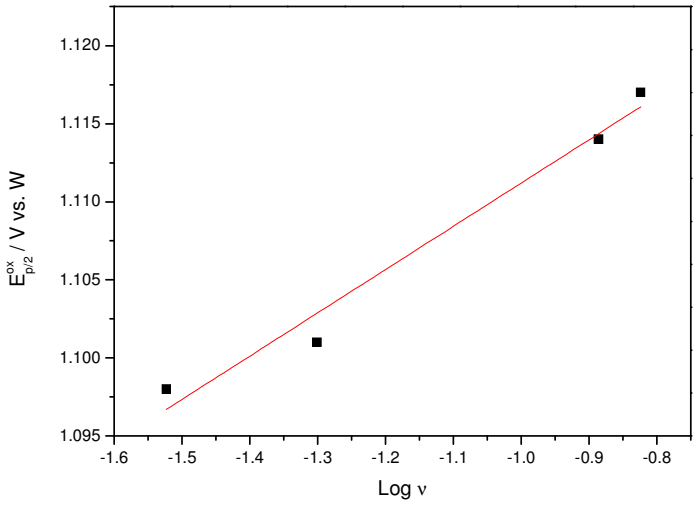

Figure 10.37: Variation of anodic peak potential $E^{ox}_{p/2}$ with CV sweep rate at a platinum electrode at 298 K in acetonitrile solution containing 0.1 M TBAP and 3 mM 1,4-dimethoxybenzene.

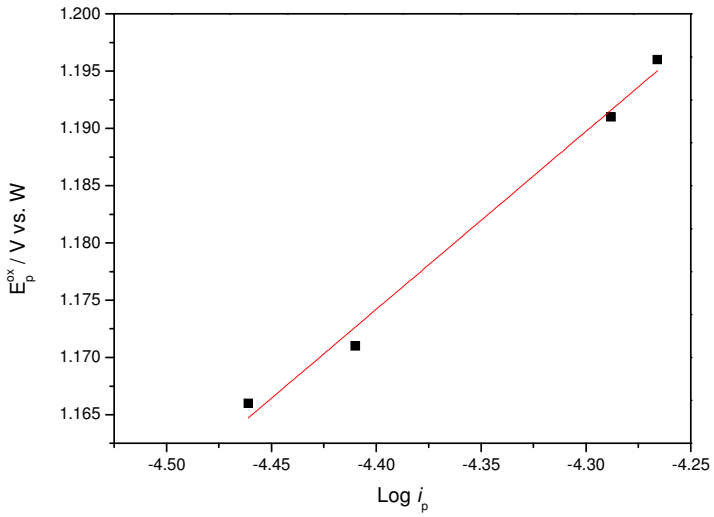

Figure 10.38: Variation of anodic peak potential E^{ox}_{p} with peak current at a platinum electrode at 298 K in acetonitrile solution containing 0.1 M TBAP and 3 mM 1,4-dimethoxybenzene.

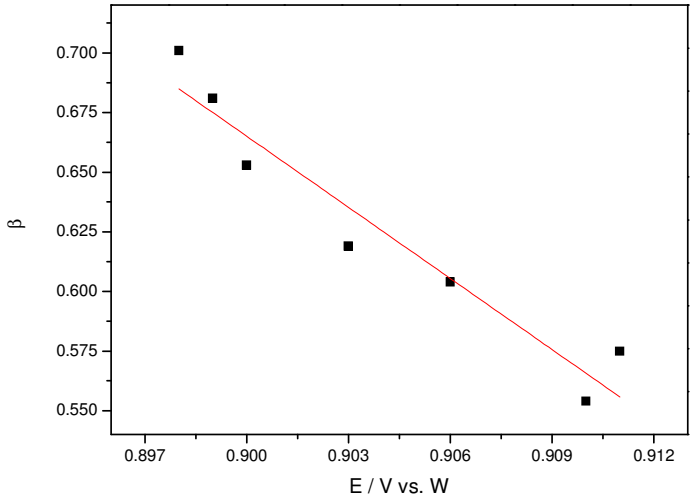

Figure 10.39: Dependence of the heterogeneous electron transfer beta with the applied electrode potential E for the 1,4-dimethoxybenzene.

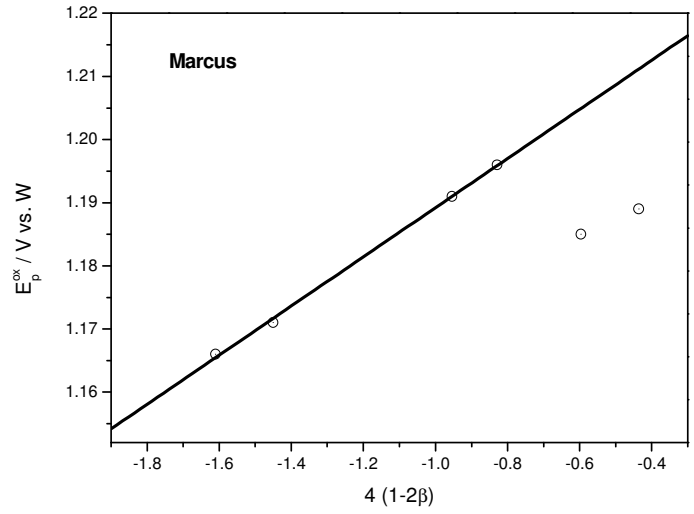

Figure 10.40: The oxidation peak potential E_p^{ox} of 1,4-dimethoxybenzene plotted as a function of the transfer coefficient β based on the Marcus free energy relationship, see equation (2.45).

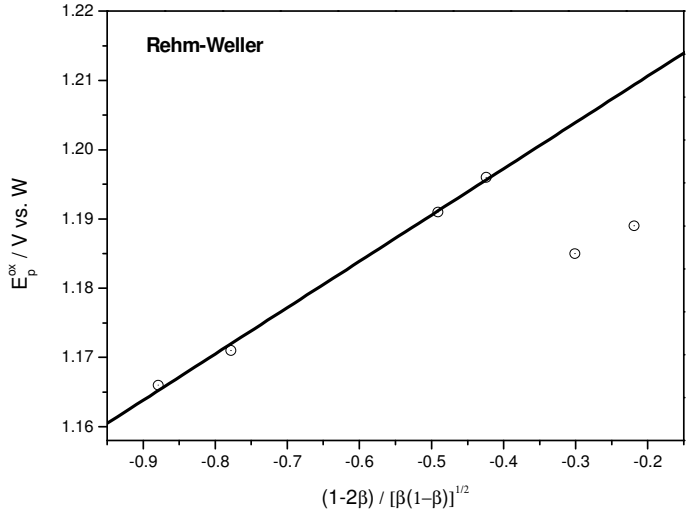

Figure 10.41: The oxidation peak potential E_p^{ox} of 1,4-dimethoxybenzene plotted as a function of the transfer coefficient β based on the Rehm-Weller free energy relationship, see equation (2.43).

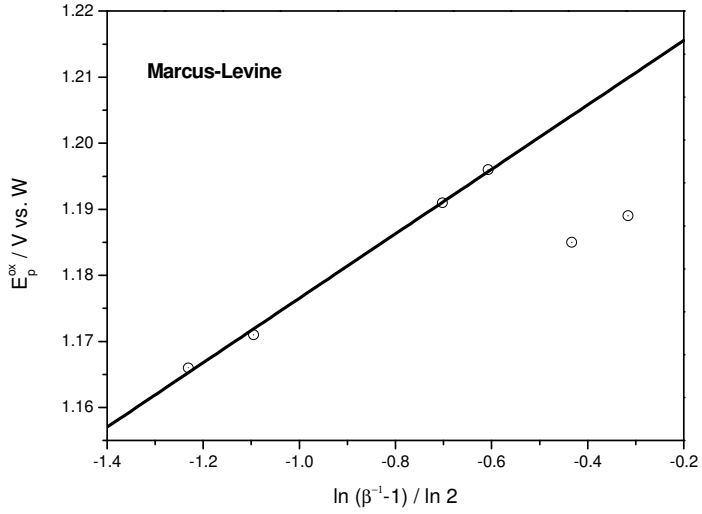

Figure 10.42: The oxidation peak potential E_p^{ox} of 1,4-dimethoxybenzene plotted as a function of the transfer coefficient β based on the Marcus-Levine free energy relationship, see equation (2.46).

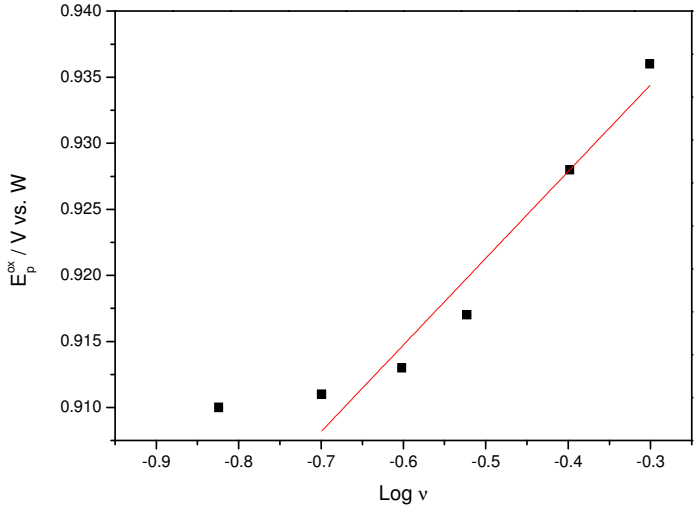

Figure 10.43: Variation of anodic peak potential E_p^{ox} with CV sweep rate at a platinum electrode at 298 K in acetonitrile solution containing 0.1 M TBAP and 2.6 mM 1,2,4-trimethoxybenzene.

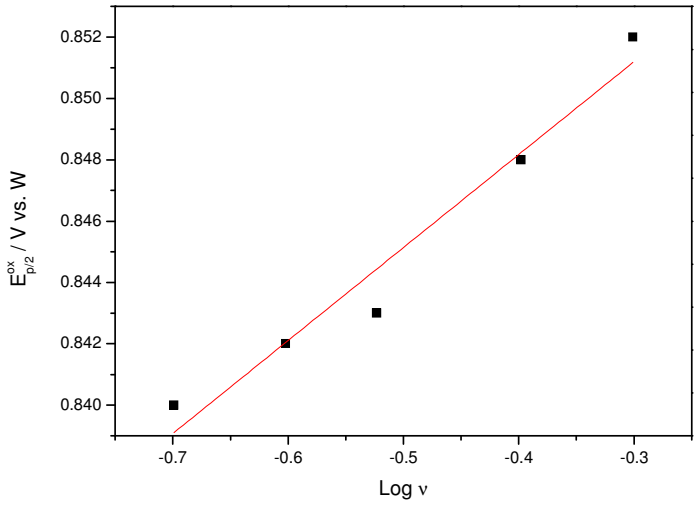

Figure 10.44: Variation of anodic peak potential $E_{p/2}^{ox}$ with CV sweep rate at a platinum electrode at 298 K in acetonitrile solution containing 0.1 M TBAP and 2.6 mM 1,2,4-trimethoxybenzene.

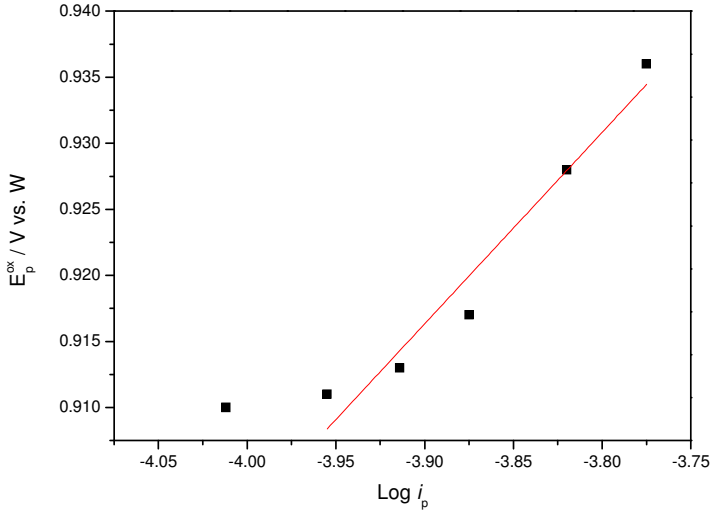

Figure 10.45: Variation of anodic peak potential E_p^{ox} with peak current at a platinum electrode at 298 K in acetonitrile solution containing 0.1 M TBAP and 2.6 mM 1,2,4-trimethoxybenzene.

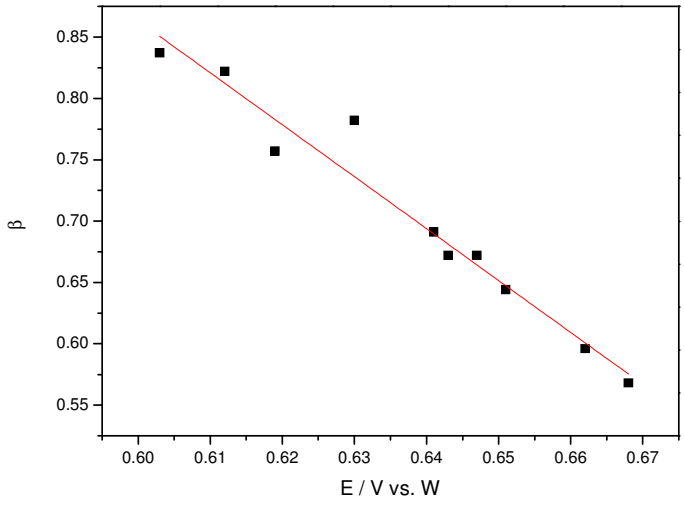

Figure 10.46: Dependence of the heterogeneous electron transfer beta with the applied electrode potential E for the 1,2,4-trimethoxybenzene.

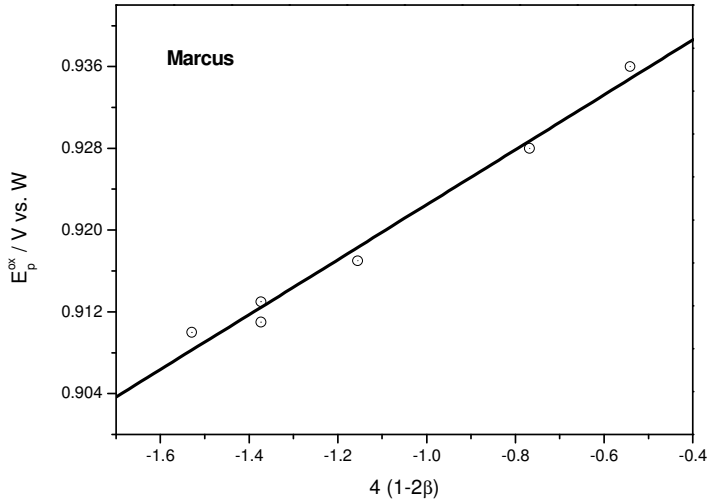

Figure 10.47: The oxidation peak potential E_p^{ox} of 1,2,4-trimethoxybenzene plotted as a function of the transfer coefficient β based on the Marcus free energy relationship, see equation (2.45).

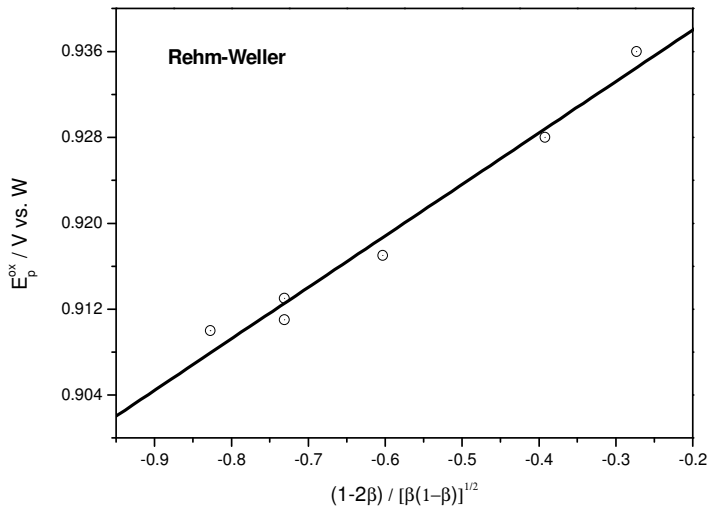

Figure 10.48: The oxidation peak potential E_p^{ox} of 1,2,4-trimethoxybenzene plotted as a function of the transfer coefficient β based on the Rehm-Weller free energy relationship, see equation (2.43).

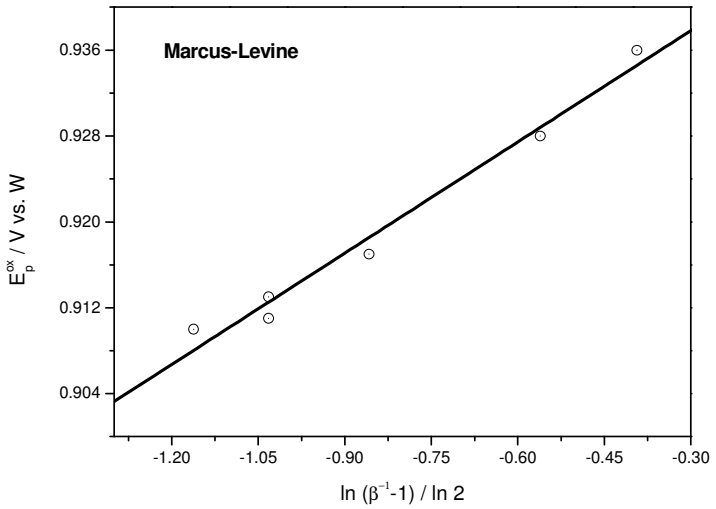

Figure 10.49: The oxidation peak potential E_p^{ox} of 1,2,4-trimethoxybenzene plotted as a function of the transfer coefficient β based on the Marcus-Levine free energy relationship, see equation (2.46).

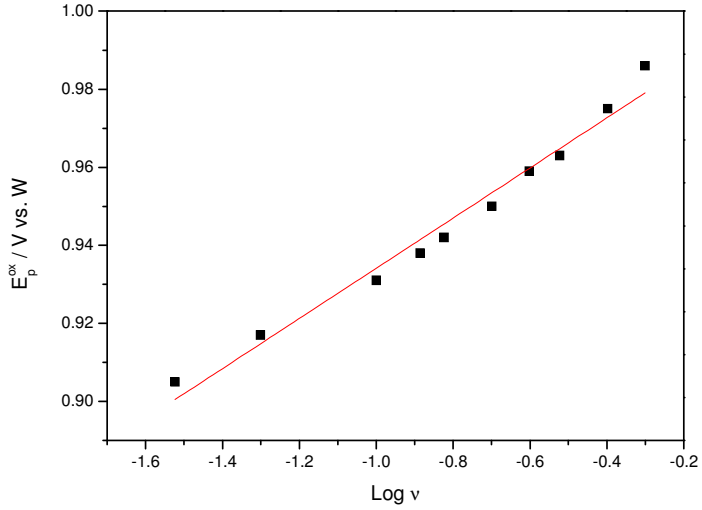

Figure 10.50: Variation of anodic peak potential E_p^{ox} with CV sweep rate at a platinum electrode at 298 K in acetonitrile solution containing 0.1 M TBAP and 3.1 mM N,N´-dimethylaniline.

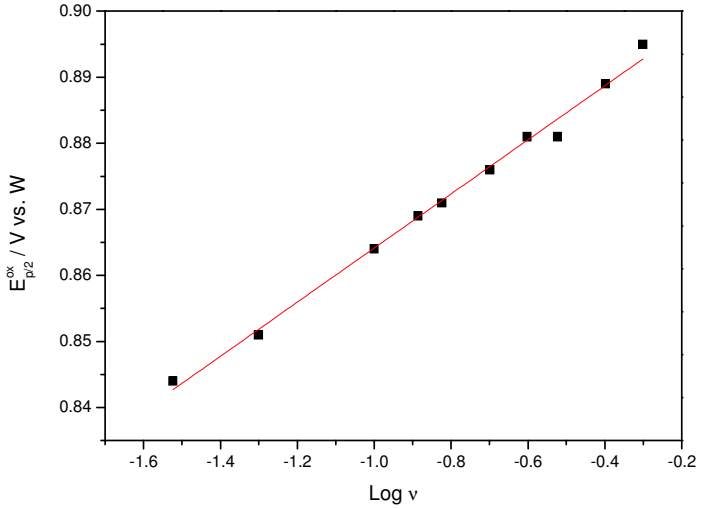

Figure 10.51: Variation of anodic peak potential $E^{ox}_{p/2}$ with CV sweep rate at a platinum electrode at 298 K in acetonitrile solution containing 0.1 M TBAP and 3.1 mM N,N´-dimethylaniline.

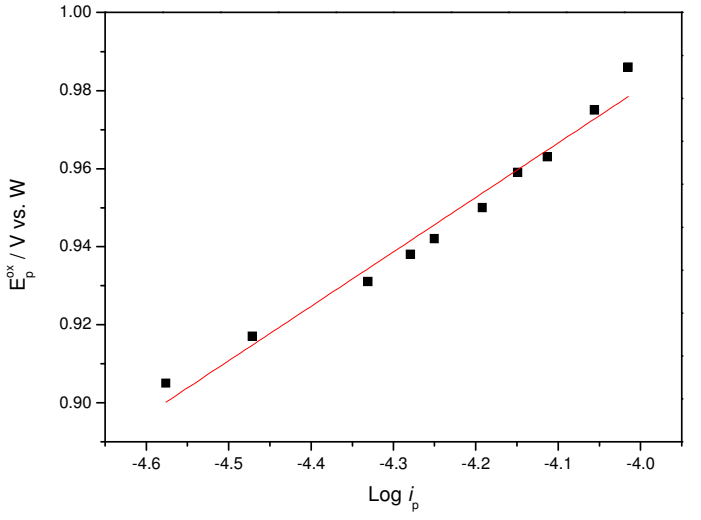

Figure 10.52: Variation of anodic peak potential E^{ox}_{p} with peak current at a platinum electrode at 298 K in acetonitrile solution containing 0.1 M TBAP and3.1 mM N,N´-dimethylaniline.

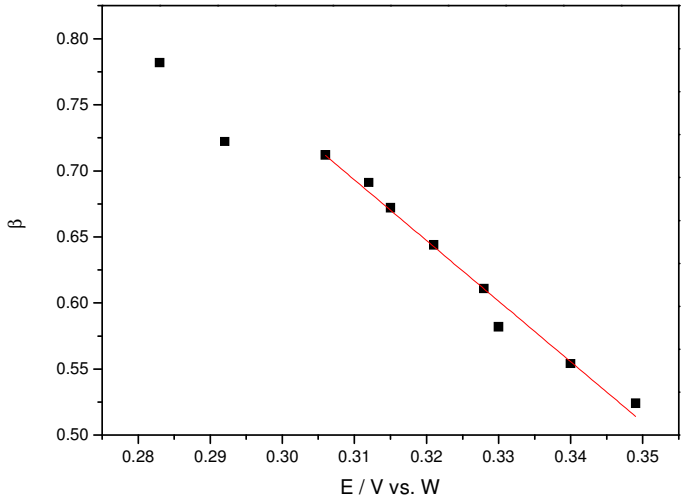

Figure 10.53: Dependence of the heterogeneous electron transfer beta with the applied electrode potential E for the N,N´-dimethylaniline.

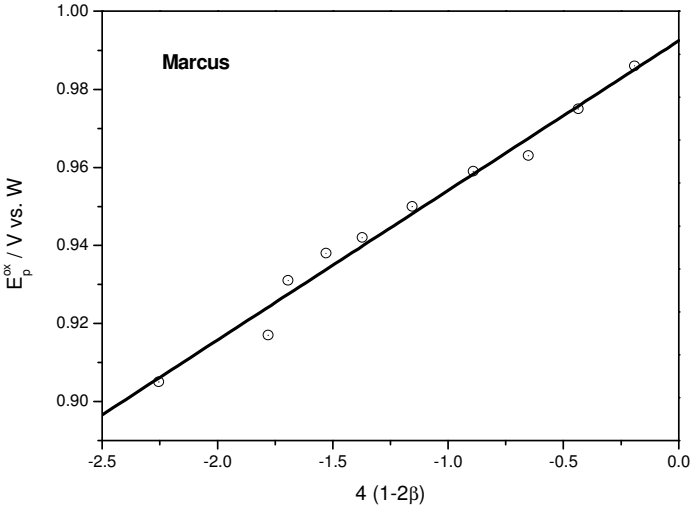

Figure 10.54: The oxidation peak potential E_p^{ox} of N,N´-dimethylaniline plotted as a function of the transfer coefficient β based on the Marcus free energy relationship, see equation (2.45).

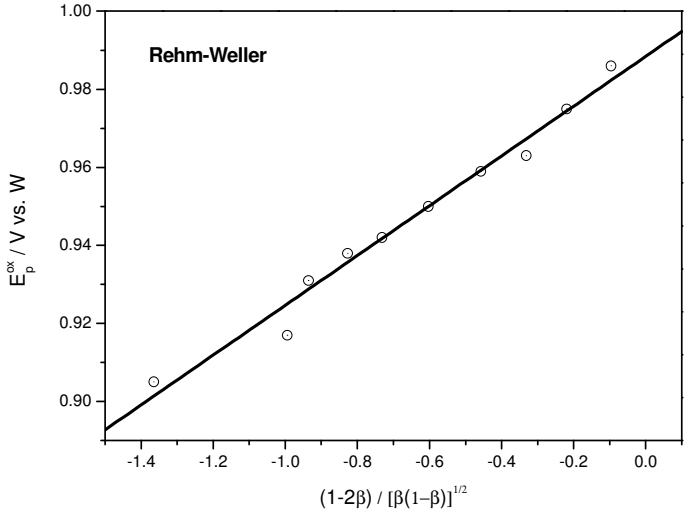

Figure 10.55: The oxidation peak potential E_p^{ox} of N,N´-dimethylaniline plotted as a function of the transfer coefficient β based on the Rehm-Weller free energy relationship, see equation (2.43).

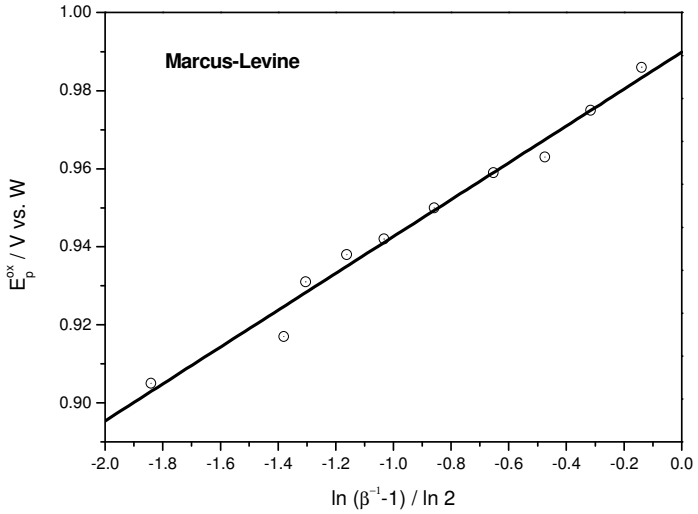

Figure 10.56: The oxidation peak potential E_p^{ox} of N,N´-dimethylaniline plotted as a function of the transfer coefficient β based on the Marcus-Levine free energy relationship, see equation (2.46).

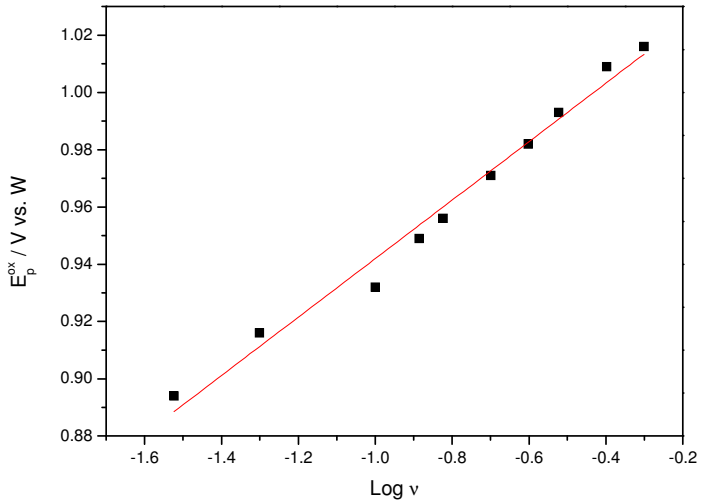

Figure 10.57: Variation of anodic peak potential E_p^{ox} with CV sweep rate at a platinum electrode at 298 K in acetonitrile solution containing 0.1 M TBAP and 3.1 mM N,N´-diethylaniline.

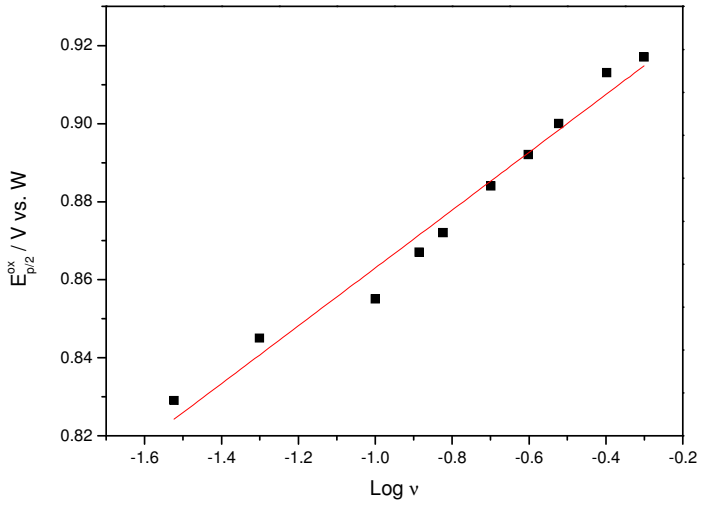

Figure 10.58: Variation of anodic peak potential $E_{p/2}^{ox}$ with CV sweep rate at a platinum electrode at 298 K in acetonitrile solution containing 0.1 M TBAP and 3.1 mM N,N´-diethylaniline.

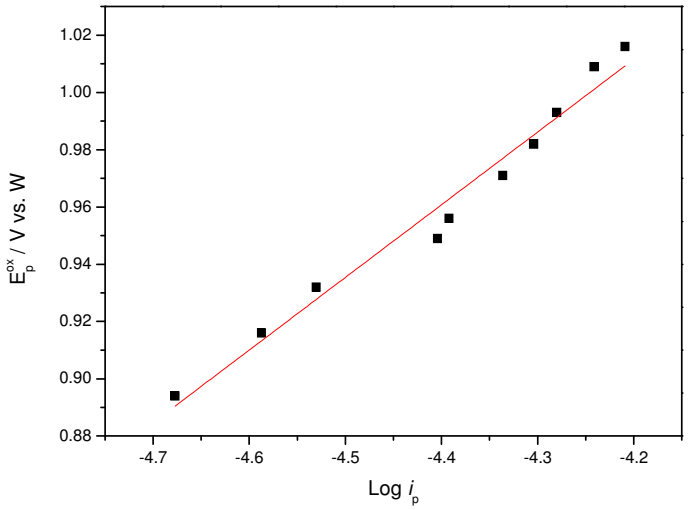

Figure 10.59: Variation of anodic peak potential E_p^{ox} with peak current at a platinum electrode at 298 K in acetonitrile solution containing 0.1 M TBAP and3.1 mM N,N´-diethylaniline.

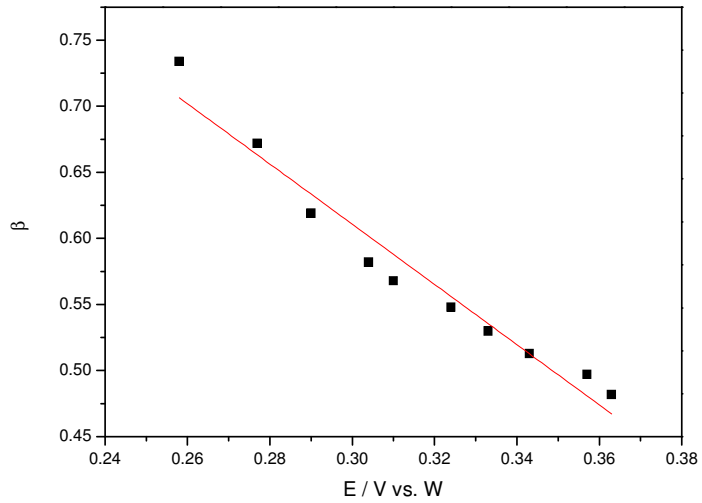

Figure 10.60: Dependence of the heterogeneous electron transfer beta with the applied electrode potential E for the N,N´-diethylaniline.

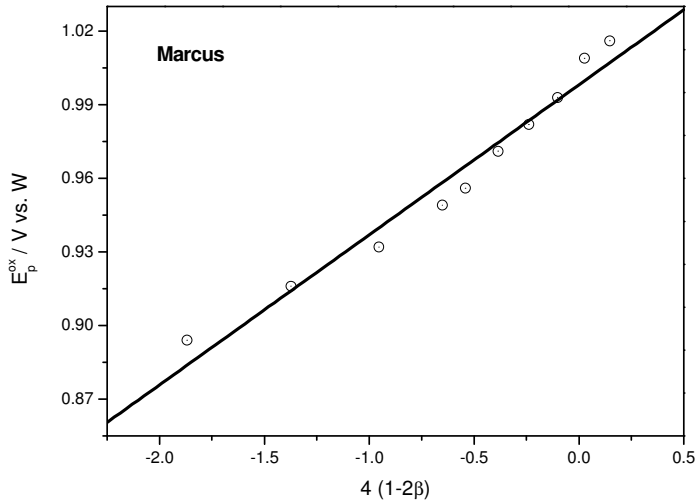

Figure 10.61: The oxidation peak potential E_p^{ox} of N,N´-dimethylaniline plotted as a function of the transfer coefficient β based on the Marcus free energy relationship, see equation (2.45).

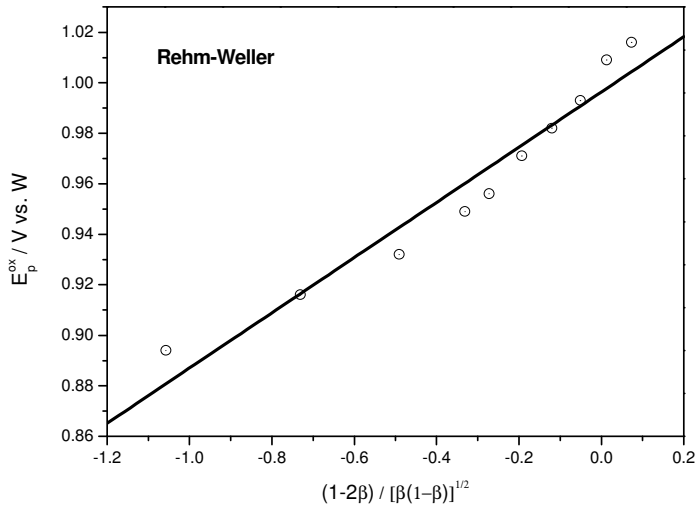

Figure 10.62: The oxidation peak potential E_p^{ox} of N,N´-dimethylaniline plotted as a function of the transfer coefficient β based on the Rehm-Weller free energy relationship, see equation (2.43).

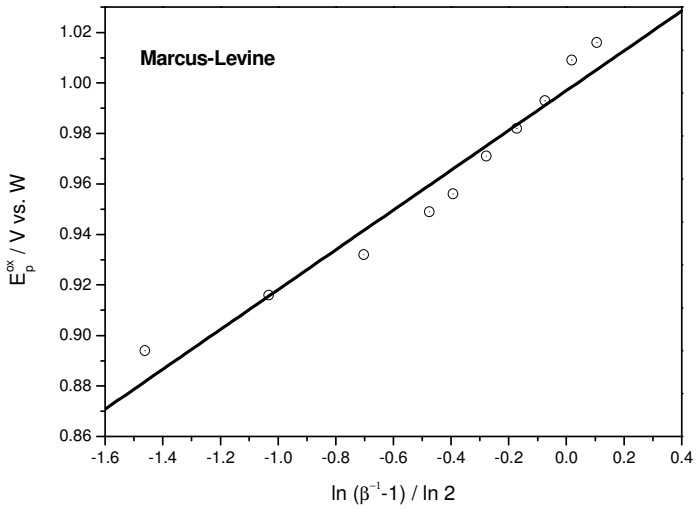

Figure 10.63: The oxidation peak potential E_p^{ox} of N,N´-diethylaniline plotted as a function of the transfer coefficient β based on the Marcus-Levine free energy relationship, see equation (2.46).

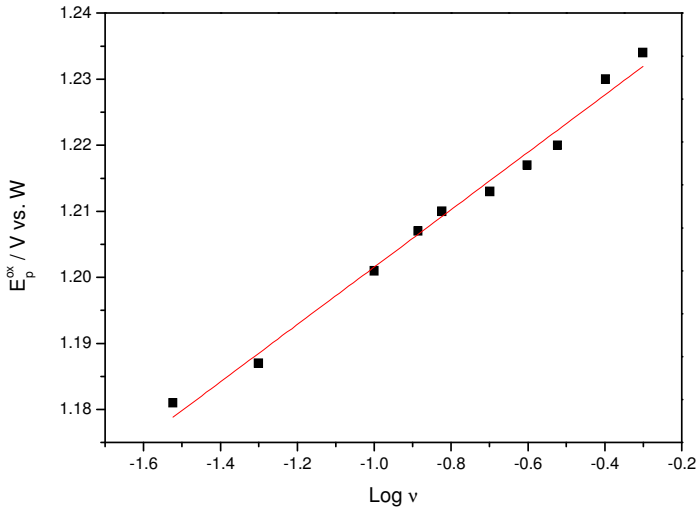

Figure 10.64: Variation of anodic peak potential E_p^{ox} with CV sweep rate at a platinum electrode at 298 K in acetonitrile solution containing 0.1 M TBAP and 3.1 mM triphenylamine.

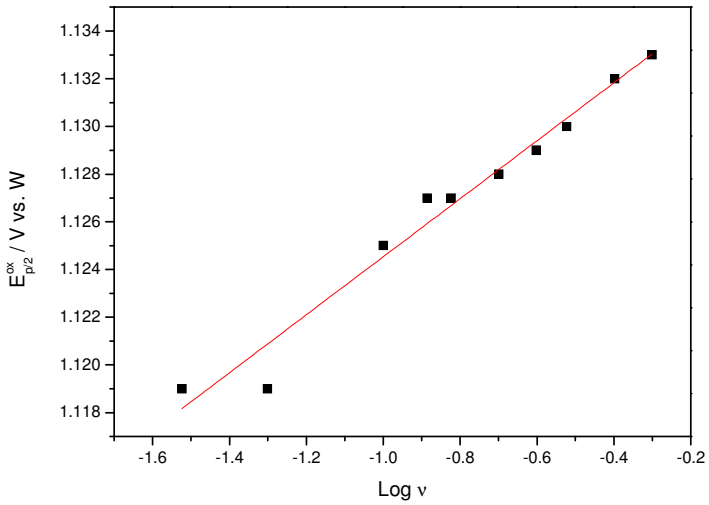

Figure 10.65: Variation of anodic peak potential $E^{ox}_{p/2}$ with CV sweep rate at a platinum electrode at 298 K in acetonitrile solution containing 0.1 M TBAP and 3.1 mM triphenylamine.

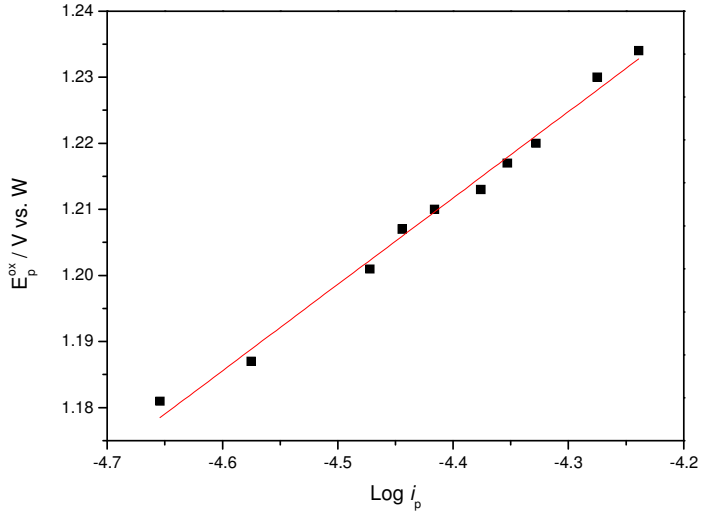

Figure 10.66: Variation of anodic peak potential E^{ox}_{p} with peak current at a platinum electrode at 298 K in acetonitrile solution containing 0.1 M TBAP and3.1 mM triphenylamine.

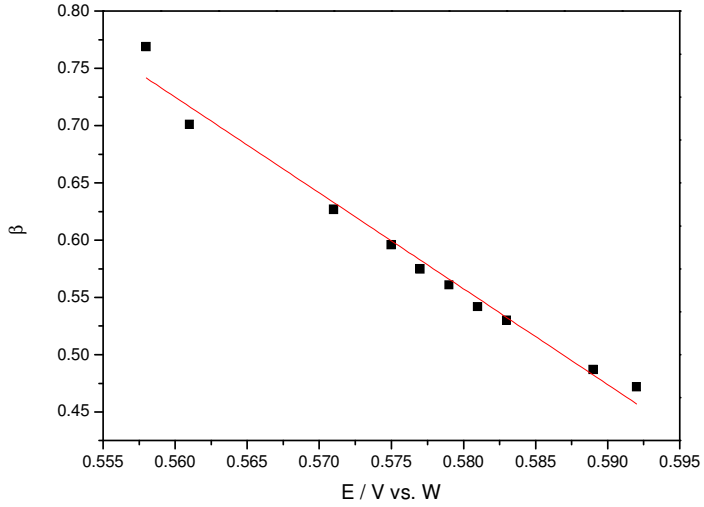

Figure 10.67: Dependence of the heterogeneous electron transfer beta with the applied electrode potential E for the triphenylamine.

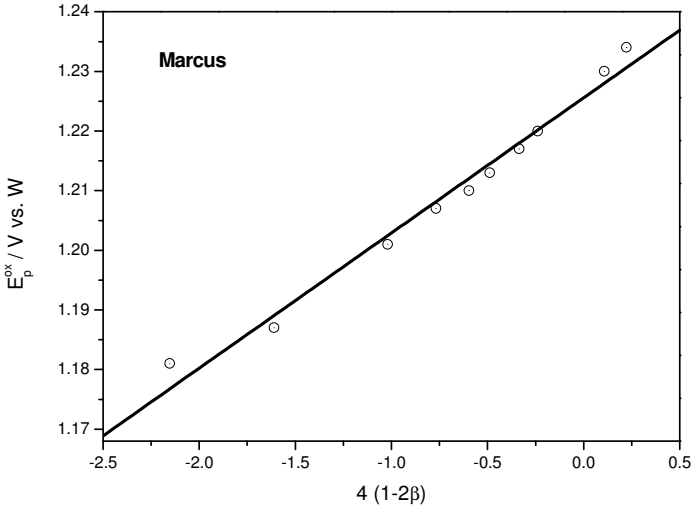

Figure 10.68: The oxidation peak potential E_p^{ox} of triphenylamine plotted as a function of the transfer coefficient β based on the Marcus free energy relationship, see equation (2.45).

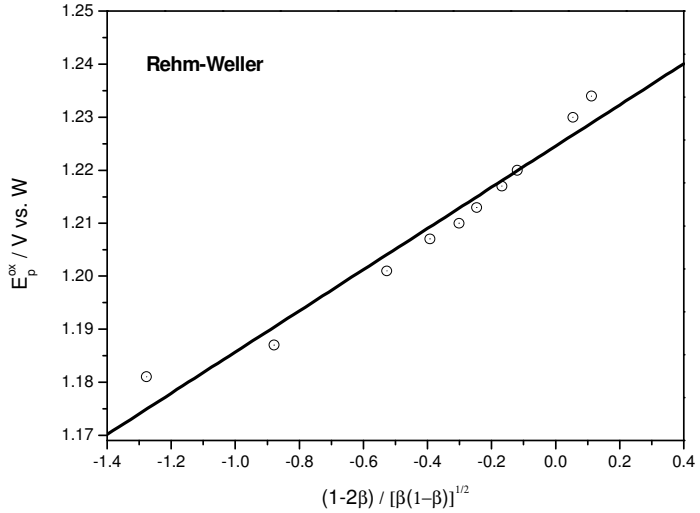

Figure 10.69: The oxidation peak potential E_p^{ox} of triphenylamine plotted as a function of the transfer coefficient β based on the Rehm-Weller free energy relationship, see equation (2.43).

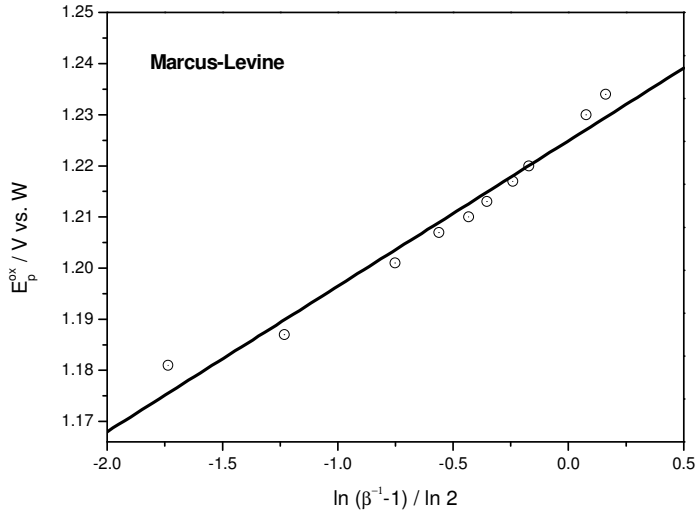

Figure 10.70: The oxidation peak potential E_p^{ox} of triphenylamine plotted as a function of the transfer coefficient β based on the Marcus-Levine free energy relationship, see equation (2.46).

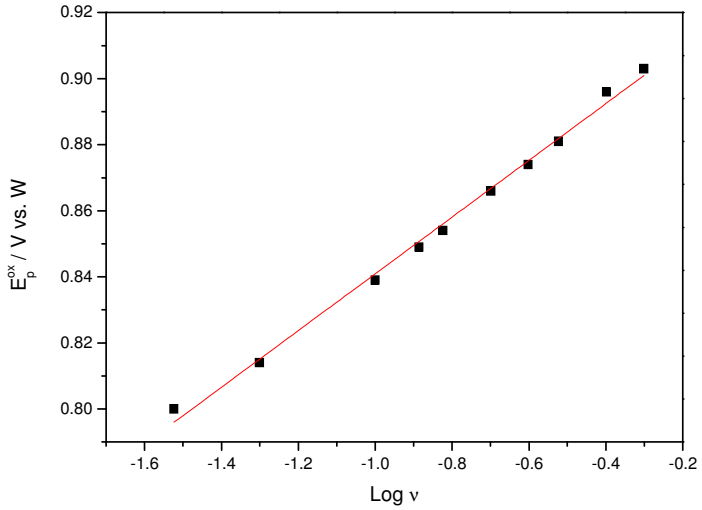

Figure 10.71: Variation of anodic peak potential E_p^{ox} with CV sweep rate at a platinum electrode at 298 K in acetonitrile solution containing 0.1 M TBAP and 3.1 mM DABCO.

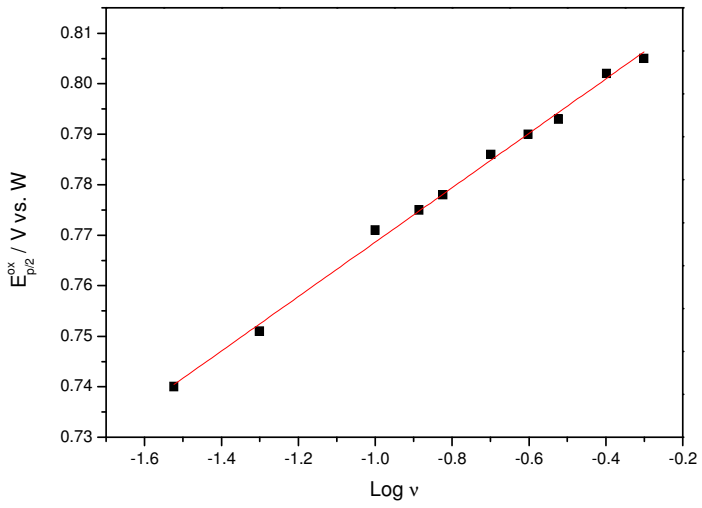

Figure 10.72: Variation of anodic peak potential $E_{p/2}^{ox}$ with CV sweep rate at a platinum electrode at 298 K in acetonitrile solution containing 0.1 M TBAP and 3.1 mM DABCO.

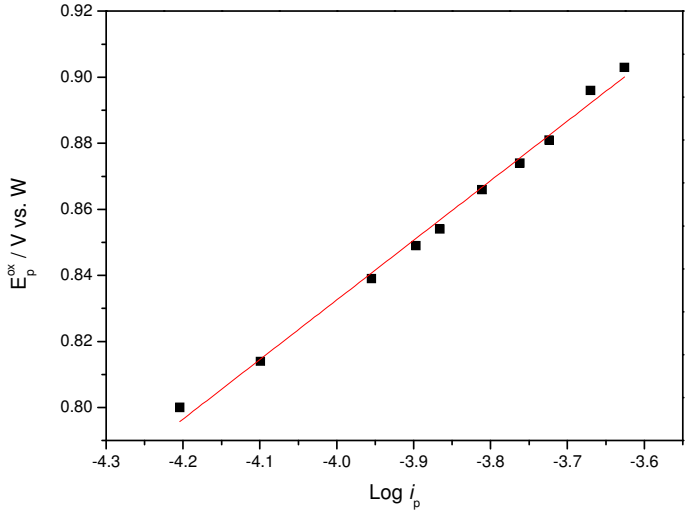

Figure 10.73: Variation of anodic peak potential E_p^{ox} with peak current at a platinum electrode at 298 K in acetonitrile solution containing 0.1 M TBAP and3.1 mM DABCO.

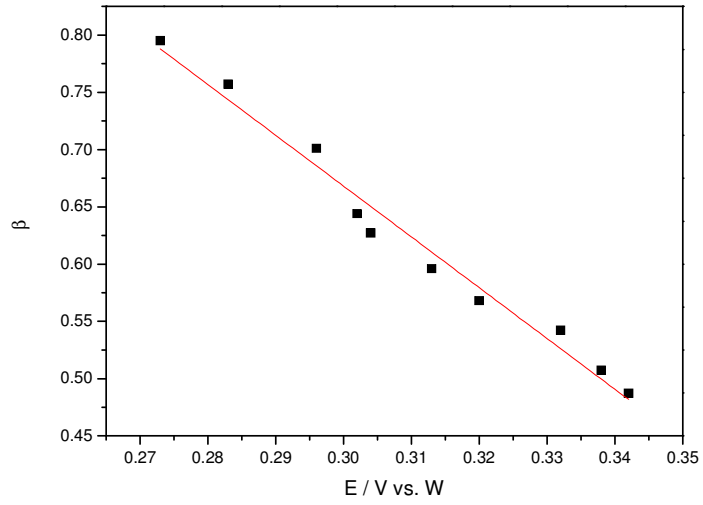

Figure 10.74: Dependence of the heterogeneous electron transfer beta with the applied electrode potential E for the DABCO.

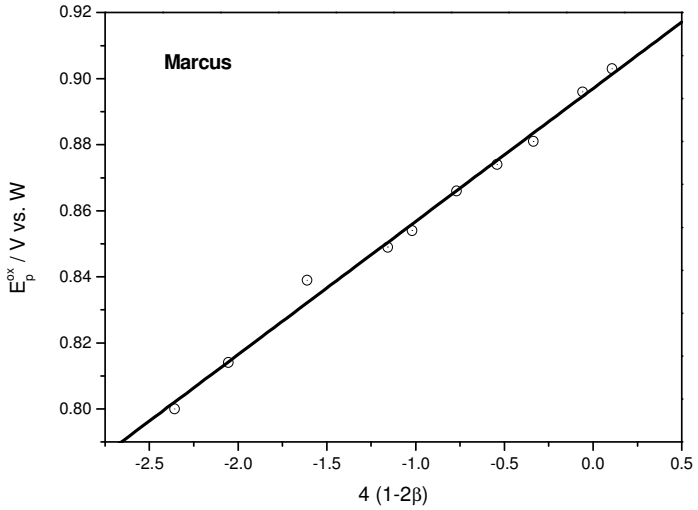

Figure 10.75: The oxidation peak potential E_p^{ox} of DABCO plotted as a function of the transfer coefficient β based on the Marcus free energy relationship, see equation (2.45).

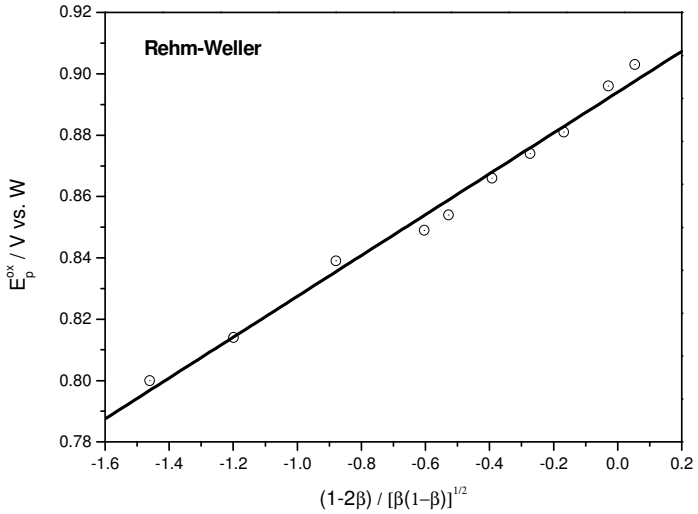

Figure 10.76: The oxidation peak potential E_p^{ox} of DABCO plotted as a function of the transfer coefficient β based on the Rehm-Weller free energy relationship, see equation (2.43).

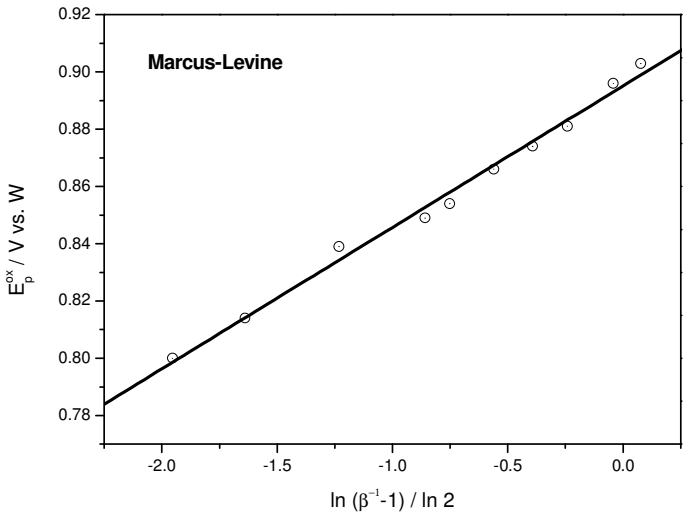

Figure 10.77: The oxidation peak potential E_p^{ox} of DABCO plotted as a function of the transfer coefficient β based on the Marcus-Levine free energy relationship, see equation (2.46).

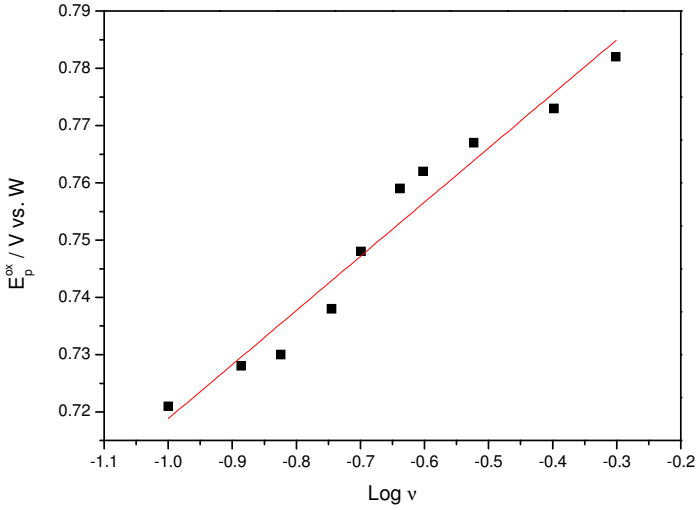

Figure 10.78: Variation of anodic peak potential E_p^{ox} with CV sweep rate at a platinum electrode at 298 K in acetonitrile solution containing 0.1 M TBAP and 3.1 mM DMPM.

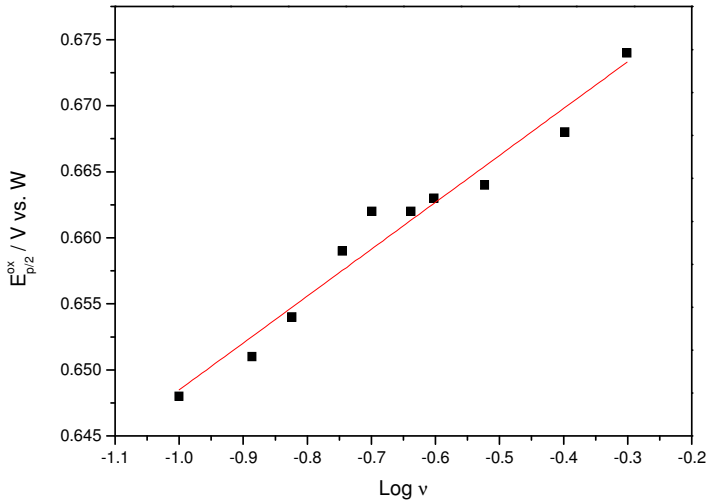

Figure 10.79: Variation of anodic peak potential $E^{ox}_{p/2}$ with CV sweep rate at a platinum electrode at 298 K in acetonitrile solution containing 0.1 M TBAP and 3.1 mM DMPM.

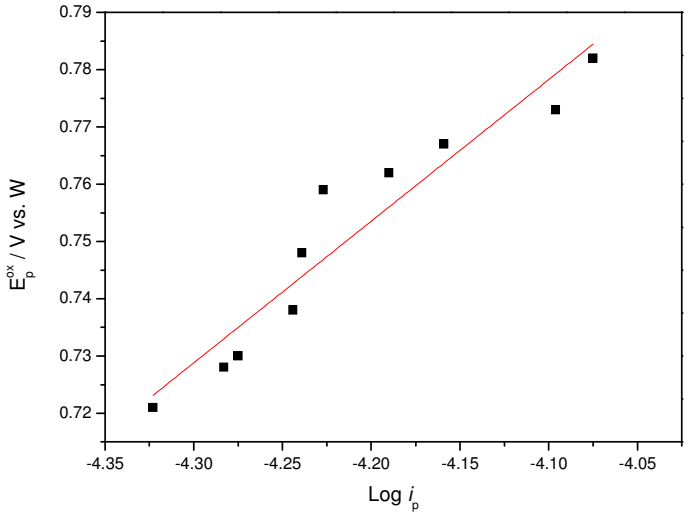

Figure 10.80: Variation of anodic peak potential E^{ox}_{p} with peak current at a platinum electrode at 298 K in acetonitrile solution containing 0.1 M TBAP and3.1 mM DMPM.

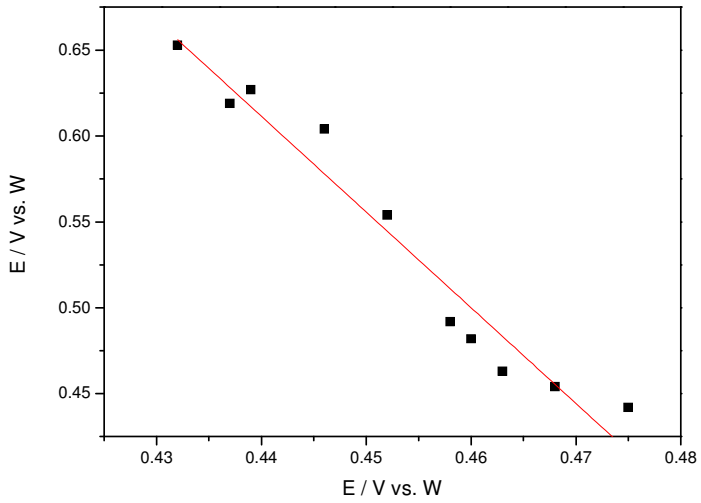

Figure 10.81: Dependence of the heterogeneous electron transfer beta with the applied electrode potential E for the DMPM.

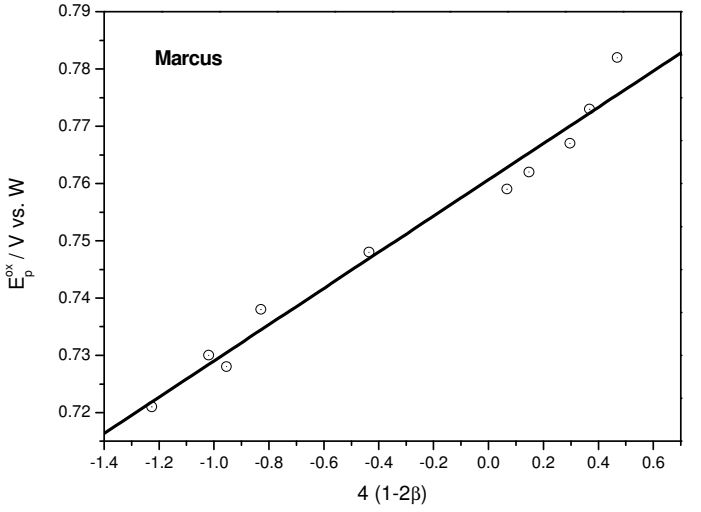

Figure 10.82: The oxidation peak potential E_p^{ox} of DMPM plotted as a function of the transfer coefficient β based on the Marcus free energy relationship, see equation (2.45).

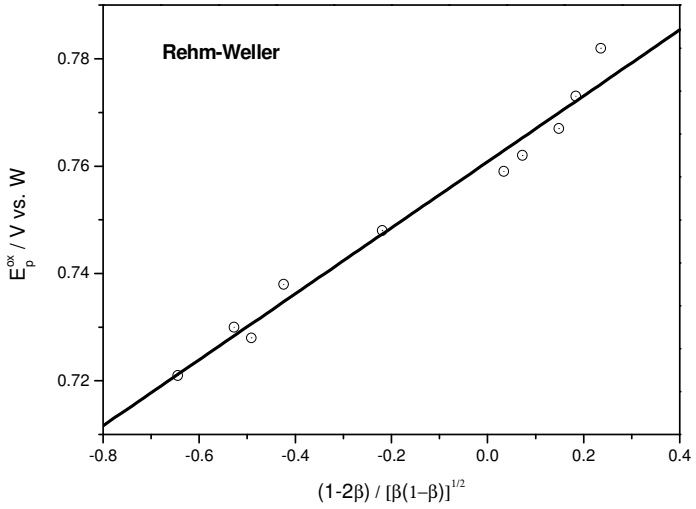

Figure 10.83: The oxidation peak potential E_p^{ox} of DMPM plotted as a function of the transfer coefficient β based on the Rehm-Weller free energy relationship, see equation (2.43).

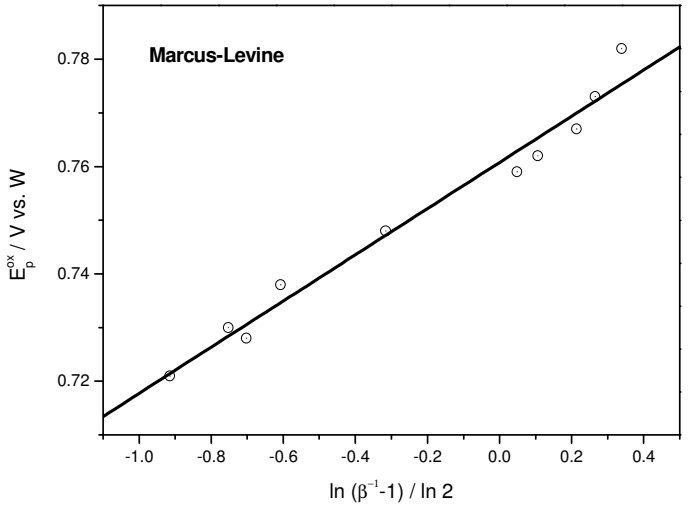

Figure 10.84: The oxidation peak potential E_p^{ox} of DMPM plotted as a function of the transfer coefficient β based on the Marcus-Levine free energy relationship, see equation (2.46).

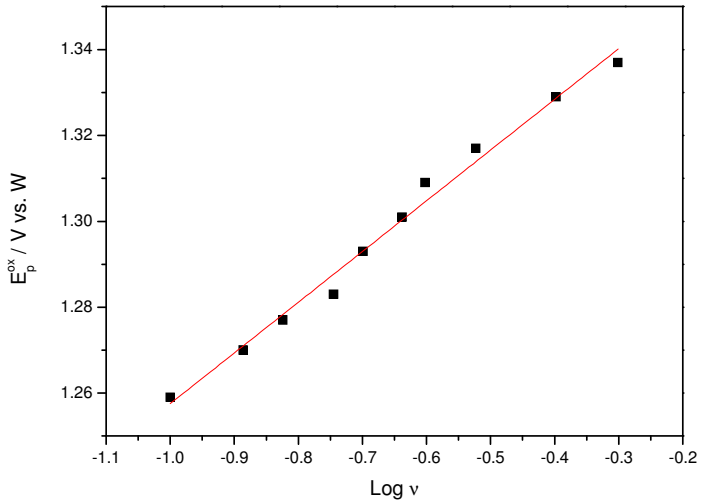

Figure 10.85: Variation of anodic peak potential E_p^{ox} with CV sweep rate at a platinum electrode at 298 K in acetonitrile solution containing 0.1 M TBAP and 3.1 mM N-methylpyrrole.

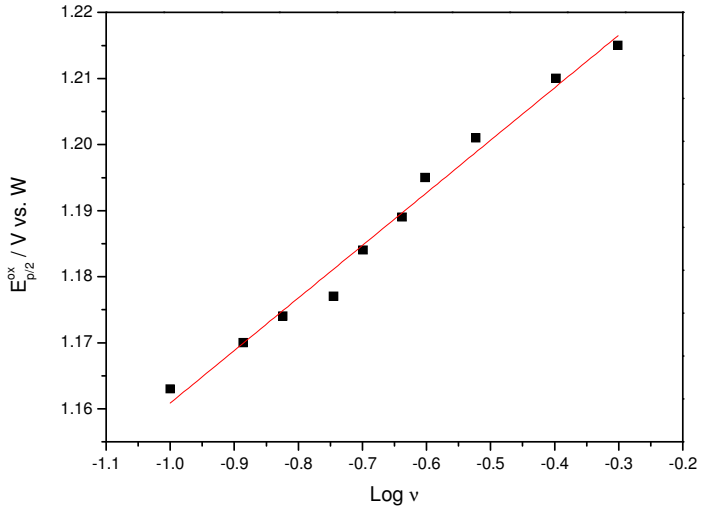

Figure 10.86: Variation of anodic peak potential $E_{p/2}^{ox}$ with CV sweep rate at a platinum electrode at 298 K in acetonitrile solution containing 0.1 M TBAP and 3.1 mM N-methylpyrrole.

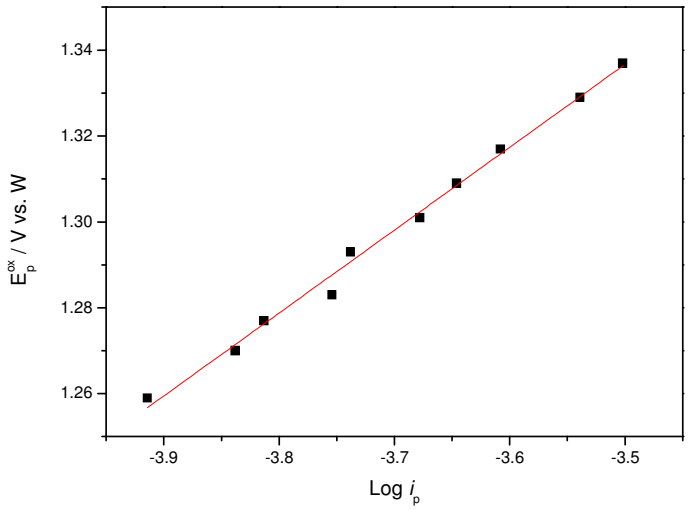

Figure 10.87: Variation of anodic peak potential E_p^{ox} with peak current at a platinum electrode at 298 K in acetonitrile solution containing 0.1 M TBAP and3.1 mM N-methylpyrrole.

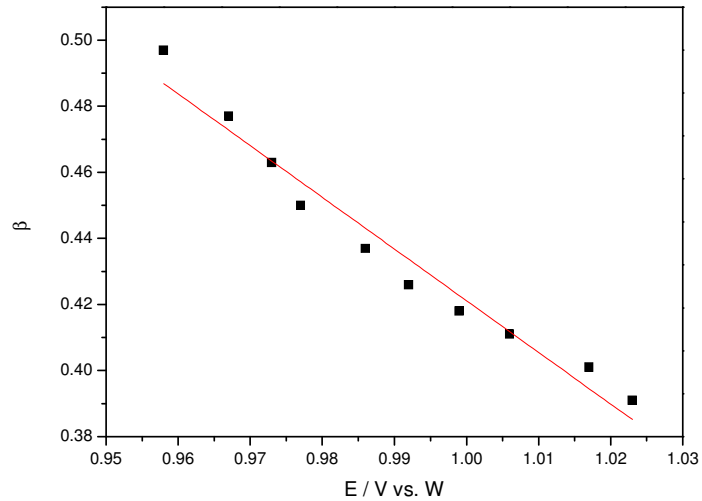

Figure 10.88: Dependence of the heterogeneous electron transfer beta with the applied electrode potential E for the N-methylpyrrole.

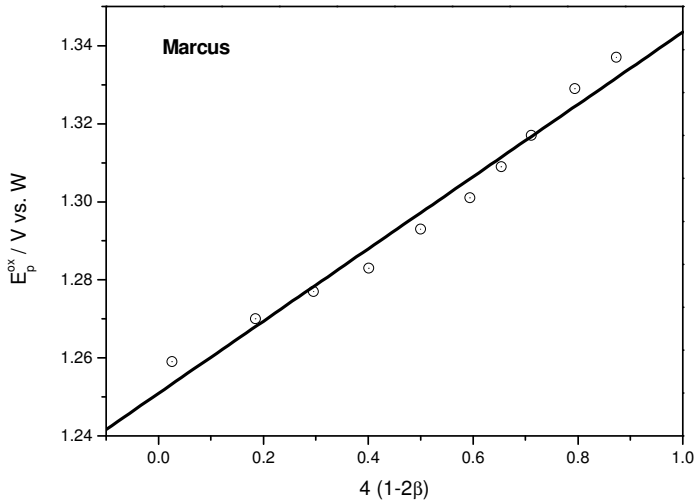

Figure 10.89: The oxidation peak potential E_p^{ox} of N-methylpyrrole plotted as a function of the transfer coefficient β based on the Marcus free energy relationship, see equation (2.45).

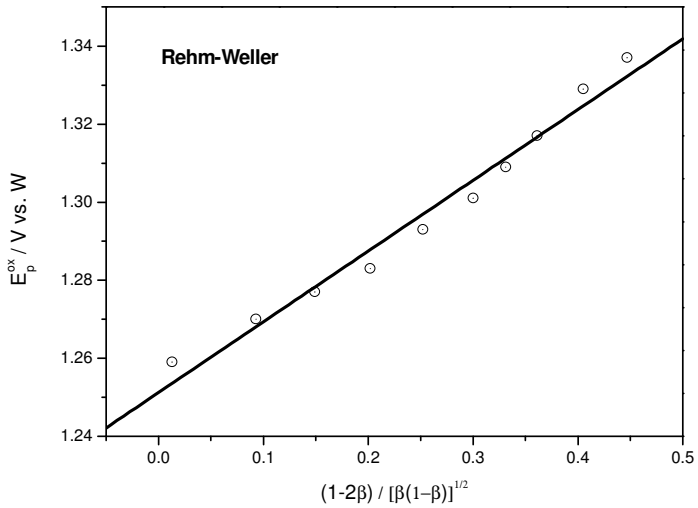

Figure 10.90: The oxidation peak potential E_p^{ox} of N-methylpyrrole plotted as a function of the transfer coefficient β based on the Rehm-Weller free energy relationship, see equation (2.43).

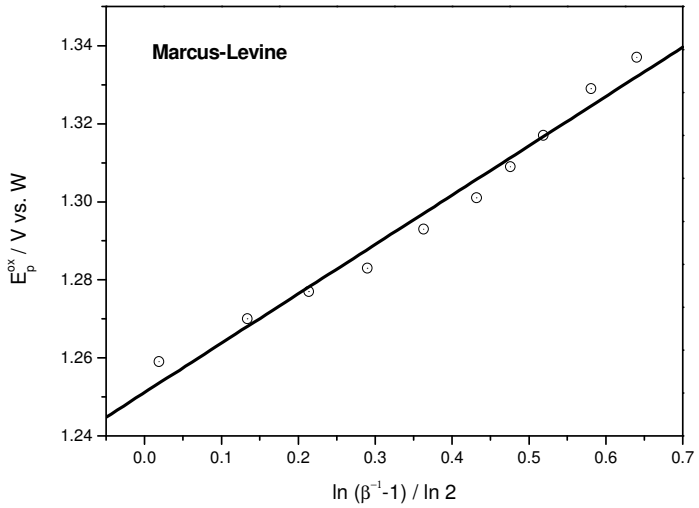

Figure 10.91: The oxidation peak potential E_p^{ox} of N-methylpyrrole plotted as a function of the transfer coefficient β based on the Marcus-Levine free energy relationship, see equation (2.46).

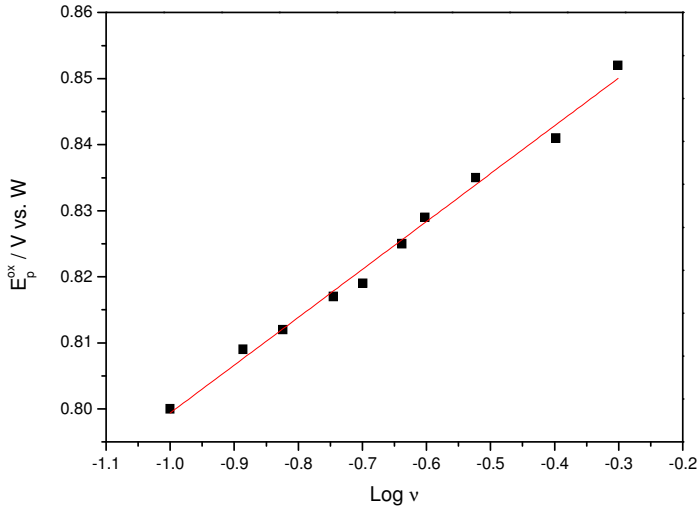

Figure 10.92: Variation of anodic peak potential E_p^{ox} with CV sweep rate at a platinum electrode at 298 K in acetonitrile solution containing 0.1 M TBAP and 3.1 mM 1,2,5-trimethylpyrrole.

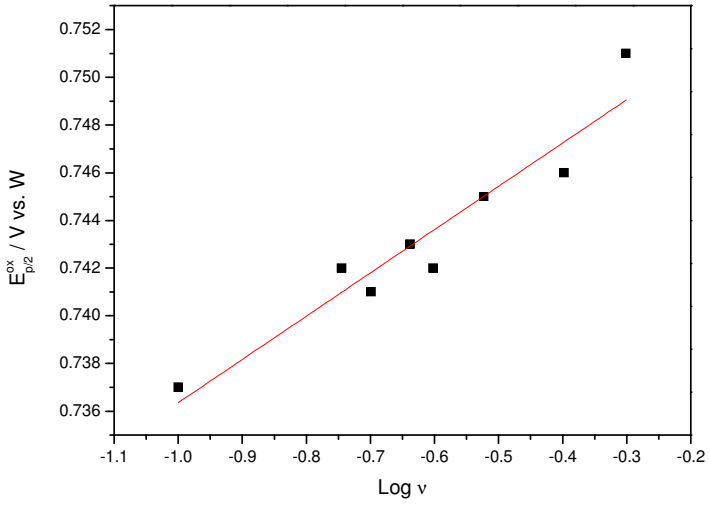

Figure 10.93: Variation of anodic peak potential $E^{ox}_{p/2}$ with CV sweep rate at a platinum electrode at 298 K in acetonitrile solution containing 0.1 M TBAP and 3.1 mM 1,2,5-trimethylpyrrole.

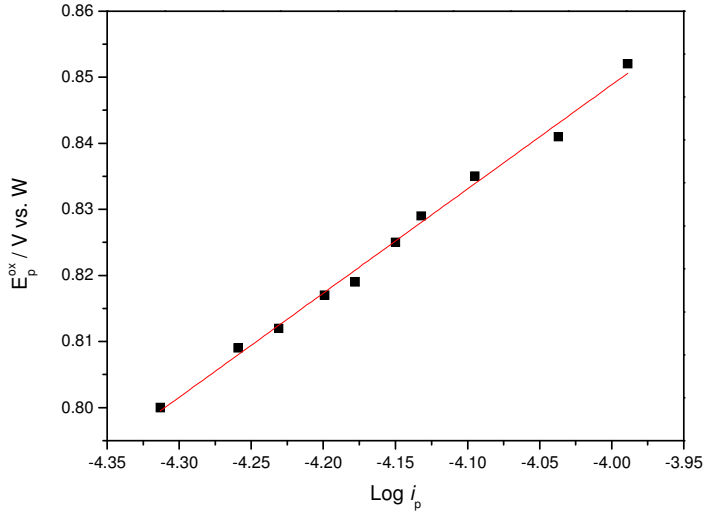

Figure 10.94: Variation of anodic peak potential E^{ox}_{p} with peak current at a platinum electrode at 298 K in acetonitrile solution containing 0.1 M TBAP and3.1 mM 1,2,5-trimethylpyrrole.

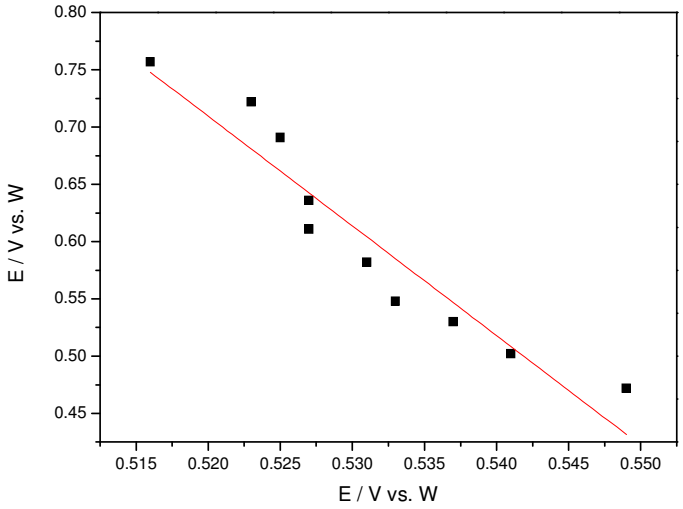

Figure 10.95: Dependence of the heterogeneous electron transfer beta with the applied electrode potential E for the 1,2,5-trimethylpyrrole.

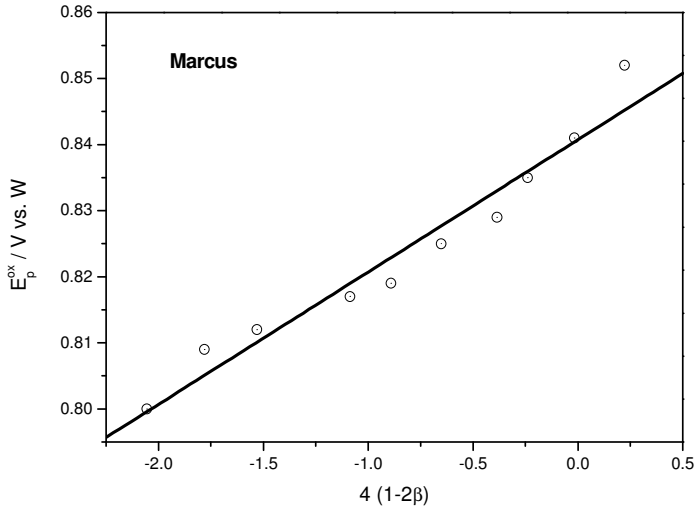

Figure 10.96: The oxidation peak potential E_p^{ox} of 1,2,5-trimethylpyrrole plotted as a function of the transfer coefficient β based on the Marcus free energy relationship, see equation (2.45).

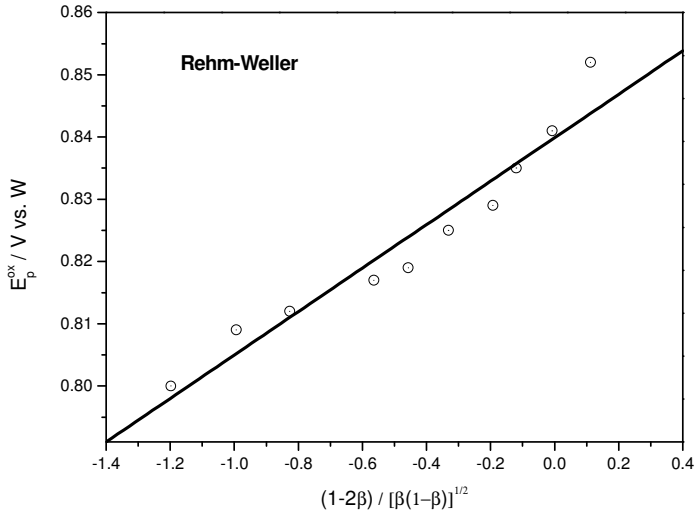

Figure 10.97: The oxidation peak potential E_p^{ox} of 1,2,5-trimethylpyrrole plotted as a function of the transfer coefficient β based on the Rehm-Weller free energy relationship, see equation (2.43).

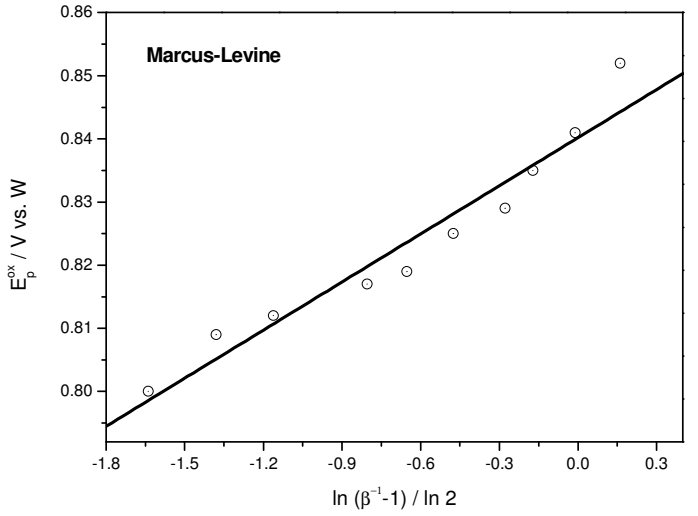

Figure 10.98: The oxidation peak potential E_p^{ox} of 1,2,5-trimethylpyrrole plotted as a function of the transfer coefficient β based on the Marcus-Levine free energy relationship, see equation (2.46).

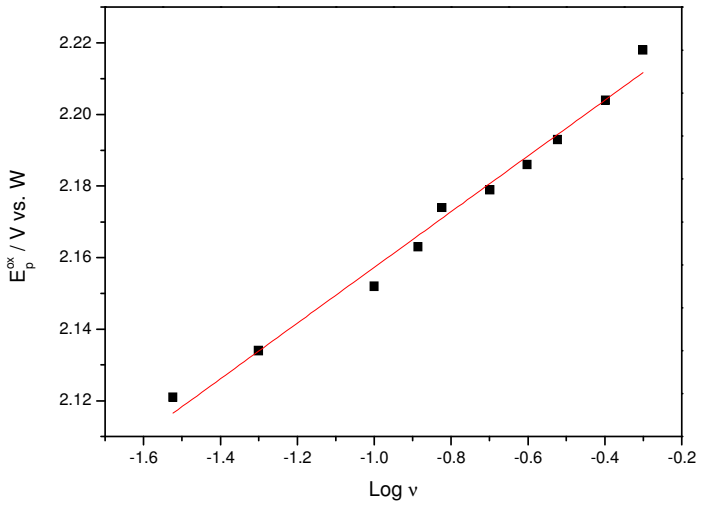

Figure 10.99: Variation of anodic peak potential E_p^{ox} with CV sweep rate at a platinum electrode at 298 K in acetonitrile solution containing 0.1 M TBAP and 3.1 mM PTPA.

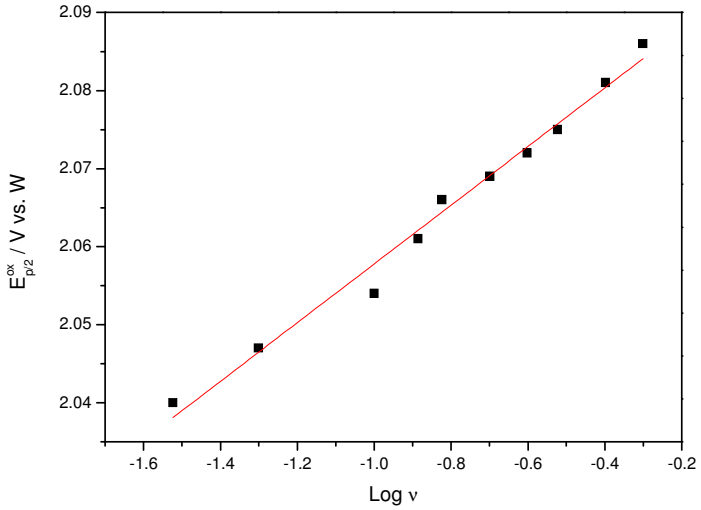

Figure 10.100: Variation of anodic peak potential $E_{p/2}^{ox}$ with CV sweep rate at a platinum electrode at 298 K in acetonitrile solution containing 0.1 M TBAP and 3.1 Mm PTPA.

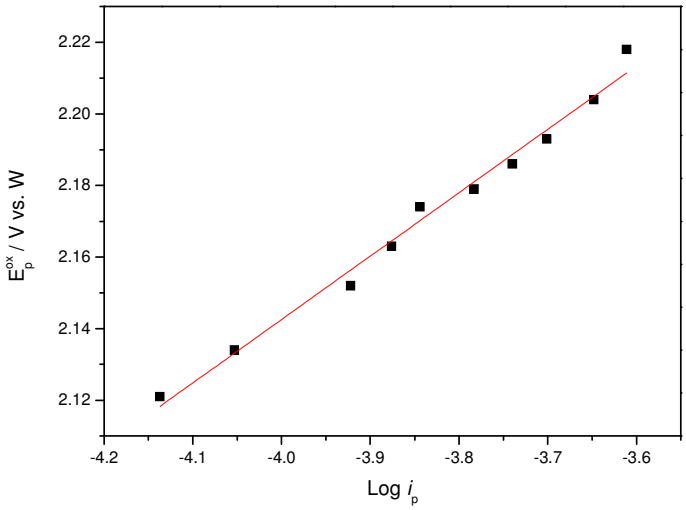

Figure 10.101: Variation of anodic peak potential E_p^{ox} with peak current at a platinum electrode at 298 K in acetonitrile solution containing 0.1 M TBAP and3.1 mM PTPA.

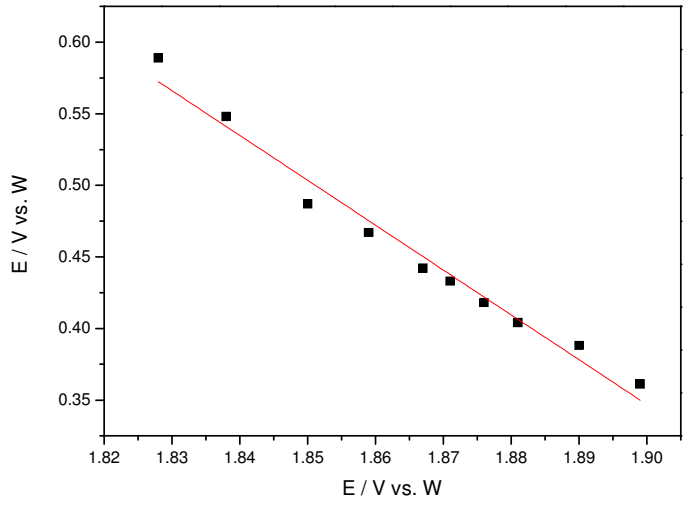

Figure 10.102: Dependence of the heterogeneous electron transfer beta with the applied electrode potential E for the PTPA.

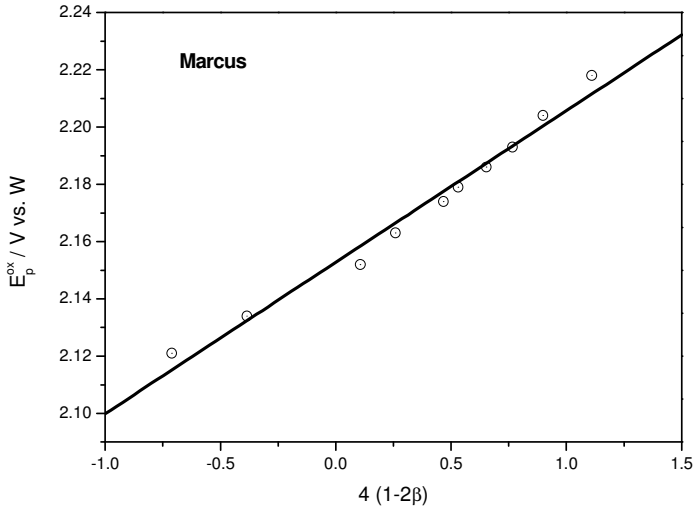

Figure 10.103: The oxidation peak potential E_p^{ox} of PTPA plotted as a function of the transfer coefficient β based on the Marcus free energy relationship, see equation (2.45).

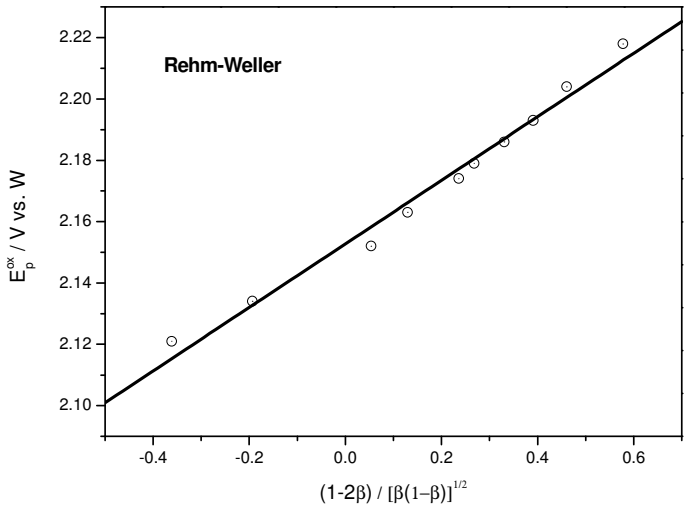

Figure 10.104: The oxidation peak potential E_p^{ox} of PTPA plotted as a function of the transfer coefficient β based on the Rehm-Weller free energy relationship, see equation (2.43).

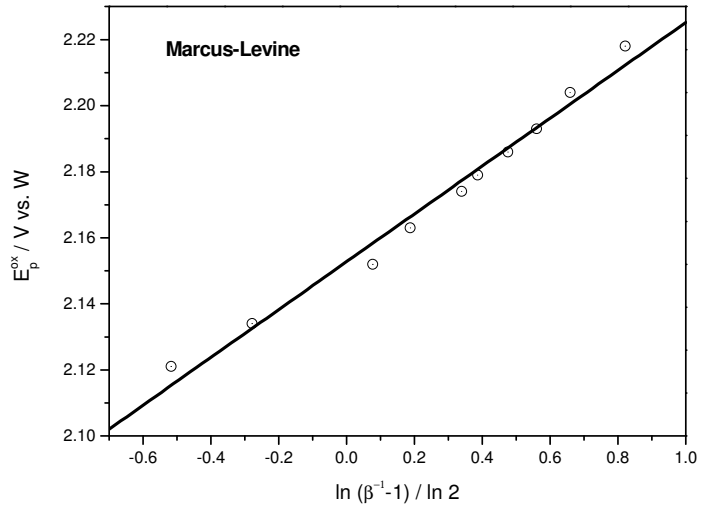

Figure 10.105: The oxidation peak potential E_p^{ox} of PTPA plotted as a function of the transfer coefficient β based on the Marcus-Levine free energy relationship, see equation (2.46).

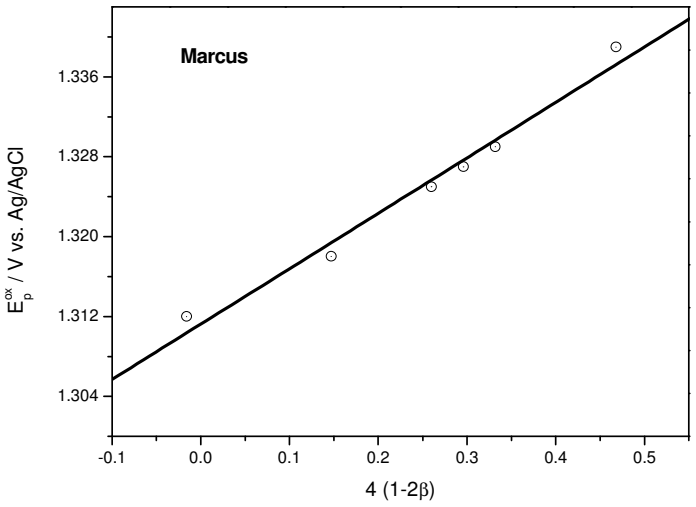

Figure 10.106: The oxidation peak potential E_p^{ox} of adenosine plotted as a function of the transfer coefficient β based on the Marcus free energy relationship; see equation (2.45), at pH 4.

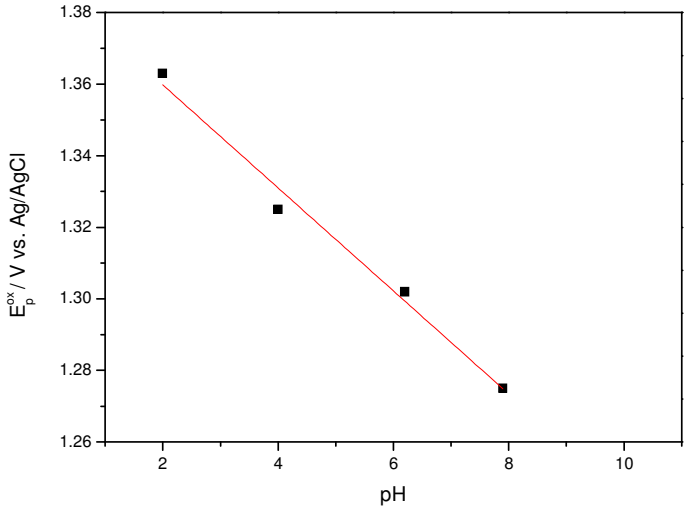

Figure 10.107: The oxidation peak potential E_p^{ox} of adenosine plotted as a function pH obtained at 298 K, 100 mVs^{-1}

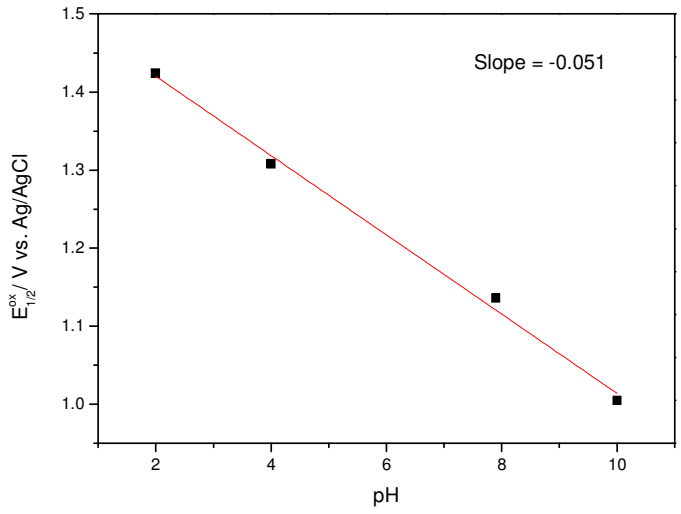

Figure 10.108: The oxidation half-wave potential $E_{1/2}^{ox}$ of adenosine plotted as a function pH obtained at 298 K, 100 mVs^{-1}

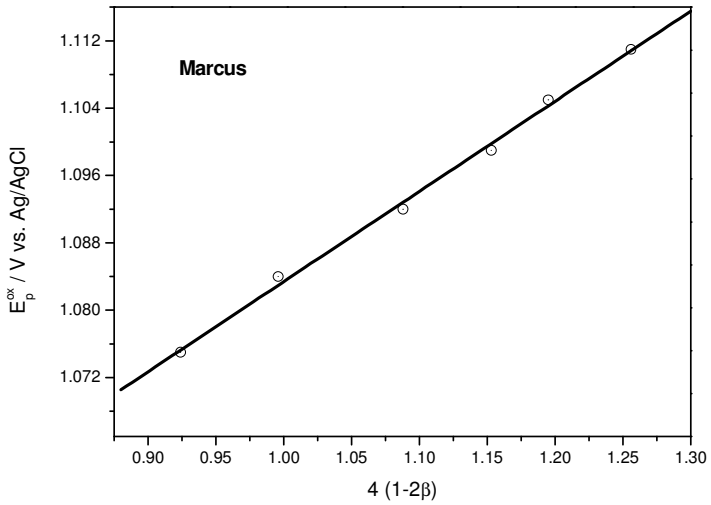

Figure 10.109: The oxidation peak potential E_p^{ox} of histidine plotted as a function of the transfer coefficient β based on the Marcus free energy relationship; see equation (2.45), at pH 6.1.

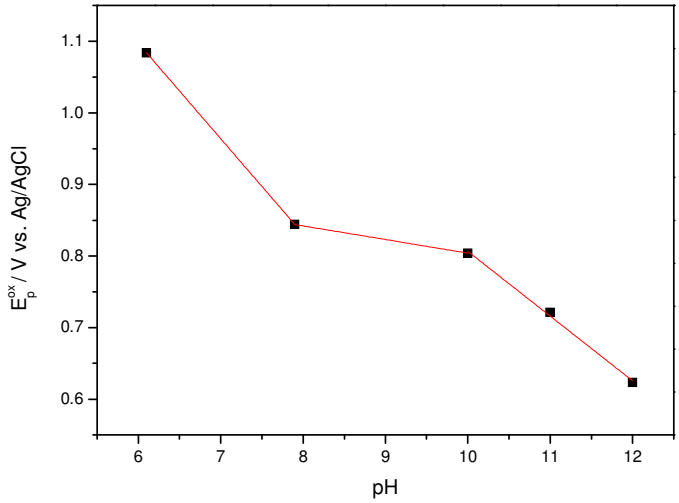

Figure 10.110: The oxidation peak potential E_p^{ox} of histidine plotted as a function pH obtained at 298 K, 100 mVs^{-1}

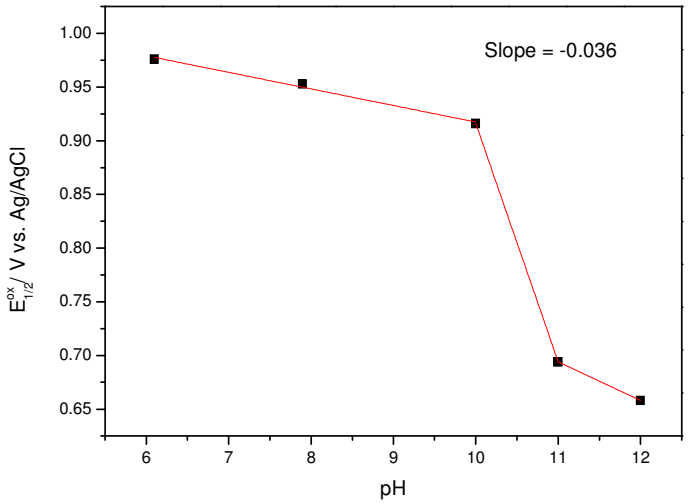

Figure 10.111: The oxidation half-wave potential $E^{ox}_{1/2}$ of histidine plotted as a function pH obtained at 298 K, 100 mVs^{-1}

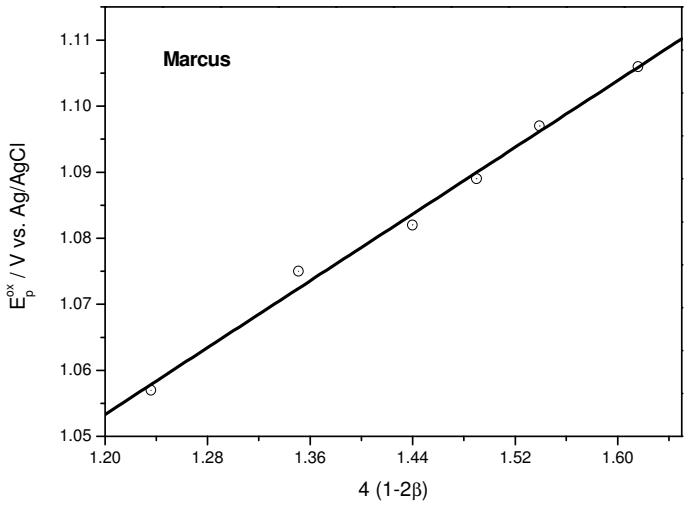

Figure 10.112: The oxidation peak potential E^{ox}_{p} of methionine plotted as a function of the transfer coefficient β based on the Marcus free energy relationship; see equation (2.45), at pH 2.

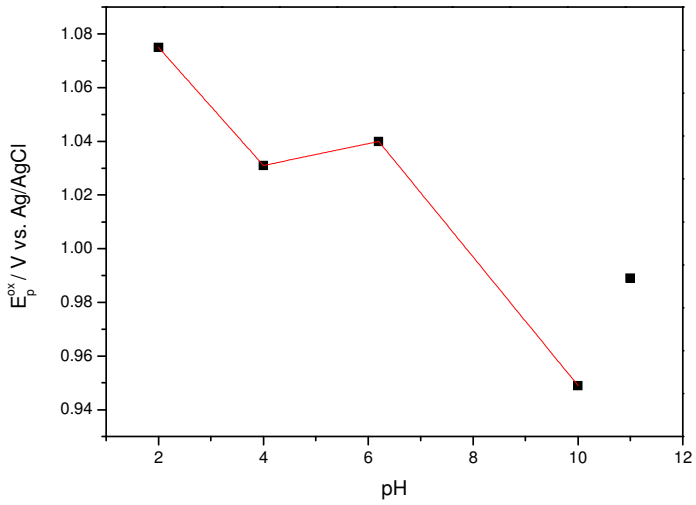

Figure 10.113: The oxidation peak potential E_p^{ox} of methionine plotted as a function pH obtained at 298 K, 100 mVs^{-1}

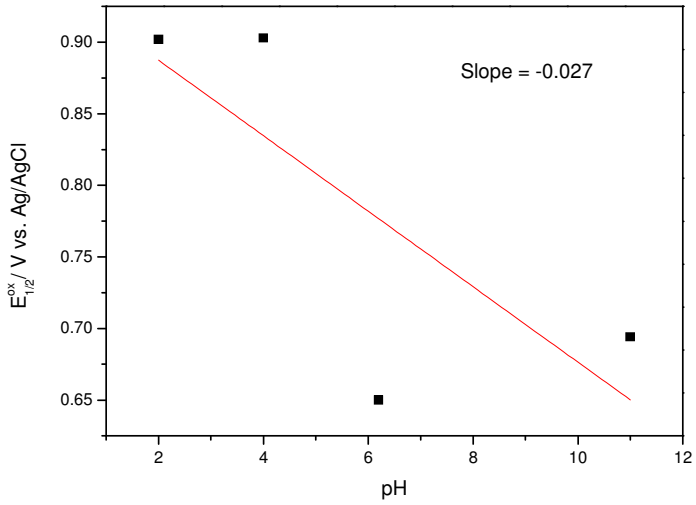

Figure 10.114: The oxidation half-wave potential $E_{1/2}^{ox}$ of methionine plotted as a function pH obtained at 298 K, 100 mVs^{-1}

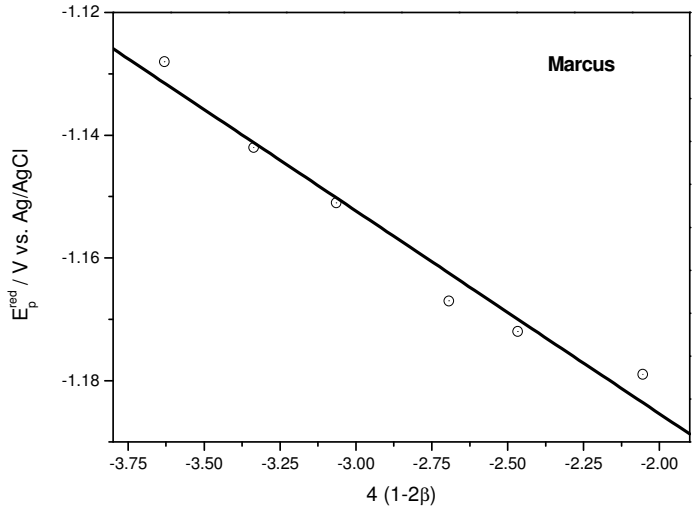

Figure 10.115: The reduction peak potential E_p^{red} of 2,2´-bipyridine plotted as a function of the transfer coefficient β based on the Marcus free energy relationship, see equation (2.54), at pH 2.

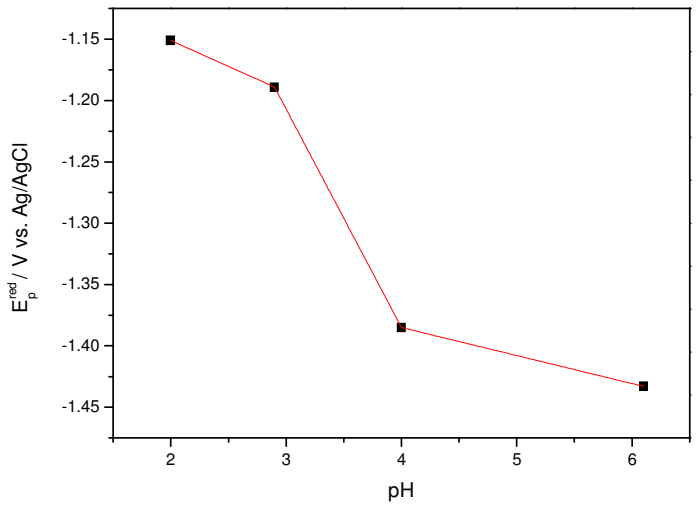

Figure 10.116: The reduction peak potential E_p^{red} 2,2´-bipyridine plotted as a function pH obtained at 298 K, 100 mVs^{-1}

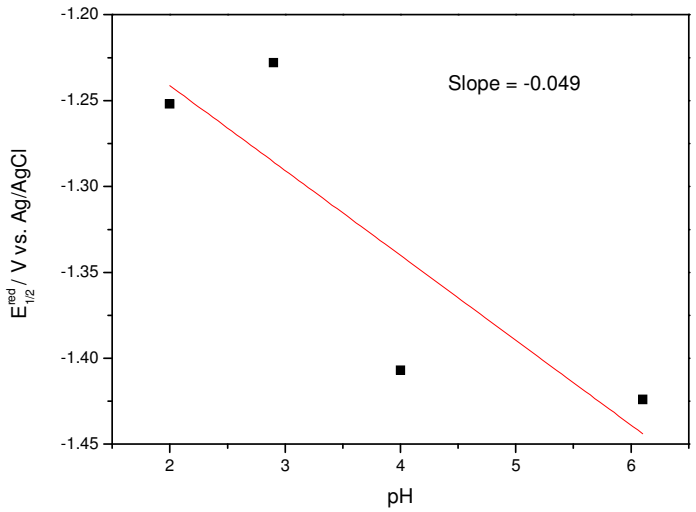

Figure 10.117: The reduction half-wave potential $E_{1/2}^{red}$ of 2,2´-bipyridine plotted as a function pH obtained at 298 K, 100 mVs^{-1}

Chapter 11. Appendix C

Table 11.1: Transfer Coefficient Determine by Several Independent Methods[a]

compd	transfer coefficient				
	E_p^{ox} *vs.* $\log \upsilon$	$E_{p/2}^{ox}$ *vs.* $\log \upsilon$	E_p^{ox} *vs.* $\log i_p$	$E_p^{ox} - E_{p/2}^{ox}$	a.v.
Thymine	0.52	0.68	0.59	0.61	0.60±0.06
Adenosine	0.66	0.53	0.79	0.76	0.69±0.11
Histidine	-	-	-	-	-
Methionine	0.42	0.77	0.49	0.32	0.50±0.19
2,2´-Bipyridine	0.48	0.63	0.28	0.89	0.57±0.25
3,3´,4,4´-Benzo-phenone tetracarboxylic acid	0.64	0.71	0.65	0.93	0.74±0.13

[a] See chapter 2. Transfer coefficient reported here obtained at pH 2.

Table 11.2: Transfer Coefficient Determine by Several Independent Methods[a]

compd	transfer coefficient				
	E_p^{ox} *vs.* $\log \upsilon$	$E_{p/2}^{ox}$ *vs.* $\log \upsilon$	E_p^{ox} *vs.* $\log i_p$	$E_p^{ox} - E_{p/2}^{ox}$	a.v.
Thymine	0.77	0.72	0.85	0.51	0.71±0.14
Adenosine	0.76	0.55	0.69	0.46	0.61±0.13
Histidine	-	-	-	-	-
Methionine	0.33	0.59	0.55	0.29	0.44±0.15
2,2´-Bipyridine	0.61	0.44	0.87	0.55	0.62±0.18
3,3´,4,4´-Benzo-phenone tetracarboxylic acid	0.83	0.77	0.55	0.63	0.70±0.12

[a] See chapter 2. Transfer coefficient reported here obtained at pH 4.

Table 11.3: Transfer Coefficient Determine by Several Independent Methods[a]

compd[b]	transfer coefficient				
	E_p^{ox} *vs.* $\log \upsilon$	$E_{p/2}^{ox}$ *vs.* $\log \upsilon$	E_p^{ox} *vs.* $\log i_p$	$E_p^{ox} - E_{p/2}^{ox}$	a.v.
Thymine	0.42	0.78	0.69	0.50	0.59±0.16
Adenosine	0.76	0.63	0.89	0.66	0.74±0.17
Histidine	0.55	0.63	0.65	0.36	0.55±0.13
Methionine	0.40	0.73	0.48	0.25	0.47±0.20
2,2´-Bipyridine	0.41	0.77	0.28	0.47	0.48±0.20
3,3´,4,4´-Benzo-phenone tetracarboxylic acid	0.72	0.81	0.67	0.78	0.75±0.06

[a] See chapter 2. [b] Transfer coefficient reported here obtained at pH 6.2.

Table 11.4: Transfer Coefficient Determine by Several Independent Methods[a]

compd[b]	transfer coefficient				
	E_p^{ox} *vs.* $\log \upsilon$	$E_{p/2}^{ox}$ *vs.* $\log \upsilon$	E_p^{ox} *vs.* $\log i_p$	$E_p^{ox} - E_{p/2}^{ox}$	a.v.
Thymine	0.86	0.91	0.76	0.57	0.77±0.15
Adenosine	0.41	0.99	0.42	0.32	0.54±0.30
Histidine	0.26	0.34	0.45	0.54	0.40±0.12
Methionine	-	-	-	-	-
2,2´-Bipyridine	-	-	-	-	-
3,3´,4,4´-Benzo-phenone tetracarboxylic acid	-	-	-	-	-

[a] See chapter 2. [b] Transfer coefficient reported here obtained at pH 7.9.

Table 11.5: Transfer Coefficient Determine by Several Independent Methods[a]

compd[b]	transfer coefficient				
	E_p^{ox} *vs.* $\log \upsilon$	$E_{p/2}^{ox}$ *vs.* $\log \upsilon$	E_p^{ox} *vs.* $\log i_p$	$E_p^{ox} - E_{p/2}^{ox}$	a.v.
Thymine	0.83	0.89	0.88	0.47	0.77±0.20
Adenosine	0.39	0.63	0.39	0.31	0.43±0.13
Histidine	0.25	0.68	0.47	0.56	0.49±0.18
Methionine	0.36	0.95	0.48	0.36	0.54±0.20
2,2´-Bipyridine	-	-	-	-	-
3,3´,4,4´-Benzo-phenone tetracarboxylic acid	-	-	-	-	-

[a] See chapter 2. [b] Transfer coefficient reported here obtained at pH 10.

Table 11.6: Transfer Coefficient Determine by Several Independent Methods[a]

compd[b]	transfer coefficient				
	E_p^{ox} *vs.* $\log \upsilon$	$E_{p/2}^{ox}$ *vs.* $\log \upsilon$	E_p^{ox} *vs.* $\log i_p$	$E_p^{ox} - E_{p/2}^{ox}$	a.v.
Thymine	0.91	0.90	0.89	0.75	0.87±0.07
Adenosine	-	-	-	-	-
Histidine	0.54	0.67	0.65	0.68	0.64±0.06
Methionine	-	-	-	-	-
2,2´-Bipyridine	-	-	-	-	-
3,3´,4,4´-Benzo-phenone tetracarboxylic acid	-	-	-	-	-

[a] See chapter 2. [b] Transfer coefficient reported here obtained at pH 12.

Acronyms

Solvents

MeCN	Acetonitrile
DMSO	Dimethyl sulfoxide
WA	Water
PrOH	2-Propanol

Solutes

TBAP	Tetrabutylammonium perchlorate
TBATFB	Tetrabuylammonium tetrafluoroborate
Bu_4NBF_4	Tetrabuylammonium tetrafluoroborate
KNO_3	Potassium nitrate
NaOH	Sodium hydroxide
HCl	Hydrochloric acid
DMA	N,N´-Dimethylaniline
DEA	N,N´-Diethylaniline
TP	Triphenylamine
DABCO	1,4-Diazabicyclo[2.2.2]octane
DMPM	4,4´-Bis(dimethylamino) diphenylmethane
TMB	1,2,4-Trimethoxybenzene
3DMB	1,3-Dimethoxybenzene
4DMB	1,4-Dimethoxybenzene
BA	2-Bromoanisole
2MA	2-Methylanisole
3MA	3-Methylanisole
4MA	4-Methylanisole
MB	Methoxybenzene
TMP	1,2,5-Trimethylpyrrole
TMB	N,N,N´,N´-Tetramethylbenzidine
MP	N-Methylpyrrole
PTPA	N-phenyl-tetrachlorophthalimide
Fc	Ferrocene
BP	2,2´-Bipyridine
BPTCA	3,3´,4,4´-Benzophenone tetracarboxylic acid

Others

PMV	Photomodulated Voltammetry
CV	Cyclic Voltammetry
SHACV	Second-harmonic alternating current voltammetry
P-SHACV	Phase-selective second-harmonic alternating current voltammetry
DNA	Deoxyribonucleic acid
PET	Photoinduced Electron Transfer Reactions

Symbols

Symbol	Meaning	Units
M	molecule	-
Q	quencher	-
A	area of electrode	cm^2
α	electron transfer coefficient for reversible process	none
β	electron transfer coefficient for irreversible process	none
C_o^*	concentration of O	M, mol/cm^3
F	faraday constant	C
E	potential of a electrode versus a reference	V
E_p	Peak potential	V
E_p^{ox}	Oxidation peak potential	V
E_p^{red}	Reduction peak potential	V
$E_{1/2}$	half-wave potential	V
$E_{1/2}^{ox}$	Half-wave oxidation potential	V
$E_{1/2}^{red}$	Half-wave reduction potential	V
E^o	standard potential	V
$E_{p/2}$	potential at half peak	V
$\left(E_p\right)_a$	anodic peak potential	V
$\left(E_p\right)_c$	cathodic peak potential	V
i	current	A
i_o	exchange current density	A/cm^2
i_p	peak current	A
$i_{p/2}$	current at half peak	A
$\left(i_p\right)_a$	anodic peak current	A
$\left(i_p\right)_c$	cathodic peak current	A
K	equilibrium constant	none
ΔG^o	standard Gibbs free energy	j/mole
ΔG	Gibbs free energy	j/mole
$\Delta G^{\ddagger}$	Activation free energy	j/mole
$\Delta G^{\ddagger}(0)$	Intrinsic barrier	j/mole
λ	reorganization energy	j/mole
λ_o	Salvation energy	j/mole
λ_i	Vibrational energy	j/mole

k_s	heterogeneous rate constant	cm/s
k_{diff}	diffusion rate constant	cm/s
k_{diss}	dissociation rate constant	cm/s
k_e	rate constant for forward electron transfer	cm/s
k_{-e}	rate constant for reverse electron transfer	cm/s
k_{decay}	decay rate constant to ground state	cm/s
k_q	quenching rate constant	cm/s
$k^{\ddagger}$	frequency factor	-
w_r	work term to bring reactant together	-
w_p	work term to bring product together	-
N_A	Avogadro's number	per mole
D	diffusion coefficient for	cm^2/sec
D_M	Diffusion coefficient for molecule	cm^2/sec
D_Q	Diffusion coefficient for quencher	cm^2/sec
ΔV	volume of the encounter complex	cm^3
χ (bt)	normalized current for a reversible system in LSV and CV	none
n	number of electrons	none
t	time	sec
v	scan rate	volts/sec
Ag/AgCl	silver-silver chloride Reference electrode	-
W	tungsten reference electrode	-
Fc^+/Fc	internal reference electrode	-

Bibliography

[1] C. R. Bock, J. A. Connor, A. R. Gutierrez, T. J. Meyer, D. G. Whitten, B. P. Sullivan and J. K. Nagle, *J Am Chem Soc* **1979**, *101*, 4815-4824.

[2] N. Sutin and C. Creutz, *J Chem Educ* **1983**, *60*, 809-814.

[3] D. Rehm and A. Weller, *Israel J Chem* **1970**, *8*, 259-271.

[4] R. A. Marcus, *J Phys Chem* **1963**, *67*, 853-857.

[5] R. A. Marcus, *Annu Rev Phys Chem* **1964**, *15*, 155-196.

[6] R. A. Marcus, *Angew Chem Int Edit* **1993**, *32*, 1111-1121.

[7] R. A. Marcus, *Angew Chem Int Edit* **1993**, *32*, 1111-1121.

[8] R. A. Marcus and N. Sutin, *Biochim Biophys Acta* **1985**, *811*, 265-322.

[9] R. D. Levine, *J Phys Chem* **1979**, *83*, 159-170.

[10] E. Ahlberg and V. D. Parker, *Acta Chem Scand* **1980**, *B 34*, 91-96.

[11] C. P. Andrieux, P. Hapiot, J. Pinson and J. M. Saveant, *J Am Chem Soc* **1993**, *115*, 7783-7788.

[12] M. R. Wasielewski and R. Breslow, *J Am Chem Soc* **1976**, *98*, 4222-4229.

[13] A. M. Bond and D. E. Smith, *Anal Chem* **1974**, *46*, 1946-1951.

[14] E. Ahlberg and V. D. Parker, *Acta Chem Scand* **1980**, *B 34*, 97-102.

[15] A. G. Larsen, *Master Thesis Department of Chemistry, Arhus University* **2001**.

[16] D. D. M. Wayner and D. Griller, *J Am Chem Soc* **1985**, *107*, 7764-7765.

[17] D. D. M. Wayner, D. J. McPhee and D. Griller, *J Am Chem Soc* **1988**, *110*, 132-137.

[18] R. Ballardini, G. Varani, M. T. Indelli, F. Scandola and V. Balzani, *J Am Chem Soc* **1978**, *100*, 7219-7223.

[19] S. Fukuzumi, K. Hironaka, N. Nishizawa and T. Tanaka, *B Chem Soc Jpn* **1983**, *56*, 2220-2227.

[20] C. Society, *Photochemistry*, Royal Society of Chemistry, **1985**, 18.

[21] F. Scandola, V. Balzani and G. B. Schuster, *J Am Chem Soc* **1981**, *103*, 2519-2523.

[22] L. Poulsen, A. Z. Ruiz, S. U. Pedersen and P. R. Ogilby, *J Chem Educ* **2003**, *80*, 819-821.

[23] C. R. Bock, T. J. Meyer and D. G. Whitten, *J Am Chem Soc* **1975**, *97*, 2909-2911.

[24] D. A. Labianca, G. N. Taylor and G. S. Hammond, *J Am Chem Soc* **1972**, *94*, 3679-3683.

[25] G. B. Schuster, *J Am Chem Soc* **1979**, *101*, 5851-5853.

[26] P. F. Barbara, T. J. Meyer and M. A. Ratner, *J Phys Chem* **1996**, *100*, 13148-13168.

[27] N. S. Hush, A. A. Vlcek, D. R. Stranks, R. A. Marcus, J. Weiss, R. P. Bell, J. Halpern, L. E. Orgel, A. W. Adamson, F. S. Dainton, R. J. P. Williams, H. Taube, I. A. W. Shimi, W. C. E. Higginson, J. B. Stead, G. M. Waind, D. R. Rosseinsky, C. F. Wells, L. H. Sutcliffe, P. J. Proll, E. L. King, D. R. Stranks, R. G. Pearson, F. Basolo, A. J. Poe, M. H. Fordsmith, N. Sutin, R. W. Dodson and C. Baughan, *Discuss Faraday Soc* **1960**, 113-136.

[28] N. S. Hush, *Trans Faraday Soc* **1961**, *57*, 557-580.

[29] N. Sutin, *Theory of Electron Transfer Reactions: Insights and Hindsights*, John Wiley & Sons, Inc., **2007**, p. 441-498.

[30] F. Scandola and V. Balzani, *J Am Chem Soc* **1979**, *101*, 6140-6142.

[31] N. Agmon and R. D. Levine, *Chem Phys Lett* **1977**, *52*, 197-201.

[32] J. K. Nagle, W. J. Dressick and T. J. Meyer, *J Am Chem Soc* **1979**, *101*, 3993-3995.

[33] A. P. Darmanyan, W. S. Jenks and P. Jardon, *J Phys Chem A* **1998**, *102*, 7420-7426.

[34] J. G. Velasco, *Electroanalysis* **1997**, *9*, 880-882.

[35] J. González-Velasco, *Electroanalysis* **1994**, *6*, 711-724.

[36] D. R. Arnold, X. Y. Du and K. M. Henseleit, *Can J Chem* **1991**, *69*, 839-852.

[37] T. Yago, Y. Kobori, K. Akiyama and S. Tero-Kubota, *J Phys Chem B* **2002**, *106*, 10074-10081.

[38] Y. Kobori, T. Yago, K. Akiyama and S. Tero-Kubota, *J Am Chem Soc* **2001**, *123*, 9722-9723.

[39] R. J. Klinger and J. K. Kochi, *J Am Chem Soc* **1980**, *102*, 4790-4798.

[40] R. S. Nicholson and I. Shain, *Anal Chem* **1964**, *36*, 706-723.

[41] R. S. Nicholson, *Anal Chem* **1965**, *37*, 1351-1355.

[42] A. Bard and L. Faulkner, *Electrochemical methods: fundamentals and applications*, Wiley, **2001**.

[43] C. Hamann, A. Hamnett and W. Vielstich, *Electrochemistry*, Wiley-VCH, **2007**.

[44] J. Heinze, *Angew Chem Int Edit* **1984**, *23*, 831-847.

[45] P. T. Kissinger and W. R. Heineman, *J Chem Educ* **1983**, *60*, 702-706.

[46] G. A. Mabbott, *J Chem Educ* **1983**, *60*, 697-702.

[47] D. Pletcher and S. E. Group, *Instrumental methods in electrochemistry*, Ellis Horwood, **2001**.

[48] F. Scholz, *Electroanalytical Methods: Guide to Experiments and Applications*, Springer, **2010**.

[49] J. J. Van Benschoten, J. Y. Lewis, W. R. Heineman, D. A. Roston and P. T. Kissinger, *J Chem Educ* **1983**, *60*, 772-776.

[50] R. J. Klingler and J. K. Kochi, *J Phys Chem* **1981**, *85*, 1731-1741.

[51] I. Lavagnini, R. Antiochia and F. Magno, *Electroanalysis* **2004**, *16*, 505-506.

[52] W. H. Reinmuth, *Anal Chem* **1960**, *32*, 1891-1892.

[53] A. W. Bott, *Curr Separ* **1999**, *18*, 9.

[54] S. C. Brooks and M. M. Richter, *Chem Ed* **2002**, *7*, 9-13.

[55] H. S. Wang, H. X. Ju and H. Y. Chen, *Anal Chim Acta* **2002**, *461*, 243-250.

[56] A. M. Oliveira Brett and F.-M. Matysik, *J Electroanal Chem* **1997**, *429*, 95-99.

[57] M. A. T. Gilmartin and J. P. Hart, *Analyst* **1992**, *117*, 1613-1618.

[58] C. M. A. Brett, A. M. Oliveira Brett and S. H. P. Serrano, *J Electroanal Chem* **1994**, *366*, 225-231.

[59] G. Dryhurst, *Talanta* **1972**, *19*, 769-778.

[60] Y. Xu and B. J. Venton, *Phys Chem Chem Phys* **2010**, *12*, 10027-10032.

[61] G. Dryhurst, *Anal Chim Acta* **1971**, *57*, 137-149.

[62] V. Vetterl, *J Electroanal Chem Inter Electrochem* **1968**, *19*, 169-173.

[63] J. Xu, Y. Wang, Y. Xian, L. Jin and K. Tanaka, *Talanta* **2003**, *60*, 1123-1130.

[64] R. P. Deo, N. S. Lawrence and J. Wang, *Analyst* **2004**, *129*, 1076-1081.

[65] V. Brabec and V. Mornstein, *Biophys Chem* **1980**, *12*, 159-165.

[66] J. A. Reynaud, B. Malfoy and A. Bere, *J Electroanal Chem Inter Electrochem* **1980**, *116*, 595-606.

[67] J. A. Reynaud, B. Malfoy and P. Canesson, *J Electroanal Chem Inter Electrochem* **1980**, *114*, 195-211.

[68] B. Malfoy and J. A. Reynaud, *J Electroanal Chem Inter Electrochem* **1980**, *114*, 213-223.

[69] R. A. Kenley, S. E. Jackson, J. C. Martin and G. C. Visor, *J Pharm Sci* **1985**, *74*, 1082-1085.

[70] A. M. Oliveira Brett and F.-M. Matysik, *Bioelectrochem Bioenerg* **1997**, *42*, 111-116.

[71] G. Jones, S. F. Griffin, C. Y. Choi and W. R. Bergmark, *J Organic Chem* **1984**, *49*, 2705-2708.

[72] C. A. M. Seidel, A. Schulz and M. H. M. Sauer, *J Phys Chem* **1996**, *100*, 5541-5553.

[73] M. Z. Hoffman, M. G. Simic, Q. G. Mulazzani, S. Emmi, P. G. Fuochi and M. Venturi, *Rad Phys Chem (1977)* **1978**, *12*, 111-113.

[74] C. Costentin, C. Louault, M. Robert and J.-M. Savéant, *Proceedings of the National Academy of Sciences 106*, 18143-18148.

[75] C. Costentin, M. Robert, J.-M. Savéant and A.-L. Teillout, *Proceedings of the National Academy of Sciences* **2009**, *106*, 11829-11836.

[76] R. Breslow and R. Goodin, *J Am Chem Soc* **1976**, *98*, 6076-6077.

[77] M. Patz, H. Mayr, J. Maruta and S. Fukuzumi, *Angew Chem Int Edit* **1995**, *34*, 1225-1227.

[78] B. Jaun, J. Schwarz and R. Breslow, *J Am Chem Soc* **1980**, *102*, 5741-5748.

[79] R. Breslow and J. L. Grant, *J Am Chem Soc* **1977**, *99*, 7745-7746.

[80] E. M. Arnett, K. Amarnath, N. G. Harvey and J. Cheng, *J Am Chem Soc* **1990**, *112*, 344-355.

[81] T. G. McCord and D. E. Smith, *Anal Chem* **1969**, *41*, 1423-1441.

[82] T. G. McCord and D. E. Smith, *Anal Chem* **1968**, *40*, 289-304.

[83] D. E. Smith and W. H. Reinmuth, *Anal Chem* **1961**, *33*, 482-485.

[84] W. L. Underkofler and I. Shain, *Anal Chem* **1965**, *37*, 218-222.

[85] H. Blutstein and A. M. Bond, *Anal Chem* **1974**, *46*, 1934-1941.

[86] A. M. Bond, *Anal Chim Acta* **1975**, *74*, 163-175.

[87] G. Grampp, S. Landgraf and C. Muresanu, *Electrochim Acta* **2004**, *49*, 537-544.

[88] G. Grampp, C. Muresanu and S. Landgraf, *J Electroanal Chem* **2005**, *582*, 171-178.

[89] D. D. M. Wayner and A. Houmam, *Acta Chem Scand* **1998**, *52*, 377-384.

[90] A. G. Larsen, A. H. Holm, M. Roberson and K. Daasbjerg, *J Am Chem Soc* **2001**, *123*, 1723-1729.

[91] D. K. Smith, W. E. Strohben and D. H. Evans, *J Electroanal Chem Inter Electrochem* **1990**, *288*, 111-128.

[92] G. Grampp, C. Muresanu and S. Landgraf, *Electrochim Acta* **2008**, *53*, 3149-3155.

[93] M. Jonsson, D. D. M. Wayner, D. A. Armstrong, D. Yu and A. Rauk, *J Chem Soc, Perkin Trans 2* **1998**, 1967-1972.

[94] T. Lund, D. D. M. Wayner, M. Jonsson, A. G. Larsen and K. Daasbjerg, *J Am Chem Soc* **2001**, *123*, 12590-12595.

[95] S. S. Jayanthi and P. Ramamurthy, *J Phys Chem A* **1998**, *102*, 511-518.

[96] T. A. Fayed, S. E.-D. H. Etaiw, S. Landgraf and G. Grampp, *Photochem Photobiol Sci* **2003**, *2*, 376-380.

[97] A. Lewandowska, G. L. Hug, G. Hörner, T. Pedzinski, P. Filipiak and B. Marciniak, *Chem Phys Chem* **2010**, *11*, 2108-2117.

[98] F. Scandola and V. Balzani, *J Chem Educ* **1983**, *60*, 814-823.

[99] R. O. Loutfy, *Tetrahedron* **1973**, *29*, 2251-2252.

[100] A. Zweig, A. H. Maurer and B. G. Roberts, *J Org Chem* **1967**, *32*, 1322-1329.

[101] S. Fukuzumi and J. K. Kochi, *J Am Chem Soc* **1981**, *103*, 7240-7252.

[102] A. Zweig, W. G. Hodgson and W. H. Jura, *J Am Chem Soc* **1964**, *86*, 4124-4129.

[103] R. J. Klinger and J. K. Kochi, *J Am Chem Soc* **1981**, *103*, 5839-5848.

[104] R. J. Klingler and J. K. Kochi, *J Am Chem Soc* **1982**, *104*, 4186-4196.

[105] S. Fukuzumi, S. Koumitsu, K. Hironaka and T. Tanaka, *J Am Chem Soc* **1987**, *109*, 305-316.

[106] S. Fukuzumi, N. Nishizawa and T. Tanaka, *J Chem Soc, Perkin Trans 2* **1985**, 371-378.

[107] R. Dietz and M. E. Peover, *Trans Faraday Soc* **1966**, *62*, 3535-3542.

[108] T. Mizoguchi and R. N. Adams, *J Am Chem Soc* **1962**, *84*, 2058-2061.

[109] L. R. Sharma, A. K. Manchanda, G. Singh and R. S. Verma, *Electrochim Acta* **1982**, *27*, 223-233.

[110] E. T. Seo, R. F. Nelson, J. M. Fritsch, L. S. Marcoux, D. W. Leedy and R. N. Adams, *J Am Chem Soc* **1966**, *88*, 3498-3503.

[111] Z.-R. Zheng, D. H. Evans and S. F. Nelsen, *J Organic Chem* **2000**, *65*, 1793-1798.

[112] K. Yuan Chiu, T. Xiang Su, J. Hong Li, T.-H. Lin, G.-S. Liou and S.-H. Cheng, *J Electroanal Chem* **2005**, *575*, 95-101.

[113] H. Yang, D. O. Wipf and A. J. Bard, *J Electroanal Chem* **1992**, *331*, 913-924.

[114] G. Wang, Z. LIU, L. X. Wang, X. B. Jing and F. S. Wang, *Chinese Chem Lett* **2002**, *13*, 422-425.

[115] A. Zweig, M. T. Neglia, J. E. Lancaster and W. H. Jura, *J Am Chem Soc* **1964**, *86*, 4130-4136.

[116] V. Brabec and V. Mornstein, *Biochim Biophys Acta (BBA) - Protein Structure* **1980**, *625*, 43-50.

[117] N. Ogawa, I. Watanabe and S. Ikeda, *Anal Chim Acta* **1982**, *141*, 123-129.

[118] H. H. Bauer, *J Electroanal Chem (1959)* **1960**, *1*, 256-258.